

AD-A246 406



MTL TR 91-55

AD



AN ASSESSMENT OF A FRICTION JOINT CONCEPT FOR THE ROADWHEEL HOUSING ATTACHMENT OF THE COMPOSITE INFANTRY FIGHTING VEHICLE

STEVEN M. SERABIAN, CHRISTOPHER CAVALLARO,
ROBERT B. DOOLEY, and KRISTEN D. WEIGHT
MECHANICS AND STRUCTURES BRANCH

December 1991

Approved for public release; distribution unlimited.

DTIC
SELECTED
FEB 27 1992
S B D



US ARMY
LABORATORY COMMAND
MATERIALS TECHNOLOGY LABORATORY

U.S. ARMY MATERIALS TECHNOLOGY LABORATORY
Watertown, Massachusetts 02172-0001

92-04660



1 62 2 24 070

The findings in this report are not to be construed as an official Department of the Army position, unless so designated by other authorized documents.

Mention of any trade names or manufacturers in this report shall not be construed as advertising nor as an official indorsement or approval of such products or companies by the United States Government.

DISPOSITION INSTRUCTIONS

Destroy this report when it is no longer needed.
Do not return it to the originator.

UNCLASSIFIED

SECURITY CLASSIFICATION OF THIS PAGE (When Data Entered)

REPORT DOCUMENTATION PAGE		READ INSTRUCTIONS BEFORE COMPLETING FORM
1. REPORT NUMBER MTL TR 91-55	2. GOVT ACCESSION NO.	3. RECIPIENT'S CATALOG NUMBER
4. TITLE (and Subtitle) AN ASSESSMENT OF A FRICTION JOINT CONCEPT FOR THE ROADWHEEL HOUSING ATTACHMENT OF THE COMPOSITE INFANTRY FIGHTING VEHICLE	5. TYPE OF REPORT & PERIOD COVERED Final Report	
	6. PERFORMING ORG. REPORT NUMBER	
7. AUTHOR(s) Steven M. Serabian, Christopher Cavallaro, Robert B. Dooley, and Kristen D. Weight	6. CONTRACT OR GRANT NUMBER(s)	
9. PERFORMING ORGANIZATION NAME AND ADDRESS U.S. Army Materials Technology Laboratory Watertown, Massachusetts 02172-0001 ATTN: SLCMT-MRS	10. PROGRAM ELEMENT, PROJECT, TASK AREA & WORK UNIT NUMBERS D/A Project: 1L263102D081 AMCMS Code: 612105.AH840011	
11. CONTROLLING OFFICE NAME AND ADDRESS U.S. Army Laboratory Command 2800 Powder Mill Road Adelphi, Maryland 20783-1145	12. REPORT DATE December 1991	
	13. NUMBER OF PAGES 85	
14. MONITORING AGENCY NAME & ADDRESS (if different from Controlling Office)	15. SECURITY CLASS. (of this report) Unclassified	
	15a. DECLASSIFICATION/DOWNGRADING SCHEDULE	
16. DISTRIBUTION STATEMENT (of this Report) Approved for public release; distribution unlimited.		
17. DISTRIBUTION STATEMENT (of the abstract entered in Block 20, if different from Report)		
18. SUPPLEMENTARY NOTES		
19. KEY WORDS (Continue on reverse side if necessary and identify by block number)		
Composite materials	Friction	Roadwheels
Bolted joints	Bolt preload	Fighting vehicles
Finite element analysis	Suspension	Tanks
20. ABSTRACT (Continue on reverse side if necessary and identify by block number) (SEE REVERSE SIDE)		

Block No. 20

ABSTRACT

Evaluation of a friction joint concept was undertaken to assess its viability as a critical joining technique for the Composite Infantry Fighting Vehicle. Through thickness viscoelastic relaxation effects of the thick [(0/90/45)₄], S2 glass/polyester woven roving CIFV hull material was experimentally investigated under dynamic surface traction fatigue and static loading conditions for a single connector configuration. Joint slip load as a function of bolt preload was also experimentally determined for this specimen configuration. Using this single connector information, a computer code was developed to predict friction joint lifetimes of multiple connector joints subjected to Perryman III terrain test conditions. Joint reaction forces and moments used in this code were obtained for the Composite Infantry Fighting Vehicle from *DADS* suspension modeling results. Bolt bearing stress state conditions resulting from friction joint slippage were predicted with a 3D nonlinear elastic finite element model. Finite element constitutive equations were developed for the S2 woven roving material from mechanical properties obtained from tension, compression, intralaminar, and interlamina shear tests.

Accession For	
NTIS GRA&I	<input checked="" type="checkbox"/>
DTIC TAB	<input type="checkbox"/>
Unannounced	<input type="checkbox"/>
Justification	
By	
Distribution/	
Availability Codes	
Dist	Avail and/or Special
A-1	



Contents

	Page
INTRODUCTION.....	3
AMTL/FMC Composite Infantry Fighting Vehicle.....	3
Use of Mechanical Fastening in CIFV Design.....	4
Roadwheel Housing Attachment.....	6
Related Past Work Efforts.....	7
Scope of Work.....	7
ESTIMATION OF CIFV FRICTION JOINT CONNECTOR LOADS.....	8
Friction Joint Mechanical Analysis.....	8
Static Roadarm Displacement Conditions.....	9
Dynamic DADS Suspension Conditions.....	10
Analysis Results.....	16
EXPERIMENTAL CHARACTERIZATION OF CIFV FRICTION JOINT PERFORMANCE.....	32
Single Connector Friction Load Carrying Capability.....	32
Effects of Through Thickness Viscoelastic Material Relaxation.....	34
Static Loading Conditions.....	34
Surface Traction Fatigue Loading Conditions.....	34
Experimental Results.....	37
PREDICTION OF CIFV FRICTION JOINT PERFORMANCE.....	39
Friction Joint Mechanical Slip Analysis.....	39
Static Roadarm Displacement Results.....	45
Dynamic Perryman III Terrain Results.....	47
[(0/90/45)_n]s S2 WOVEN ROVING MECHANICAL PROPERTY CHARACTERIZATION.....	54
Tension Tests.....	54
Compression Testing.....	55
Intra and Inter Lamina Shear Testing.....	59
BOLT BEARING STRESS STATE PREDICTIONS.....	62
Single Connector Three Dimensional Finite Element Model.....	62
Constitutive Equation Development.....	64
Abaqus User Material Subroutine.....	65
Finite Element Computations.....	66
Finite Element Results.....	68
CONCLUSIONS.....	82
RECOMMENDATIONS FOR FUTURE WORK.....	84
ACKNOWLEDGMENTS.....	84

INTRODUCTION

AMTL/FMC Composite Infantry Fighting Vehicle

Increased mobility and performance requirements of next generation Army hardware systems are presently being met by exploiting the advantages of fiber reinforced composite laminates. The Composite Infantry Fighting Vehicle (CIFV), shown in Figure 1, presently being developed by FMC under the direction of Army Material Technology Laboratory is a prime example of this. Design engineers have been able to meet both structural and ballistic needs yet obtain increased weight savings by using an S2 glass/polyester woven roving to fabricate both hull and turret structures. Other benefits such as lower fabrication costs through parts consolidation, increased operational life via reduced corrosion and stress cracking, improved noise and vibration characteristics, and enhanced survivability by spall reduction have been observed.¹



Figure 1 The Composite Infantry Fighting Vehicle

Figure 2 illustrates the CIFV hull cross sectional view. As can be seen, it is constructed by joining two composite hull halves along a vertical center line. This center line has been positioned to run between numerous hull cutouts to reduce joining requirements. An aluminum chassis frame with longitudinal box beam supports and transverse torsion bar beam housings is joined between the bottom of both hull halves. Blast protection from land mines is accomplished through a composite bottom plate that is attached to the chassis frame. An aluminum turret shield is employed to transmit roof and turret inertial loads to the aluminum chassis.

1. WEERTH, D.E., *Fiber Reinforced Plastic Infantry Fighting Vehicle Technology Development*. Proceedings of the Army Symposium on Solid Mechanics: Lightening the Force. U.S. Army Materials Technology Laboratory, MTL MS-86-2, October 1986, pp.37-54.

Roadwheel arms are attached to torsion bar assemblies through roadwheel housings at the lower portions of both right and left hull halves. At these points the hull section is sandwiched between the roadwheel housings and the aluminum chassis. Torsion bar ends are anchored to respective roadwheel housings on opposing hull sides.

**COMPOSITE INFANTRY FIGHTING VEHICLE HULL PROGRAM
Hull Cross Section — Concept IV**

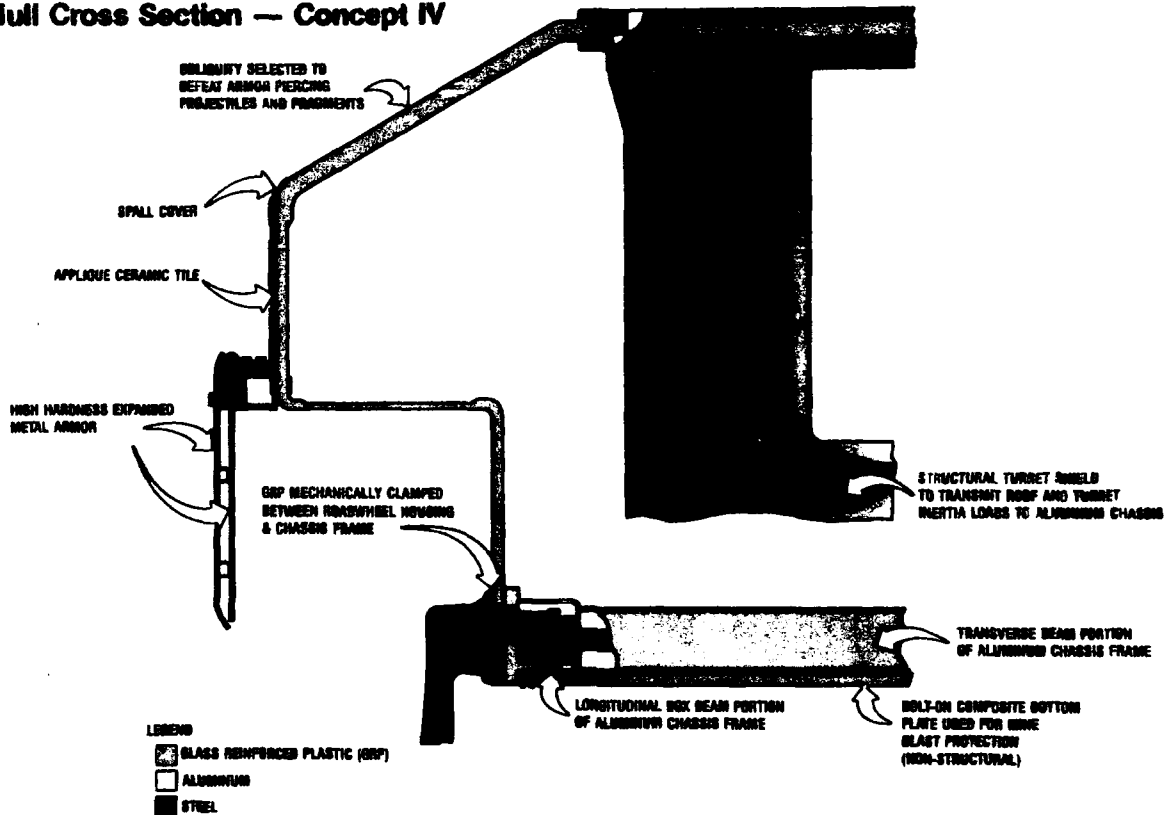


Figure 2 CIFV Hull Cross Sectional View

Use of Mechanical Fastening in CIFV Design

Although significant parts consolidation is being achieved with this basic hull design, aluminum and composite components must still be structurally joined. Mechanical fastening is employed to accomplish this. Figure 3 illustrates representative hull bolted joint configurations presently under consideration.² As can be seen, splice joints are used to join upper hull halves while a through bolting configuration is used at the hull/turret interface. A modified single lap joint bolting configuration is used for attaching the hull halves to the aluminum idler plate while an angle bracket type attachment is used for the aft plate/hull interface. A through bolt configuration is used to attach roadwheel housings to the hull halves as well as the composite bottom plate to the aluminum chassis.

2. PARA, P. *Composite Infantry Fighting Vehicle Hull Program: Test Plan Review Meeting*. July 14, 1987, Watertown, MA.

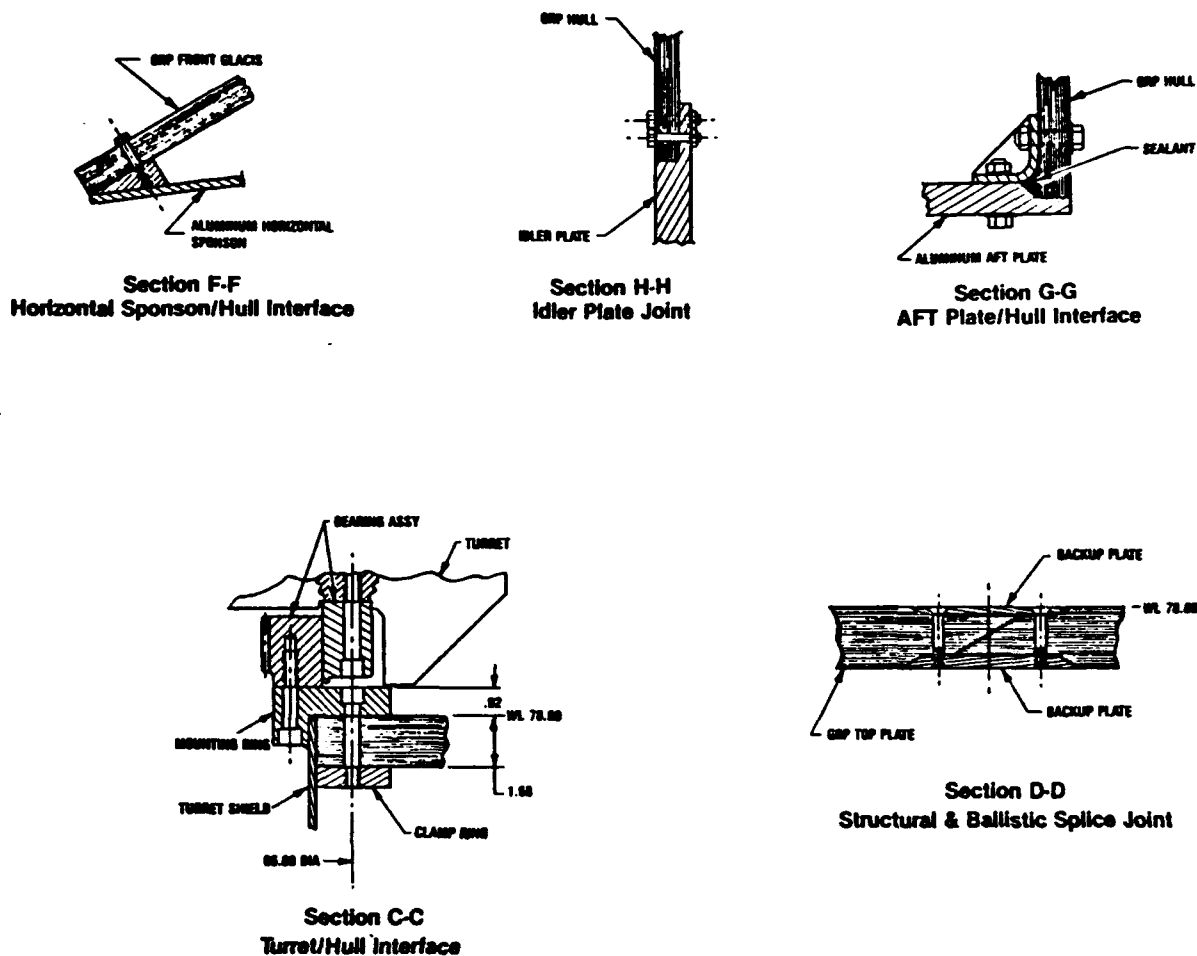


Figure 3 Representative CIFV Mechanical Fastening Configurations

Many hull joints are subjected to harsh loading environments. Generally, joint design is governed by these structural requirements alone. In some instances however; as in the upper hull splice joints, joint design is also driven by ballistic considerations as well. In these cases, joint structural integrity must be maintained even after joint ballistic damage is sustained. Maintaining both structural and ballistic integrity of hull joints become increasingly important in light of hull parts consolidation. Many joints may be termed *design critical* when both repair and integrity considerations are made.

Roadwheel Housing Attachment

The roadwheel housing attachment is a prime example of a design critical hull joint. Its function of transmitting severe dynamic roadwheel suspension loads into the hull and providing torsion bar anchoring is quite demanding. Failure of this joint could possibly necessitate hull replacement since localized repair in these highly loaded sections is improbable.

As seen in Figure 4a, the roadwheel housing multiple connector mechanically clamps the composite hull. Roadarm forces and torsion bar moments are reacted by the connectors within the joint to transmit roadwheel forces to the hull. Frictional forces generated by this mechanical clamping action are used to prevent joint slippage and bolt bearing conditions between the fasteners and hull material. The mechanics of this novel *friction joint* concept are however susceptible to bolt preload drop off from the potential viscoelastic relaxation of the thick composite hull material. Prediction of this bolt preload decay under the prevailing dynamic surface traction fatigue conditions of the roadwheel housing plate are required to estimate friction joint lifetimes. Furthermore; maximum bolt bearing state stress conditions must be predicted to insure overall roadwheel housing attachment structural integrity.

Figure 4b illustrates the dimensional characteristics of the roadwheel housing attachment. As can be seen, twelve 5/8" grade eight bolts torqued to 158 ft-lbs are used to generate a reactive frictional force. This multiple connector arrangement is the same as the one used on the current production aluminum Bradley Fighting Vehicle. A modified version of this attachment, shown in Figure 4c, that attempts to reduce frictional requirements by bolt pattern alteration, has been proposed by FMC.

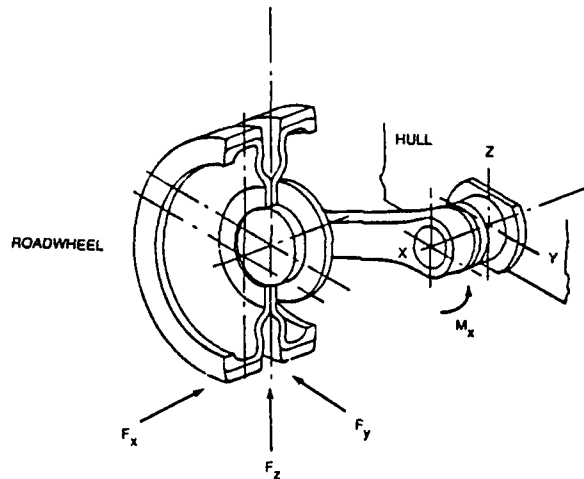


Figure 4a CIFV Roadwheel Assembly and Loading Configuration

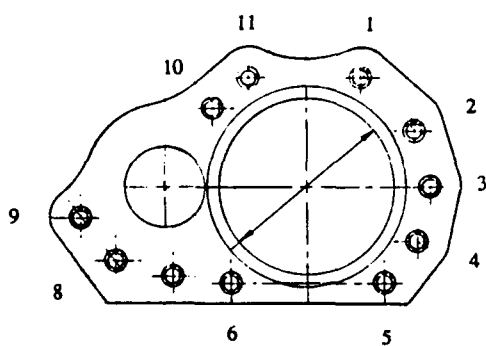


Figure 4b Original CIFV Attachment

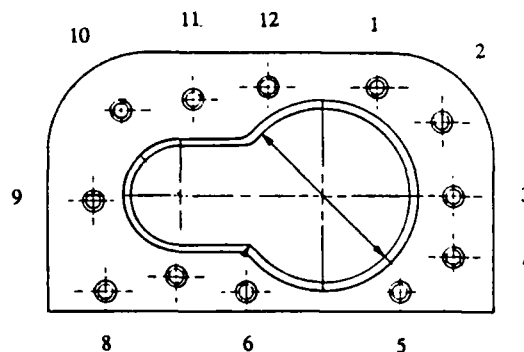


Figure 4c Modified CIFV Attachment

Related Past Work Efforts

The friction joint concept has been used in past design efforts that sought to introduce composite materials into Army mobile bridging systems. Slepetz *et al*³ investigated the friction joining of bridging tension members constructed of high modulus graphite epoxy sandwiched between aluminum plates. Improved structural joining efficiencies were achieved above those obtained from conventional bolt bearing methodologies by the use of elliptical bolt holes. Effects of bolt preload relaxation in both room and elevated temperature environments were also experimentally determined by Slepetz *et al*.⁴ Significant reductions were observed at elevated temperatures while minimal reductions were observed at room temperature. Similar trends were observed by Shivakumar and Crews.⁵ In another effort, Weerth and Ortloff developed lifetime estimations of a single axially loaded through thickness mechanical fastener in a thick Vinyl Ester/E Glass composite/metallic sandwich connector.⁶

Structural testing of both roadwheel housing joints was conducted by FMC during the same time period that this present work was being done.⁷ In that work, a full scale representative hull cross section was fatigue loaded with estimated cross country duty cycle loading. Hydraulic actuators were used to load steel I-beams that were connected to torsion bar assemblies. Test results showed that no-slip conditions prevailed for both roadwheel housing configurations. However, high load frequencies were employed to compress testing time and half magnitude vertical force joint shear loading was used to reduce actuator testing loads. It is not apparent how both these factors affected test conclusions regarding the performance of each roadwheel housing friction joint design.

Scope of Work

This effort is an attempt to provide advanced design and analysis techniques for the design critical CIFV roadwheel housing attachment. These techniques will be used to assess the load carrying capability and lifetime of a friction joint concept based on both roadwheel housing designs. Overall joint structural integrity will be reviewed by investigating maximum bolt bearing stress state conditions. It is hoped that these advanced analysis techniques will not only provide pertinent information regarding the present roadwheel housing attachment design, but will also be used in future CIFV friction joint design studies.

3. SLEPETZ, J.M. OPLINGER, D.O., and ANDREWS, B.O., *Fabrication, Testing, and Connector Design for a Metal-Composite Sandwich Panel Tension Member*. Proceedings of the Sixth Conference on Fibrous Composites in Structural Design, AMMRC MS 83-2, November 1983, pp. V1-V22.
4. SLEPETZ, J.M. OPLINGER, D.O., and ANDREWS, B.O., *Bolt Tension Relaxation in Composite Friction Joints*. Proceedings of the Seventh Conference on Fibrous Composites in Structural Design, Air Force Wright Aeronautical Laboratory, AFWAL-TR-85-3094, June 1985, pp. 119-130.
5. SHIVAKUMAR, K.N. and CREWS, J.H. Jr, *Bolt Clamp-Up Relaxation in a Graphite/Epoxy Laminate. Long Term Behavior of Composites ASTM STP-813*, American Society for Testing and Materials, 1983.
6. WEERTH, D.E. and ORTLOFF, C.R., *Creep Considerations in Reinforced Plastic Laminate Bolted Connections*. Proceedings of the Army Symposium on Solid Mechanics: Lightening the Force, Army Materials Technology Laboratory, MS-86-2, October 1986, pp.137-154.
7. PARA, P. *Composite Infantry Fighting Vehicle Program Structural Test Report*. Contract DAAL 04-86-C-0079, CDRL Sequence Item Number A005, FMC Corp., February 1988.

ESTIMATION OF CIFV FRICTION JOINT CONNECTOR LOADS

Roadwheel housing connector loads were calculated as a function of both static roadarm displacement and dynamic terrain conditions. A specially developed multiple connector shear/moment analysis computer program was written to obtain individual resultant connector loads. Both dynamic and maximum static connector loads were predicted using this analysis tool. Hull surface traction fatigue loading characteristics were calculated from roadwheel housing dynamic connector loads.

Friction Joint Mechanical Analysis

Friction joint resultant connector load histories were calculated from the *DADS* force/moment time histories by a shear/moment analysis of the roadwheel housing joint. The computer code *BJAN* (Bolted Joint ANalysis) was written for this purpose. In this two dimensional analysis, connector loads were calculated from in-plane moment and shear loads only. The composite material was assumed to behave in a linear elastic fashion precluding ductility and connector load redistribution within the joint. In-plane roadwheel arm shear forces (F_y and F_z) were replaced by equivalent in-plane shear forces ($F_{y\ eq}$ and $F_{z\ eq}$) and a couple (M_{eq}) acting through the bolt pattern center of gravity (CG) as seen in Figure 5. The total joint inplane moment (M_{xt}) was found by summing the roadwheel arm inplane moment (M_x) and the equivalent couple (M_{eq}). These relationships may be stated as;

$$M_{eq} = (F_{y\ eq} \bar{Z} + F_{z\ eq} \bar{Y}) \quad (1)$$

$$M_{xt} = (M_x + M_{eq}) \quad (2)$$

$$\bar{Z} = \frac{\sum_{j=1}^n z_j A_j}{\sum_{j=1}^n A_j} \quad (3)$$

$$\bar{Y} = \frac{\sum_{j=1}^n y_j A_j}{\sum_{j=1}^n A_j} \quad (4)$$

where

M_{eq} = roadwheel arm equivalent moment
 $F_{y\ eq}, F_{z\ eq}$ = roadwheel arm inplane shear forces
 M_{xt} = total joint inplane moment
 n = total number of connectors

M = roadwheel arm moment
 (\bar{Z}, \bar{Y}) = joint CG coordinates
 (y_i, z_i) = connector coordinates
 A_i = connector cross sectional area

For a given equivalent shear/moment loading, resultant connector loads (r_j) were calculated by vectorially summing reactive shear (f_j) and couple (t_j) connector forces. Joint shear loading was equally distributed to each connector of the joint while moment loading was distributed to each connector by connector forces acting about the joint's center of gravity.⁸

8. DEUTSCHMAN, A., MICHAELS, W., and WILSON, C., *Machine Design: Theory and Practice*. Macmillan Publishing Company, New York, 1975, pp.788-791.

This may be simply stated by the following relationships;

$$f_y = \frac{F_y \text{ eq}}{n} \quad (5)$$

$$f_z = \frac{F_z \text{ eq}}{n} \quad (6)$$

$$t_j = \frac{M_x \text{ eq} d_j}{\sum_{j=1}^n d_j^2} \quad (7)$$

$$\vec{r}_j = \vec{r}_y + \vec{r}_z + \vec{t}_j \quad (8)$$

where

f_y, f_z = connector shear force
 t_j = connector couple force

\vec{r}_j = resultant connector load
 d_j = perp. connector CG distance

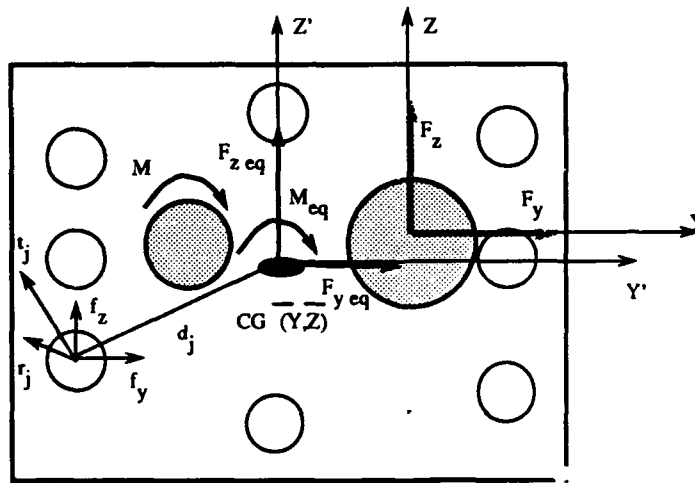


Figure 5 Shear/Moment Analysis of Roadwheel Housing Joint

Static Roadarm Displacement Conditions

Resultant connector loads were predicted as a function of roadarm displacement using the friction joint mechanical analysis of previous section. Roadarm moments from the hull cross section structural test performed by FMC were used in these calculations.

Corresponding roadwheel arm vertical shear forces were calculated from these moments and the geometrical characteristics of roadwheel arm assembly shown in Figure 6. Table 1 contains the force/moment pairs as a function of roadwheel arm displacement from these calculations as well as those used in the hull cross section structural test. These force/moment roadwheel arm displacement results were input into the **BJAN** computer code. Total resultant connector loads were calculated for both roadwheel housing configurations.

Dynamic *DADS* Suspension Conditions

The *DADS* computer code was used by FMC to model tank suspension system response and obtain estimates of CIFV roadwheel arm force/moment time histories. Requests to FMC for this information were answered with available roadwheel arm force/moment time histories for the following test conditions.⁹⁻¹⁰

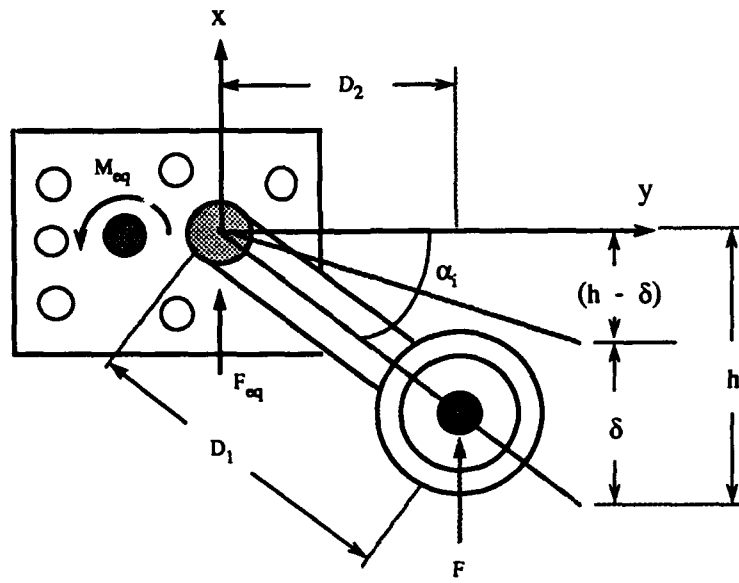
- 1) 60,000 lb (gross vehicle weight) composite hull Bradley Fighting Vehicle traversing a Perryman III cross country course at a simulated angle of 30 degrees and a speed of 4 MPH.
- 2) 43,000 lb (gross vehicle weight) aluminum hull Bradley Fighting Vehicle traversing a Perryman III cross country course at a simulated angle of 0 degrees and a speed of 20 MPH

Figures 7a through 7f and 8a through 8c illustrate the *DADS* force/moment time histories for the two test cases listed previously. The X axes of the reference coordinate frame is perpendicular to roadwheel housing while the Y axis is parallel. The Z axis is positive vertical. Each of these time histories were digitized and stored in respective computer files for creation of terrain data bases.

Resultant connector loads were calculated for each *DADS* force/moment pairs of both terrain test conditions. Both the original and modified roadwheel housing configurations were analysed. Subsequent transformation of these connector force-time histories into the frequency domain yielded CIFV hull surface traction fatigue loading spectral characteristics. These characteristics were used to determine single connector dynamic preload relaxation test conditions. The discrete fast Fourier transform subroutine (DFFT) of the International Mathematics and Statistics Library (*IMSL*) software package was used to obtain this amplitude-frequency information.

9 FATEMI, B., FMC Memo to A. Johnson (Army Materials Technology Laboratory), May 26, 1987.

10 PARA, P., FMC Memo to A. Johnson (Army Materials Technology Laboratory), February 18, 1988.



$$F = \frac{M_{FMC}}{D_2} = \frac{M_{FMC}}{[D_1^2 - (D_1 \sin \alpha_1 - \delta)^2]^{0.5}}$$

Figure 6 Geometrical Characteristics of Roadwheel Arm Assembly

Table 1 Roadwheel Arm Verticle Force/Moment Values

δ (in)	F_{FMC} (lbs)	M_{FMC} (in-lbs)	F (lbs)
2.0	3,000	97,860	6,498
4.0	3,714	121,151	7,666
6.0	4,402	143,593	8,825
8.0	5,076	165,579	10,045
10.0	5,746	187,435	11,393
12.0	6,424	209,551	12,955
14.0	7,119	232,222	14,849

$D_2 \text{ FMC} = 32.62''$
 $D_1 = 16.50''$
 $\alpha_1 = 32$

TERRAIN TEST CASE I: DADS SUSPENSION FX FORCE/TIME HISTORY
(60,000 LB COMPOSITE BFV, PERRYMAN III, 4 MPH, 30 DEGREE TRAVERSING ANGLE)

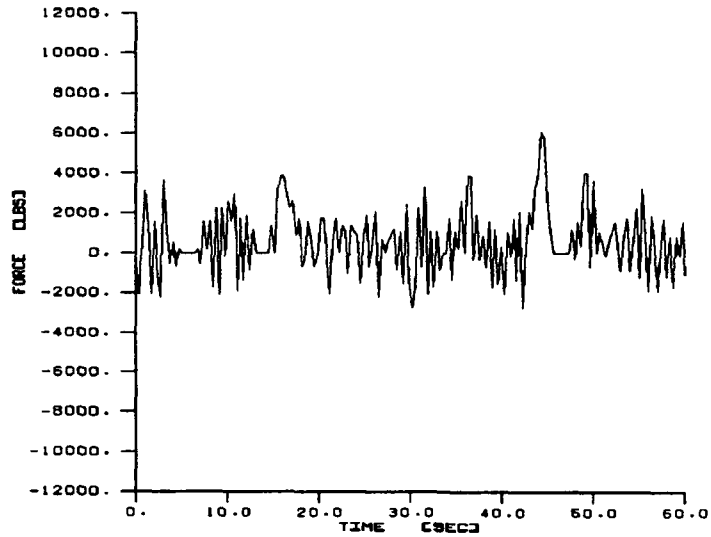


Figure 7a CIFV Roadwheel Arm F_x Time History (test case 1)

TERRAIN TEST CASE I: DADS SUSPENSION FY FORCE/TIME HISTORY
(60,000 LB COMPOSITE BFV, PERRYMAN III, 4 MPH, 30 DEGREE TRAVERSING ANGLE)

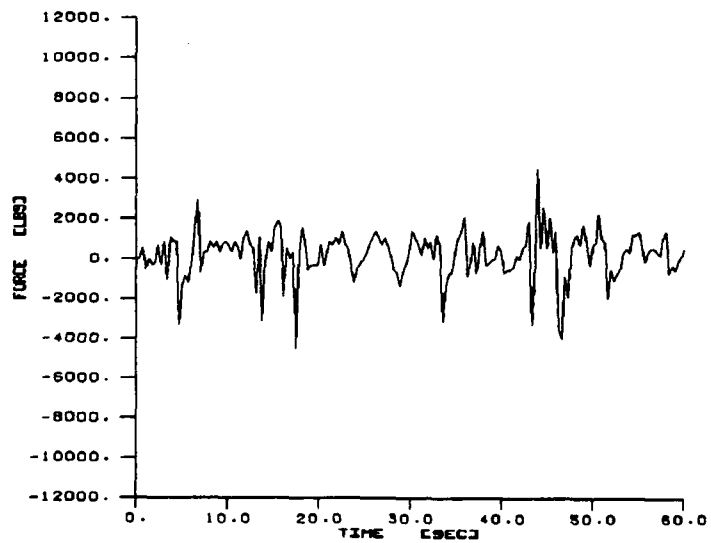


Figure 7b CIFV Roadwheel Arm F_y Time History (test case 1)

TERRAIN TEST CASE II: OADS SUSPENSION FZ FORCE/TIME HISTORY
(60,000 LB COMPOSITE BFV, PERRYMAN III, 4 MPH, 30 DEGREE TRAVERSING ANGLE)

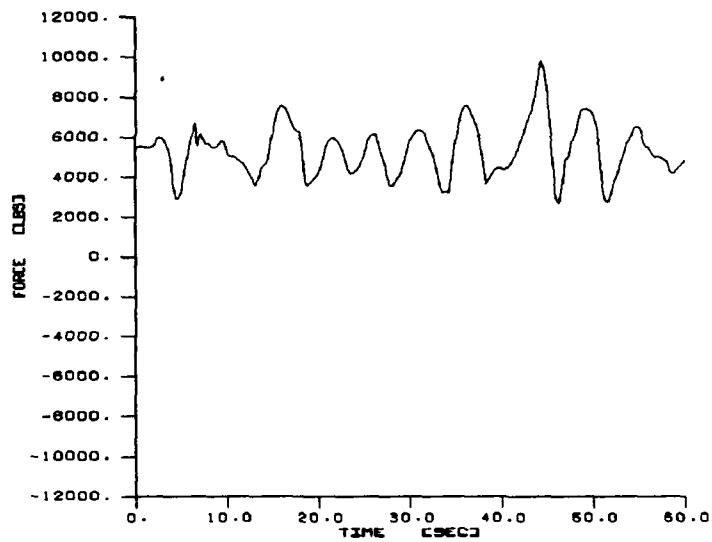


Figure 7c CIFV Roadwheel Arm F_z Time History (test case 1)

TERRAIN TEST CASE II: OADS SUSPENSION MX MOMENT/TIME HISTORY
(60,000 LB COMPOSITE BFV, PERRYMAN III, 4 MPH, 30 DEGREE TRAVERSING ANGLE)

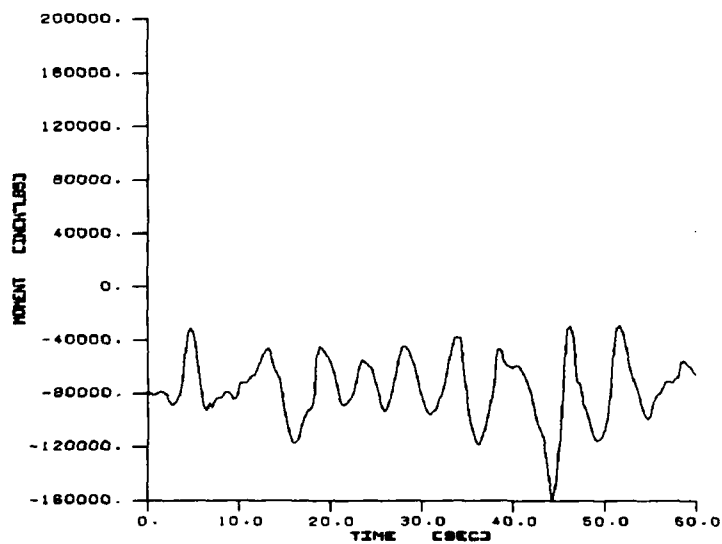


Figure 7d CIFV Roadwheel Arm M_x Time History (test case 1)

TERRAIN TEST CASE II: DADS SUSPENSION MY MOMENT/TIME HISTORY
(80,000 LB COMPOSITE BFV, PERRYMAN III, 4 MPH, 30 DEGREE TRAVERSING ANGLE)

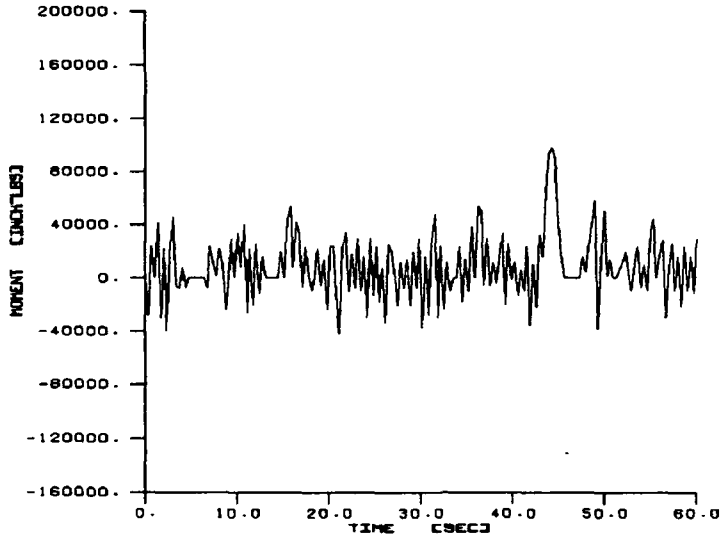


Figure 7e CIFV Roadwheel Arm M_y Time History (test case 1)

TERRAIN TEST CASE II: DADS SUSPENSION MZ MOMENT/TIME HISTORY
(80,000 LB COMPOSITE BFV, PERRYMAN III, 4 MPH, 30 DEGREE TRAVERSING ANGLE)

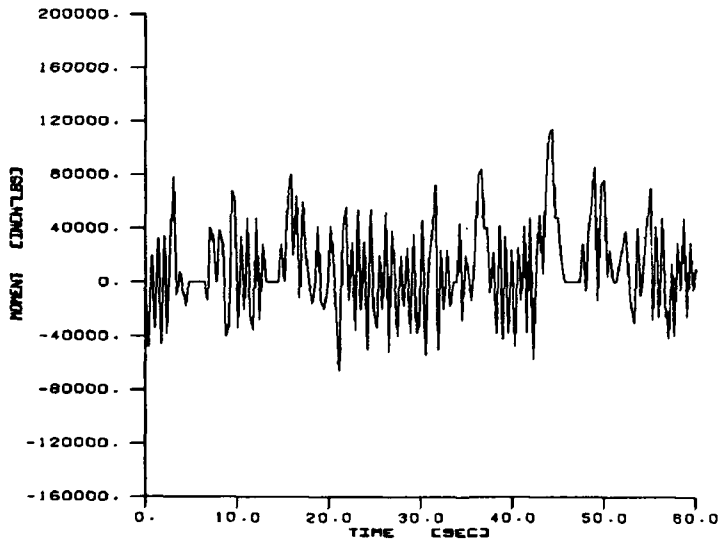


Figure 7f CIFV Roadwheel Arm M_z Time History (test case 1)

TERRAIN TEST CASE II: OADS SUSPENSION F_y FORCE/TIME HISTORY
(43,000 LB ALUMINUM SPV. PERRYMAN III. 20 MPH. 0 DEGREE TRAVERSING ANGLE)

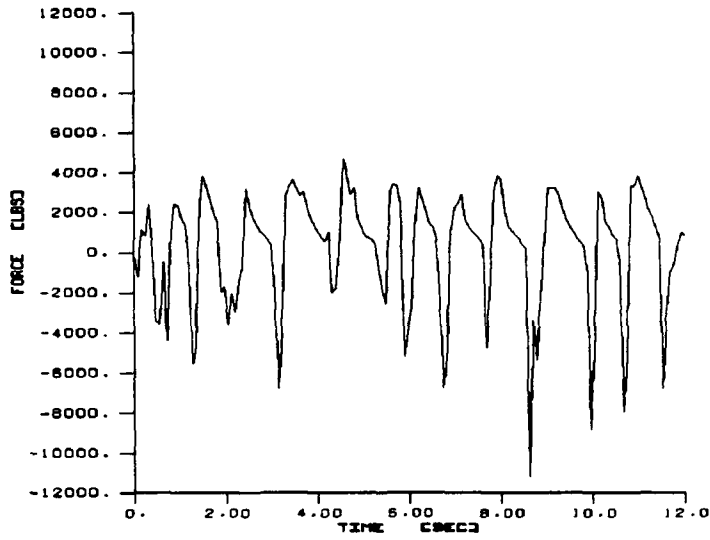


Figure 8a CIFV Roadwheel Arm F_y Time History (test case 2)

TERRAIN TEST CASE II: OADS SUSPENSION F_z FORCE/TIME HISTORY
(43,000 LB ALUMINUM SPV. PERRYMAN III. 20 MPH. 0 DEGREE TRAVERSING ANGLE)

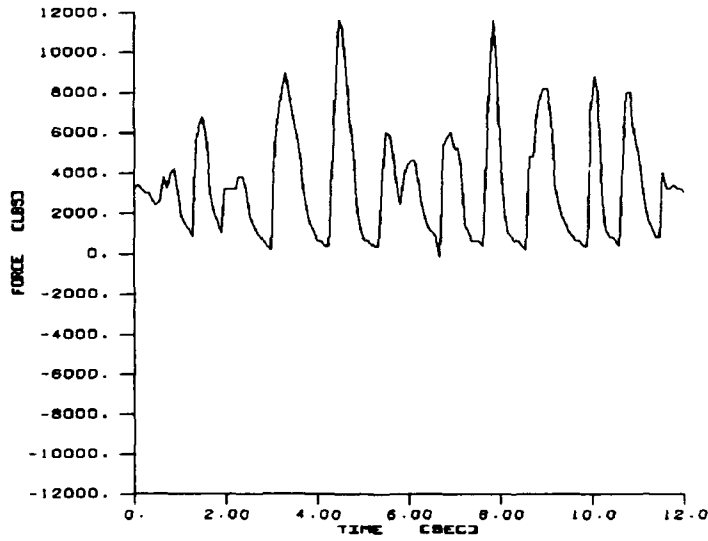


Figure 8b CIFV Roadwheel Arm F_z Time History (test case 2)

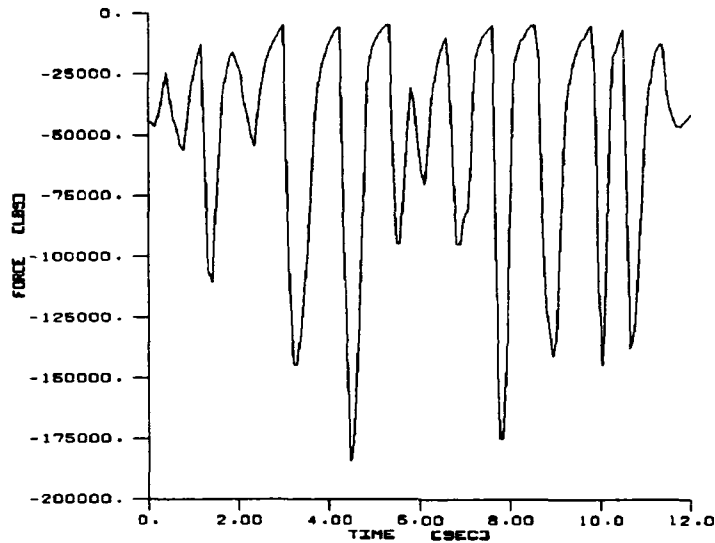


Figure 8c CIFV Roadwheel Arm M_x Time History (test case 2)

Analysis Results

Results from the friction joint mechanical analysis for the static roadwheel arm displacement and dynamic Perryman III terrain loading conditions may be seen in Figures 9 through 18. Figures 9 and 10 illustrate original and modified roadwheel housing resultant connector loads as a function of roadwheel arm displacement.

Figures 11 and 12 depict original and modified roadwheel housing design resultant connector force-time histories for terrain test case 1. Figures 13 and 14 depict similar results for terrain test case 2. Respective resultant connector amplitude-frequency content for these connector force time histories may be seen in Figures 15 through 18.

As can be seen from Figures 9 and 10, resultant connector forces increased linearly with static roadwheel arm displacement for both the original and modified roadwheel housing designs. Larger forces were generally observed for those connectors whose location maximized the magnitude of the couple force and its vector addition to the shear forces (i.e. C.G. quadrants 1 and 4). Connector forces ranged from 1,070 lbs-2,442 lbs and 2,594 lbs-5,757 lbs for respective vertical roadarm displacements of 2" and 14" for the original roadwheel housing design. Expansion of the bolt pattern in the modified roadwheel housing design reduced these ranges to 1,031 lbs-1,712 lbs and 2,164 lbs-5,205 lbs respectively.

Resultant connector forces closely profiled the F_z force and M_x moment Perryman III DADS suspension simulation results for both the original and modified roadwheel housing designs. As with the static roadarm displacement results, larger forces were generally observed for those connectors whose location maximized the magnitude of the couple force

and its vector addition to the shear forces (i.e. C.G. quadrants 1 and 4). closer to the bolt pattern center of gravity. Figures 11 through 14 indicate that terrain 1 test conditions (60,000 lb Composite BFV, Perryman III, 4 MPH, 30 degree traversing angle) were less severe than terrain 2 test conditions (43,000 lb aluminum BFV, Perryman III, 20 MPH, 0 degree traversing angle). Resultant connector forces were smaller for the modified roadwheel housing design in comparison to the original roadwheel housing design. Connector forces ranged from 300 lbs-3,936 lbs and 51 lbs-3,575 lbs for the original and modified roadwheel housing designs for terrain 1. Connector forces for terrain 2 ranged from 0 lbs-4,983 lbs and 0 lbs-4,576 lbs for the original and modified roadwheel housing designs.

Figures 15 through 18 illustrate the discrete fast fourier transform results of the resultant connector loads shown in Figures 11 through 14. As can be seen, the amplitude-frequency information generally consists of a given mean load at 0 Hz and a specific fatigue load at a higher frequency. Fatigue load frequencies were approximately 0.2 Hz for terrain 1 test conditions and 1.0 Hz for terrain 2 test conditions.

ORIGINAL ROADWHEEL HOUSING RESULTANT CONNECTOR LOADS VS ROADWHEEL ARM DISP
(INFINITE FRICTION COEFFICIENT)

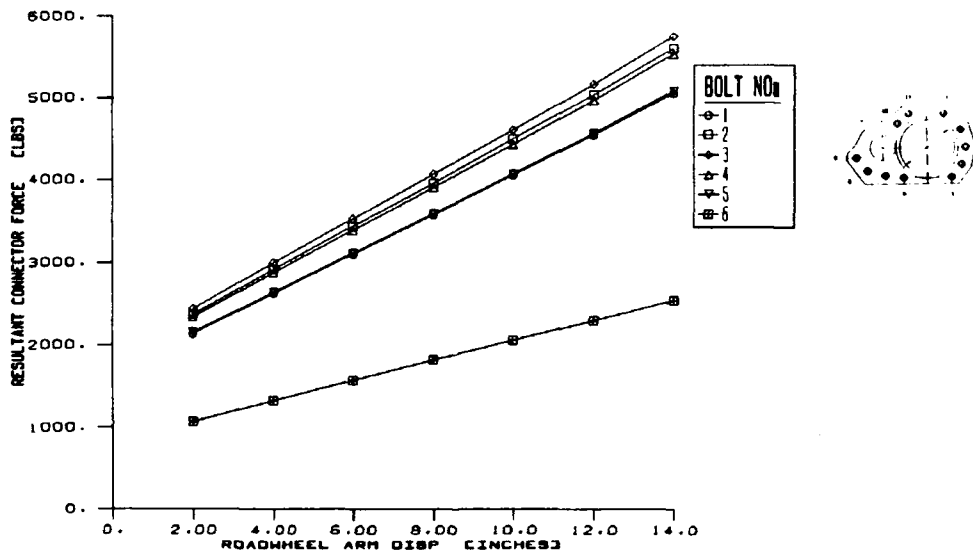


Figure 9a Original Roadwheel Housing Resultant Connector Loads as a Function of Roadwheel Arm Displacement

ORIGINAL ROADWHEEL HOUSING RESULTANT CONNECTOR LOADS VS ROADWHEEL ARM DISP.
(INFINITE FRICTION COEFFICIENT)

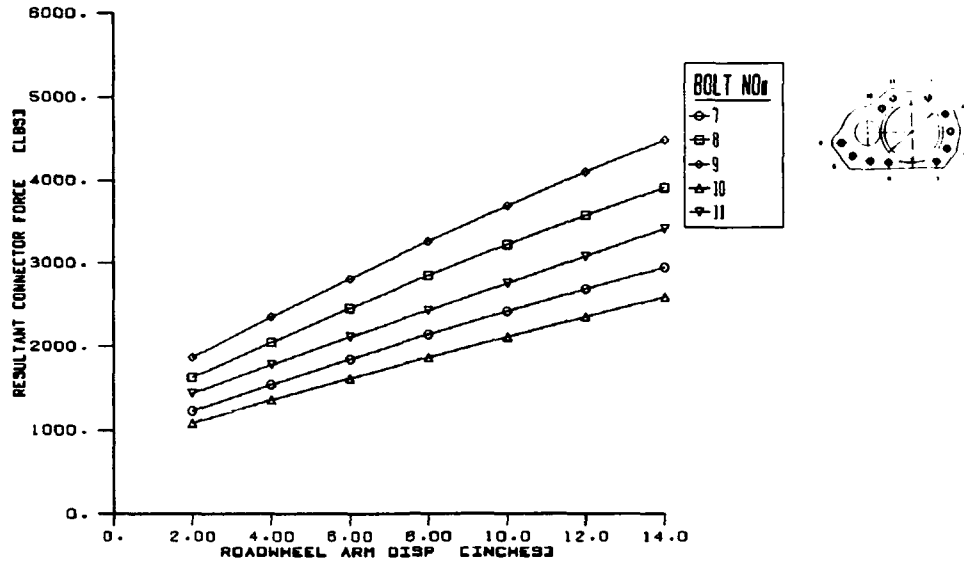


Figure 9b Original Roadwheel Housing Resultant Connector Loads as a Function of Roadwheel Arm Displacement

MODIFIED ROADWHEEL HOUSING RESULTANT CONNECTOR LOADS VS ROADWHEEL ARM DISP.
(INFINITE FRICTION COEFFICIENT)

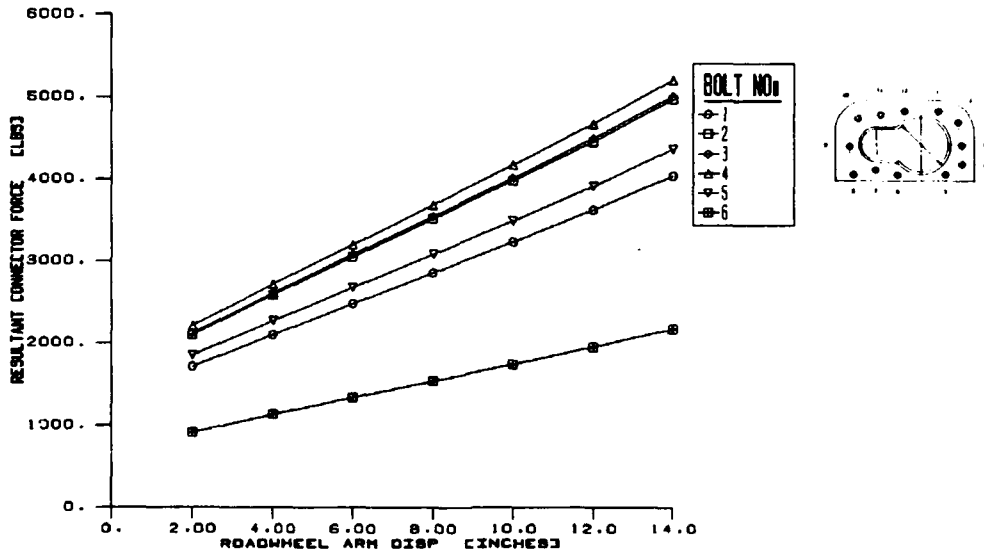


Figure 10a Modified Roadwheel Housing Resultant Connector Loads as a Function of Roadwheel Arm Displacement

MODIFIED ROADWHEEL HOUSING RESULTANT CONNECTOR LOADS VS ROADWHEEL ARM DISP
 (INFINITE FRICTION COEFFICIENT)

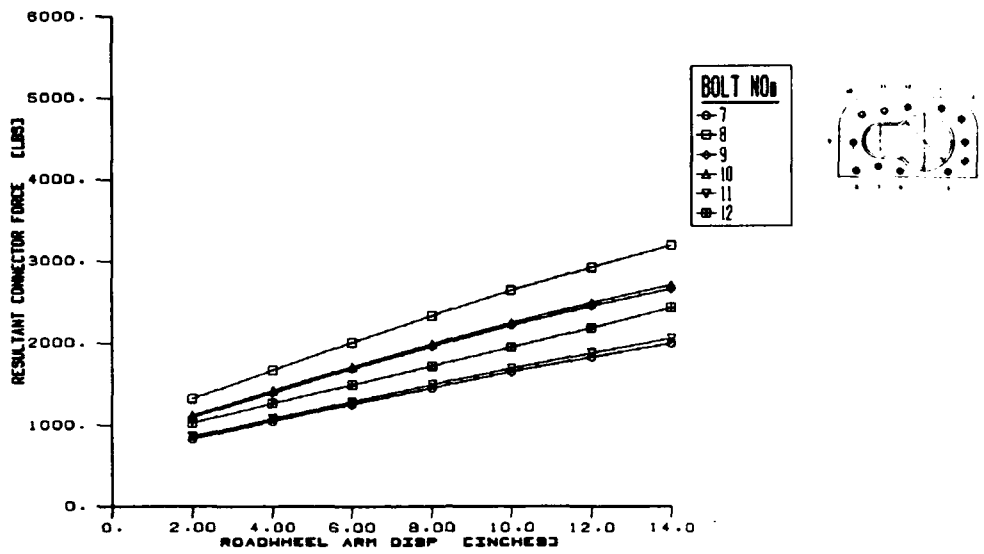


Figure 10b Modified Roadwheel Housing Resultant Connector Loads as a Function of Roadwheel Arm Displacement

ORIGINAL ROADWHEEL HOUSING RESULTANT CONNECTOR FORCE/TIME HISTORIES
 (80,000 LB COMPOSITE BPV, PERRYMAN 11), 4 MPH, 30 DEGREE TRAVERSING ANGLE
 (INFINITE SLIP LOAD)

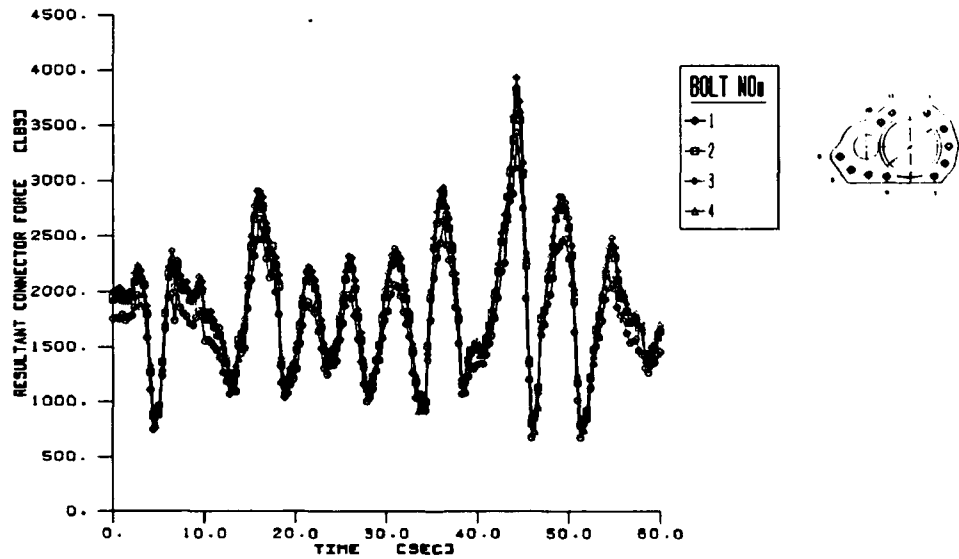


Figure 11a Original Roadwheel Housing Resultant Connector Force-Time Histories [terrain 1] [bolts 1-4]

ORIGINAL ROADWHEEL HOUSING RESULTANT CONNECTOR FORCE/TIME HISTORIES
 (80,000 LB COMPOSITE SFV. PERRYMAN III, 4 MPH, 30 DEGREE TRAVERSING ANGLE)
 (INFINITE SLIP LOAD)

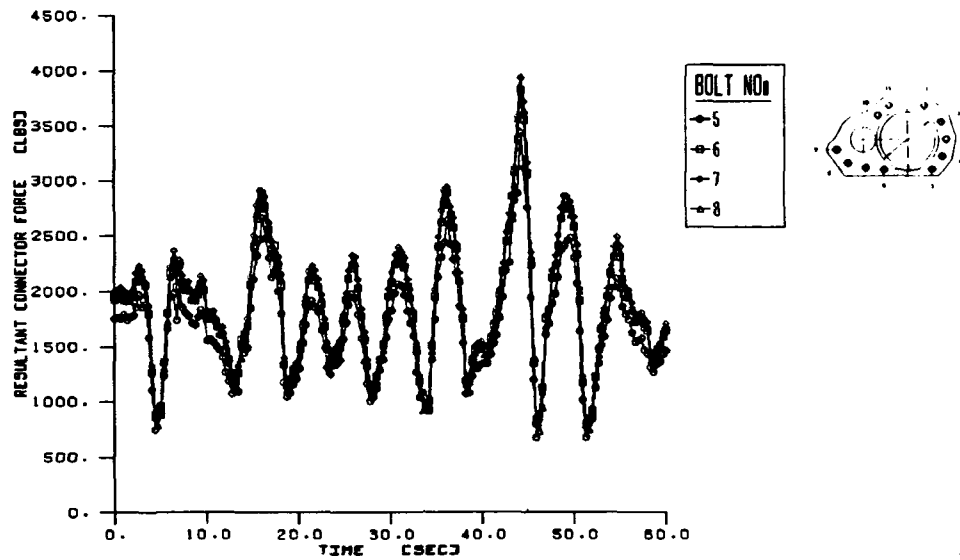


Figure 11b Original Roadwheel Housing Resultant Connector Force-Time Histories [terrain 1] [bolts 5-8]

ORIGINAL ROADWHEEL HOUSING RESULTANT CONNECTOR FORCE/TIME HISTORIES
 (80,000 LB COMPOSITE SFV. PERRYMAN III, 4 MPH, 30 DEGREE TRAVERSING ANGLE)
 (INFINITE SLIP LOAD)

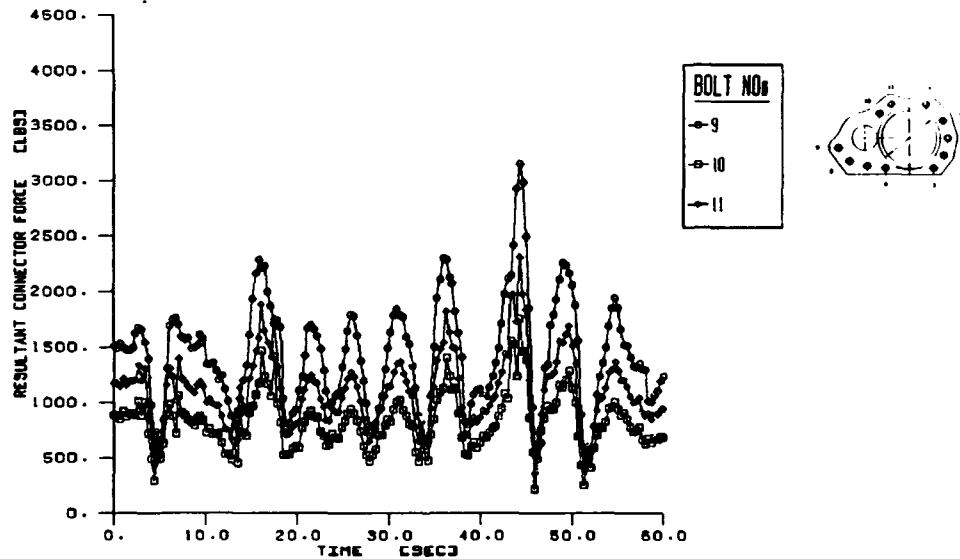


Figure 11c Original Roadwheel Housing Resultant Connector Force-Time Histories [terrain 1] [bolts 9-11]

MODIFIED ROADWHEEL HOUSING RESULTANT CONNECTOR FORCE/TIME HISTORIES
 (60,000 LB COMPOSITE SPV, PERRYMAN III), 4 MPH, 30 DEGREE TRAVERSING ANGLE)
 (INFINITE SLIP LOAD)

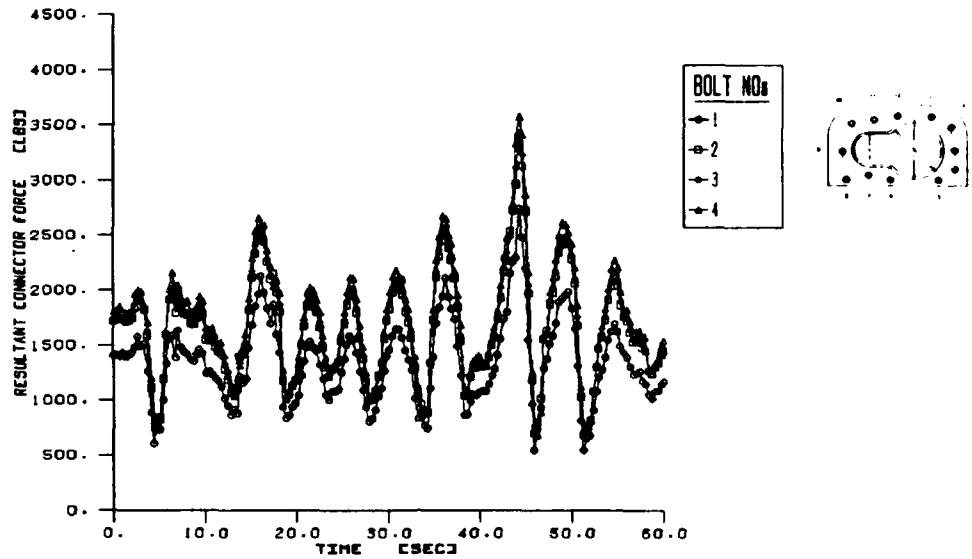


Figure 12a Modified Roadwheel Housing Resultant Connector Force-Time Histories [terrain 1] [bolts 1-4]

MODIFIED ROADWHEEL HOUSING RESULTANT CONNECTOR FORCE/TIME HISTORIES
 (60,000 LB COMPOSITE SPV, PERRYMAN III), 4 MPH, 30 DEGREE TRAVERSING ANGLE)
 (INFINITE SLIP LOAD)

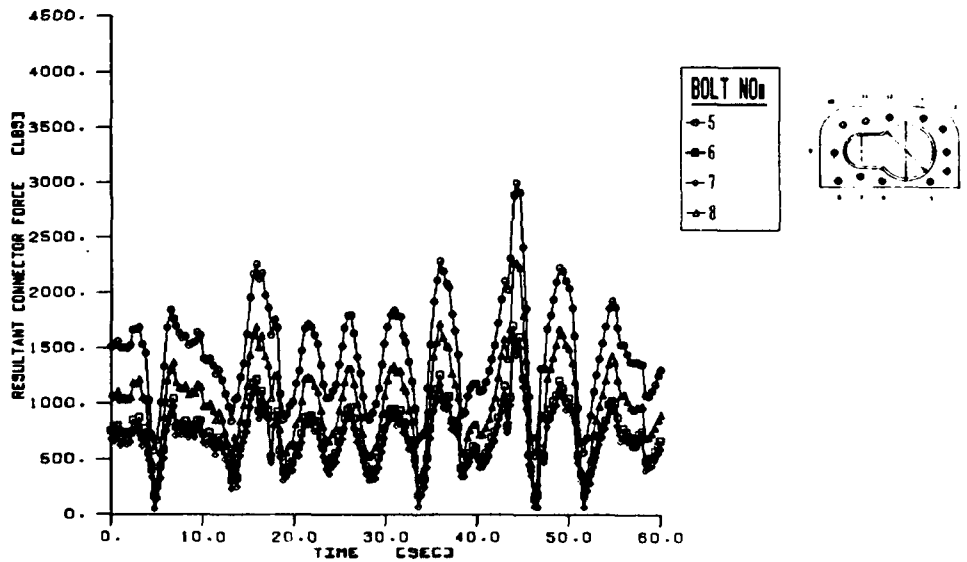


Figure 12b Modified Roadwheel Housing Resultant Connector Force-Time Histories [terrain 1] [bolts 5-9]

MODIFIED ROADWHEEL HOUSING RESULTANT CONNECTOR FORCE/TIME HISTORIES
 (80,000 LB COMPOSITE SPV. PERRYMAN III, 4 MPH, 30 DEGREE TRAVERSING ANGLE)
 (INFINITE SLIP LOAD)

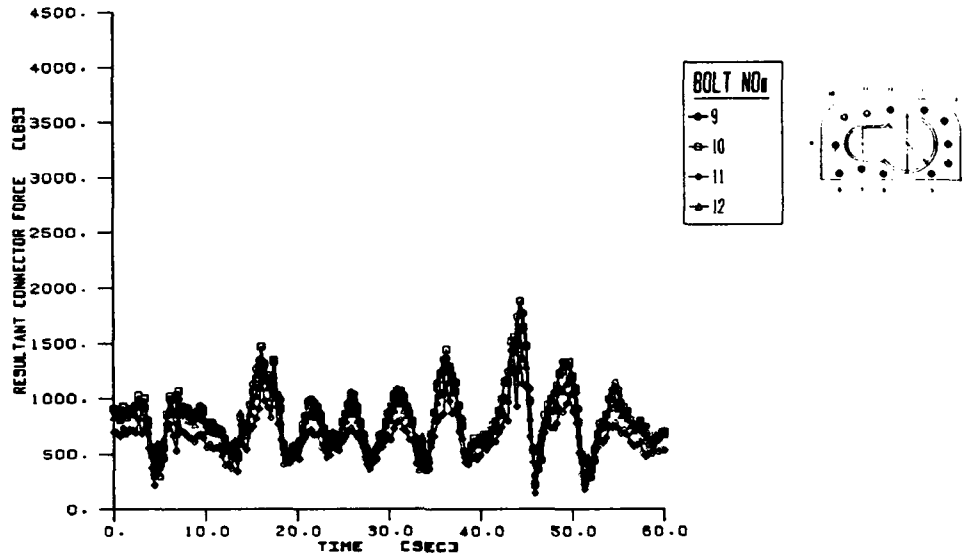


Figure 12c Modified Roadwheel Housing Resultant Connector Force-Time Histories [terrain 1] [bolts 9-12]

ORIGINAL ROADWHEEL HOUSING RESULTANT CONNECTOR FORCE/TIME HISTORIES
 (48,000 LB ALUMINUM SPV. PERRYMAN III, 20 MPH, 0 DEGREE TRAVERSING ANGLE)
 (INFINITE SLIP LOAD)

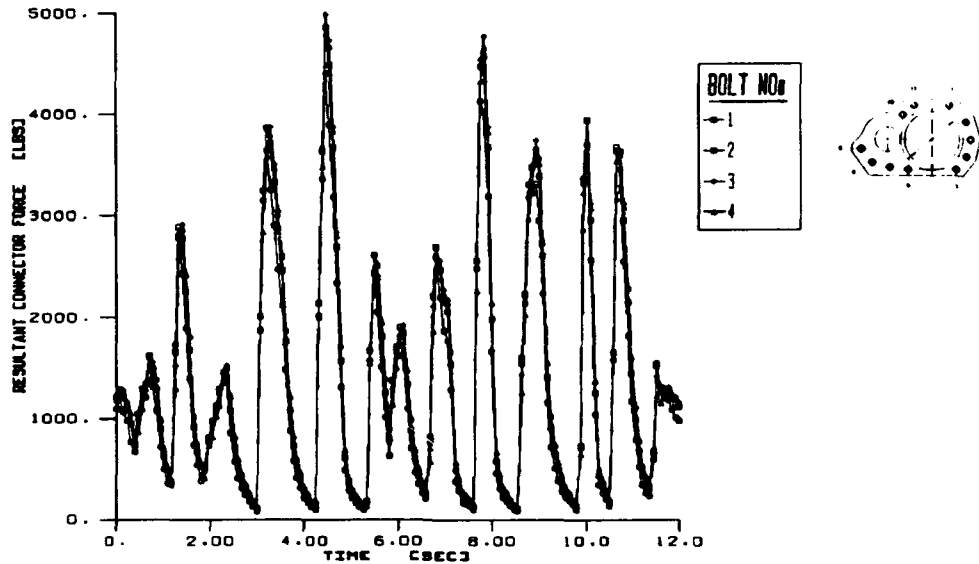


Figure 13a Original Roadwheel Housing Resultant Connector Force-Time Histories [terrain 2] [bolts 1-4]

ORIGINAL ROADWHEEL HOUSING RESULTANT CONNECTOR FORCE/TIME HISTORIES
 (49,000 LB ALUMINUM BAY, PERRYMAN III, 20 MPH, 0 DEGREE TRAVERSING ANGLE)
 (INFINITE SLIP LOAD)

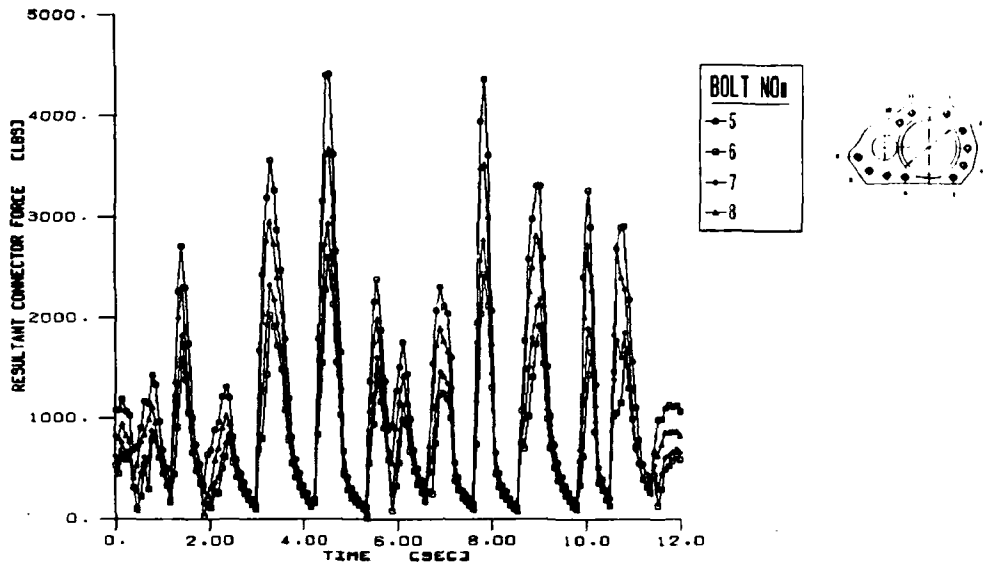


Figure 13b Original Roadwheel Housing Resultant Connector Force-Time Histories [terrain 2] [bolts 5-8]

ORIGINAL ROADWHEEL HOUSING RESULTANT CONNECTOR FORCE/TIME HISTORIES
 (49,000 LB ALUMINUM BAY, PERRYMAN III, 20 MPH, 0 DEGREE TRAVERSING ANGLE)
 (INFINITE SLIP LOAD)

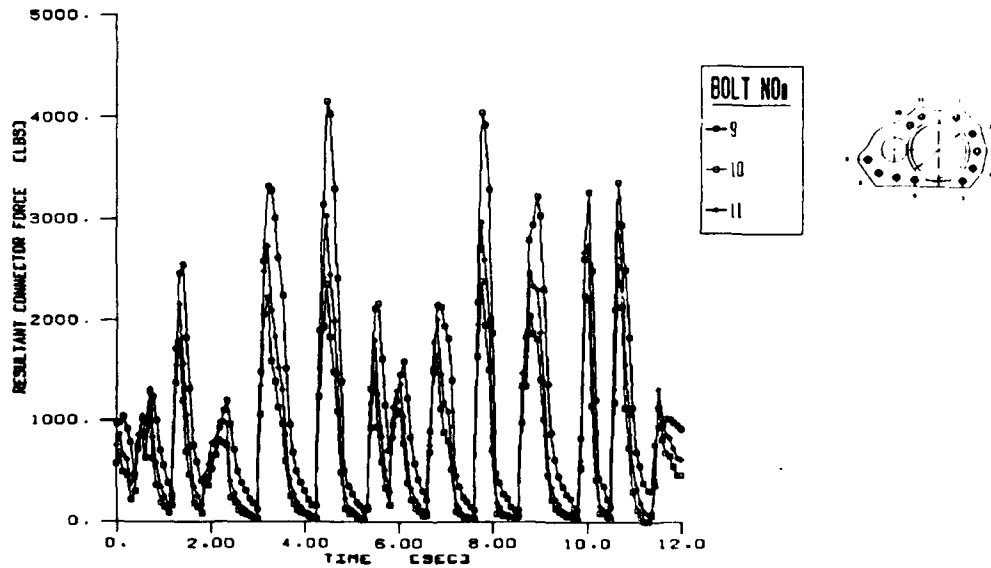


Figure 13c Original Roadwheel Housing Resultant Connector Force-Time Histories [terrain 2] [bolts 9-11]

MODIFIED ROADWHEEL HOUSING RESULTANT CONNECTOR FORCE/TIME HISTORIES
 (49,000 LB ALUMINUM SPV, PERRYMAN III, 20 MPH, 0 DEGREE TRAVERSING ANGLE)
 (INFINITE SLIP LOAD)

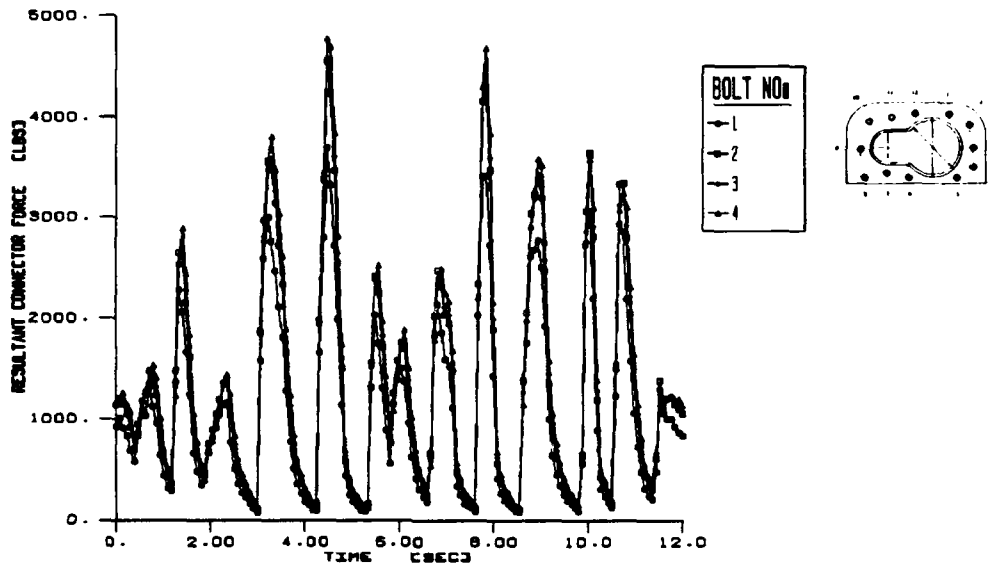


Figure 14a Modified Roadwheel Housing Resultant Connector Force-Time Histories [terrain 2] [bolts 1-4]

MODIFIED ROADWHEEL HOUSING RESULTANT CONNECTOR FORCE/TIME HISTORIES
 (49,000 LB ALUMINUM SPV, PERRYMAN III, 20 MPH, 0 DEGREE TRAVERSING ANGLE)
 (INFINITE SLIP LOAD)

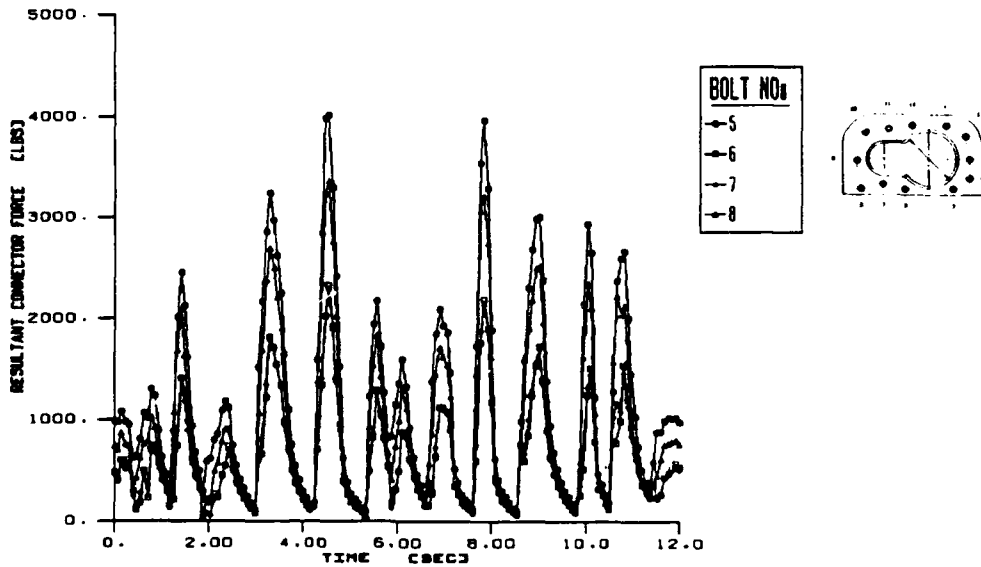


Figure 14b Modified Roadwheel Housing Resultant Connector Force-Time Histories [terrain 2] [bolts 5-8]

MODIFIED ROADWHEEL HOUSING RESULTANT CONNECTOR FORCE/TIME HISTORIES
 (43,000 LB ALUMINUM BPV, PERRYMAN III, 20 MPH, 0 DEGREE TRAVERSING ANGLE)
 (INFINITE SLIP LOAD)

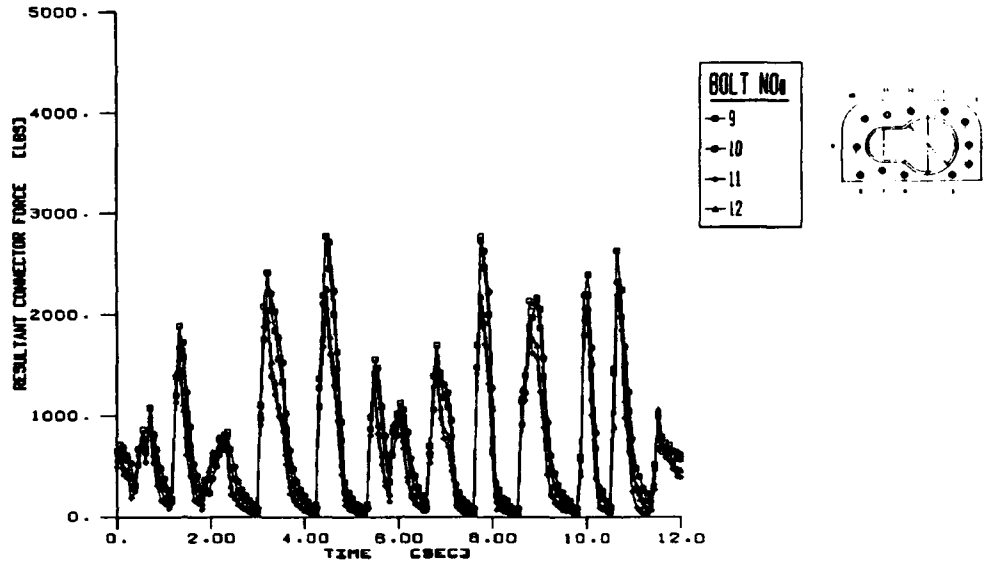


Figure 14c Modified Roadwheel Housing Resultant Connector Force-Time Histories [terrain 2] [bolts 9-12]

ORIGINAL ROADWHEEL HOUSING AMPLITUDE/FREQUENCY CONTENT
 (80,000 LB COMPOSITE BPV, PERRYMAN III, 4 MPH, 30 DEGREE TRAVERSING ANGLE)
 (INFINITE SLIP LOAD) (CONSTANT BOLT PRELOAD)

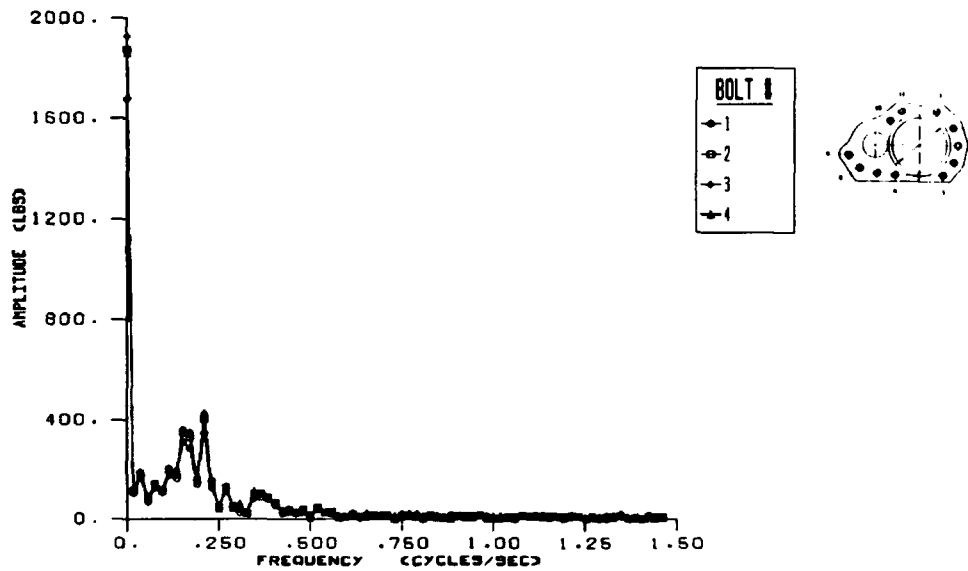


Figure 15a Original Roadwheel Housing Resultant Connector Amplitude-Frequency Content [terrain 1] [bolts 1-4]

ORIGINAL ROADWHEEL HOUSING AMPLITUDE/FREQUENCY CONTENT
 (80,000 LB COMPOSITE SPV, PERRYMAN III, 4 MPH, 30 DEGREE TRAVERSING ANGLE)
 (INFINITE SLIP LOAD) (CONSTANT BOLT PRELOAD)

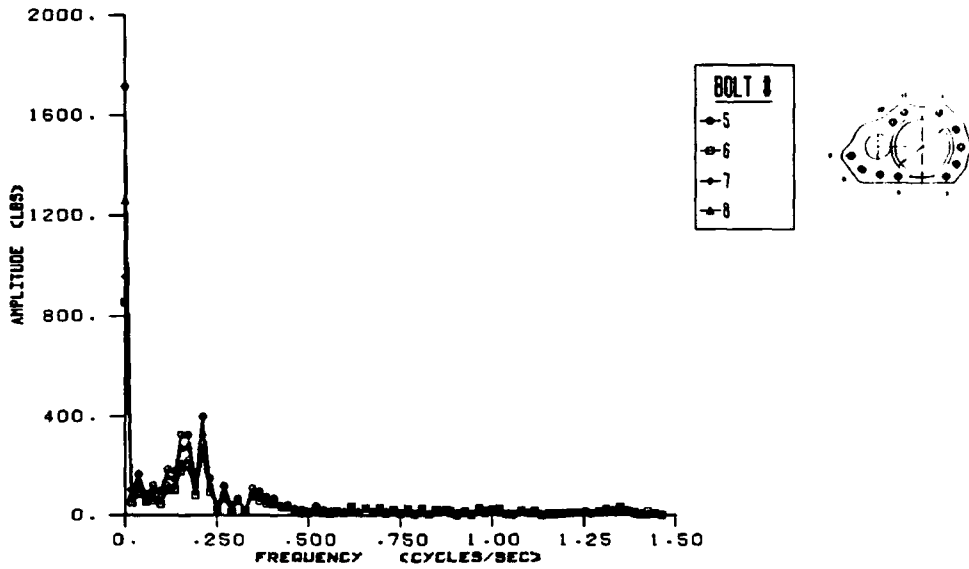


Figure 15b Original Roadwheel Housing Resultant Connector Amplitude-Frequency Content [terrain 1] [bolts 5-8]

ORIGINAL ROADWHEEL HOUSING AMPLITUDE/FREQUENCY CONTENT
 (80,000 LB COMPOSITE SPV, PERRYMAN III, 4 MPH, 30 DEGREE TRAVERSING ANGLE)
 (INFINITE SLIP LOAD) (CONSTANT BOLT PRELOAD)

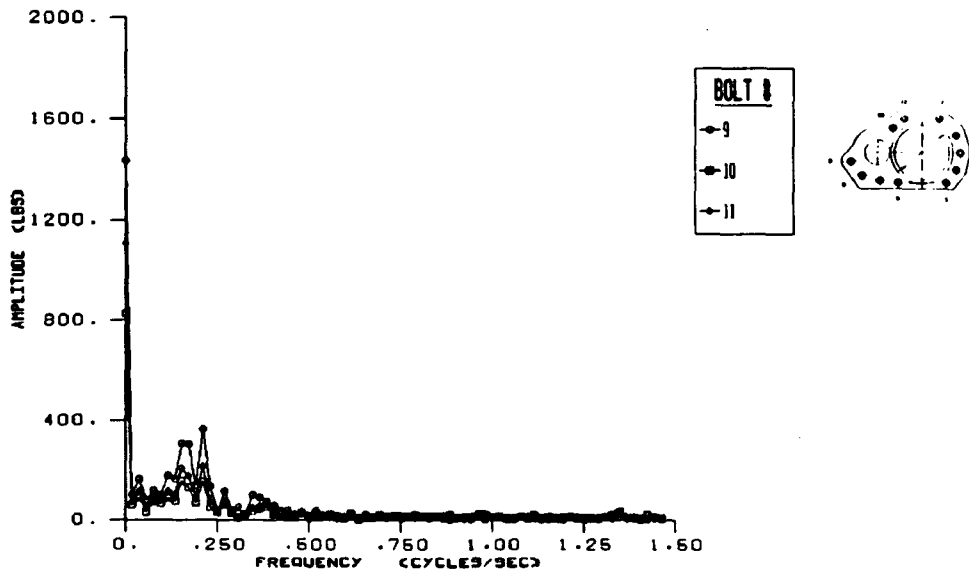


Figure 15c Original Roadwheel Housing Resultant Connector Amplitude-Frequency Content [terrain 1] [bolts 9-11]

MODIFIED ROADWHEEL HOUSING AMPLITUDE/FREQUENCY CONTENT
 (80,000 LB COMPOSITE SFV, PERRYMAN III, 4 MPH, 30 DEGREE TRAVERSING ANGLE)
 (INFINITE SLIP LOAD) (CONSTANT BOLT PRELOAD)

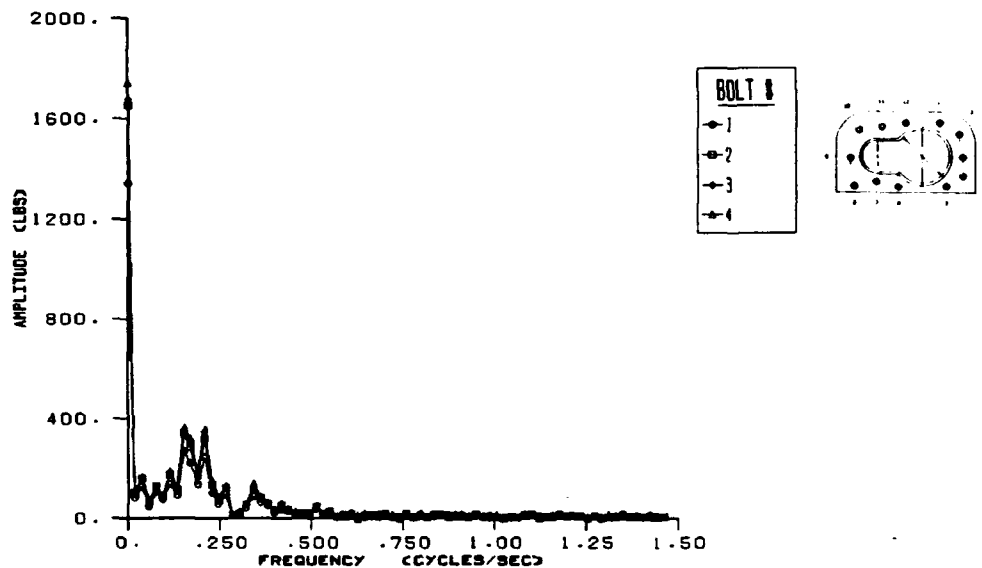


Figure 16a Modified Roadwheel Housing Resultant Connector Amplitude-Frequency Content [terrain 1] [bolts 1-4]

MODIFIED ROADWHEEL HOUSING AMPLITUDE/FREQUENCY CONTENT
 (80,000 LB COMPOSITE SFV, PERRYMAN III, 4 MPH, 30 DEGREE TRAVERSING ANGLE)
 (INFINITE SLIP LOAD) (CONSTANT BOLT PRELOAD)

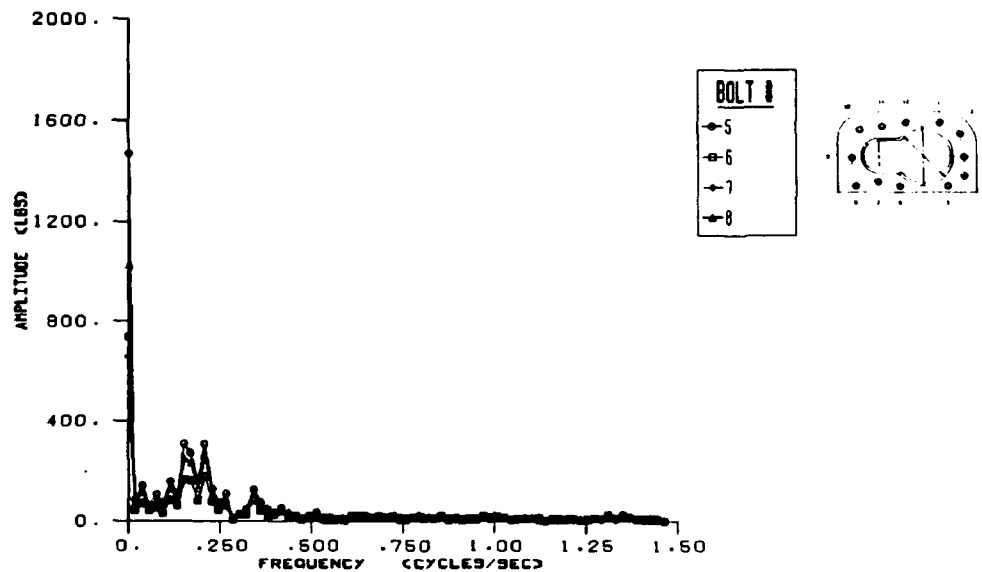


Figure 16b Modified Roadwheel Housing Resultant Connector Amplitude-Frequency Content [terrain 1] [bolts 5-8]

MODIFIED ROADWHEEL HOUSING AMPLITUDE/FREQUENCY CONTENT
 (80,000 LB COMPOSITE SPV. PERRYMAN III, 4 MPH, 30 DEGREE TRAVERSING ANGLE)
 (INFINITE SLIP LOAD) (CONSTANT BOLT PRELOAD)

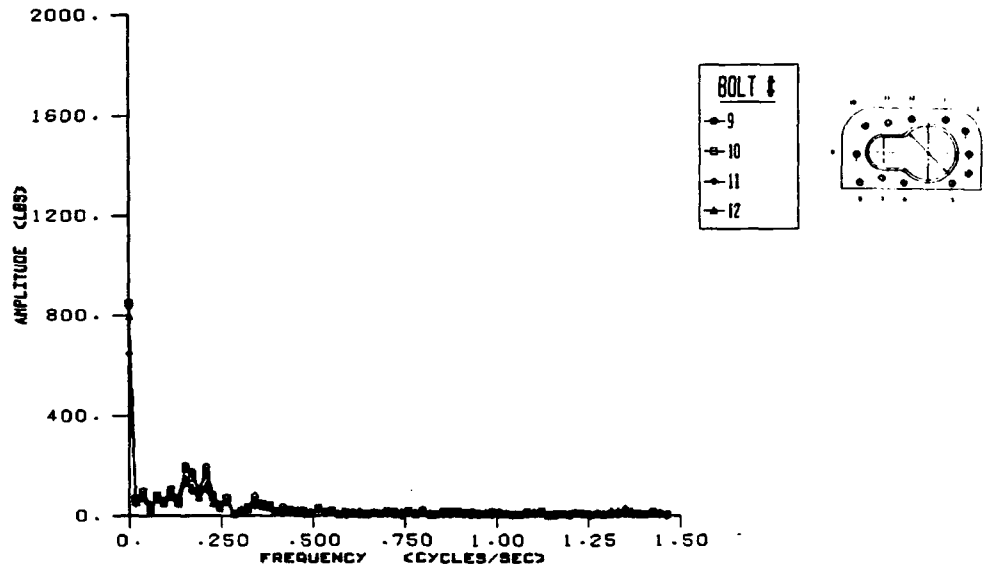


Figure 16c Modified Roadwheel Housing Resultant Connector Amplitude-Frequency Content [terrain 1] [bolts 9-12]

ORIGINAL ROADWHEEL HOUSING AMPLITUDE/FREQUENCY CONTENT
 (49,000 LB ALUMINUM SPV. PERRYMAN III, 20 MPH, 0 DEGREE TRAVERSING ANGLE)
 (INFINITE SLIP LOAD) (CONSTANT BOLT PRELOAD)

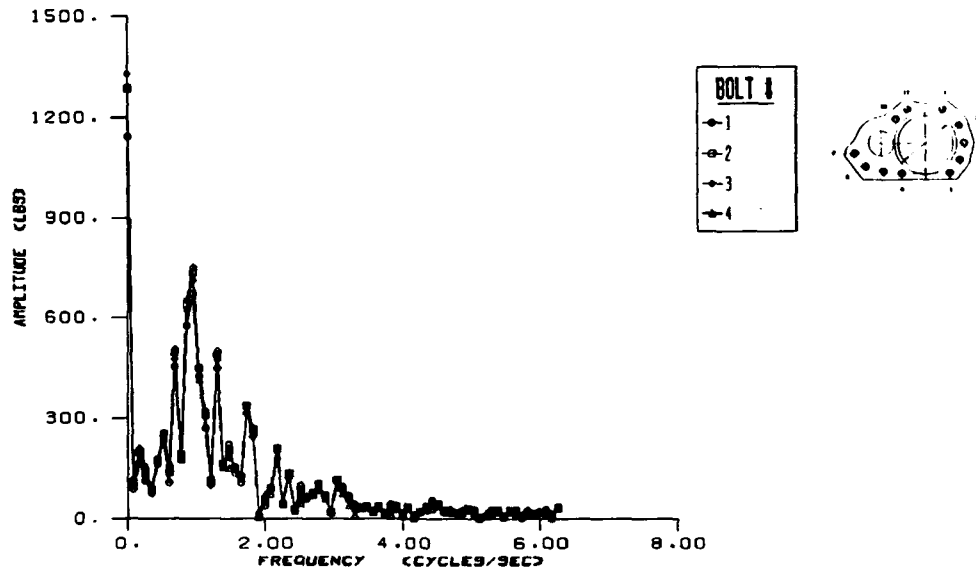


Figure 17a Original Roadwheel Housing Resultant Connector Amplitude-Frequency Content [terrain 2] [bolts 1-4]

ORIGINAL ROADWHEEL HOUSING AMPLITUDE/FREQUENCY CONTENT
 (49,000 LB ALUMINUM BFV, PERRYMAN III, 20 MPH, 0 DEGREE TRAVERSING ANGLE)
 (INFINITE SLIP LOAD) (CONSTANT BOLT PRELOAD)

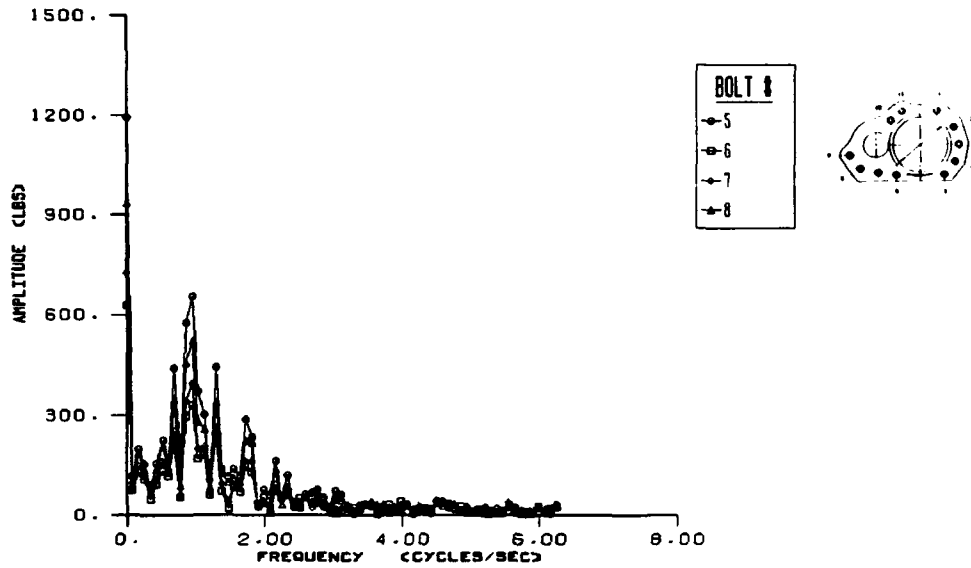


Figure 17b Original Roadwheel Housing Resultant Connector Amplitude-Frequency Content [terrain 2] [bolts 5-8]

ORIGINAL ROADWHEEL HOUSING AMPLITUDE/FREQUENCY CONTENT
 (49,000 LB ALUMINUM BFV, PERRYMAN III, 20 MPH, 0 DEGREE TRAVERSING ANGLE)
 (INFINITE SLIP LOAD) (CONSTANT BOLT PRELOAD)

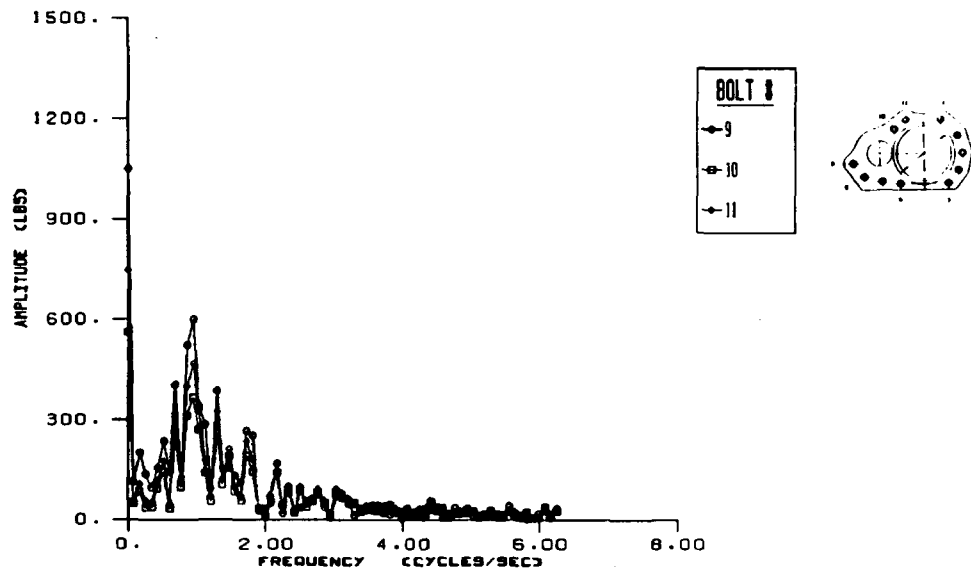


Figure 17c Original Roadwheel Housing Resultant Connector Amplitude-Frequency Content [terrain 2] [bolts 9-11]

MODIFIED ROADWHEEL HOUSING AMPLITUDE/FREQUENCY CONTENT
 (49,000 LB ALUMINUM SPV. PERRYMAN III. 20 MPH. 0 DEGREE TRAVERSING ANGLE)
 (INFINITE SLIP LOAD) (CONSTANT BOLT PRELOAD)

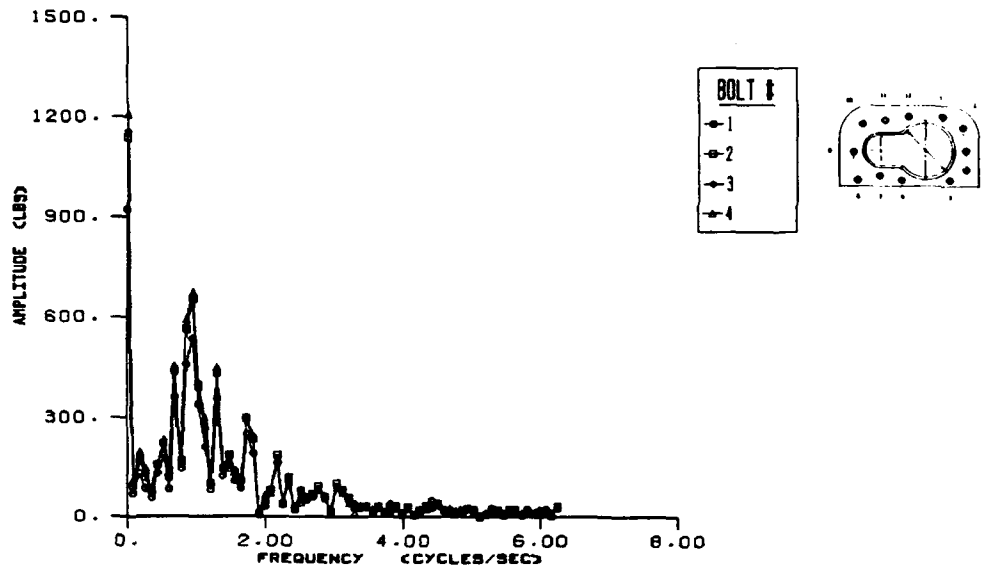


Figure 18a Modified Roadwheel Housing Resultant Connector Amplitude-Frequency Content [terrain 2] [bolts 1-4]

MODIFIED ROADWHEEL HOUSING AMPLITUDE/FREQUENCY CONTENT
 (49,000 LB ALUMINUM SPV. PERRYMAN III. 20 MPH. 0 DEGREE TRAVERSING ANGLE)
 (INFINITE SLIP LOAD) (CONSTANT BOLT PRELOAD)

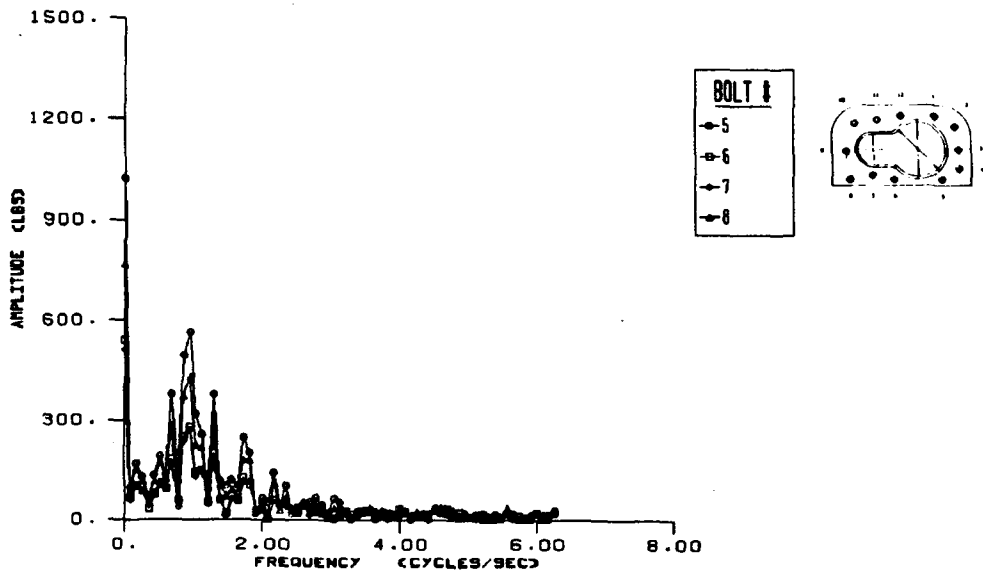


Figure 18b Modified Roadwheel Housing Resultant Connector Amplitude-Frequency Content [terrain 2] [bolts 5-8]

MODIFIED ROADWHEEL HOUSING AMPLITUDE/FREQUENCY CONTENT
 (43,000 LB ALUMINUM SPV, PERRYMAN III, 20 MPH, 0 DEGREE TRAVERSING ANGLE)
 (INFINITE SLIP LOAD) (CONSTANT BOLT PRELOAD)

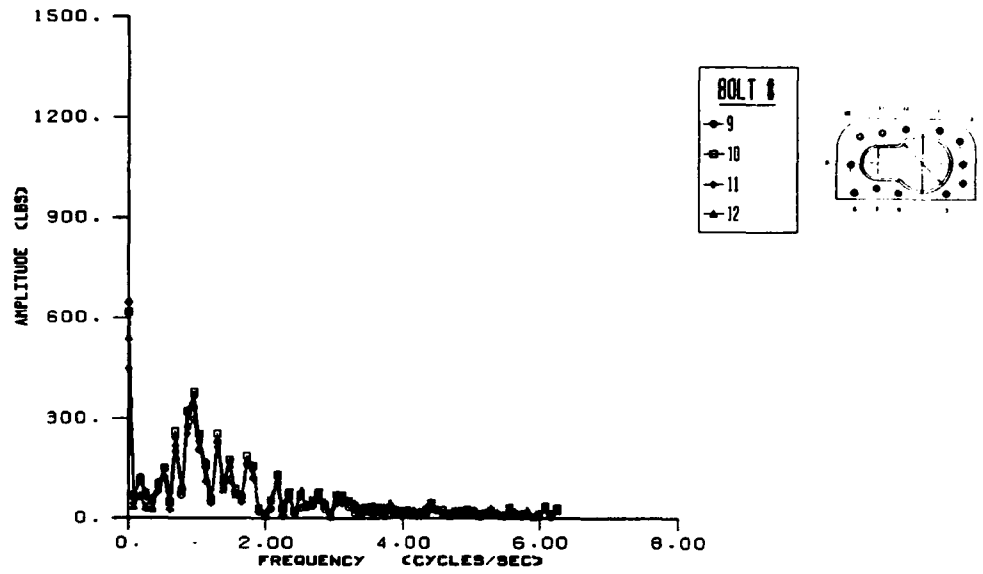


Figure 18c Modified Roadwheel Housing Resultant Connector Amplitude-Frequency Content [terrain 2] [bolts 9-12]

EXPERIMENTAL CHARACTERIZATION OF CIFV FRICTION JOINT PERFORMANCE

Experimental characterization of the CIFV friction joint performance was done on a single connector level. Single connector load carrying capability as a function of bolt preload and through thickness viscoelastic material relaxation was experimentally determined. These relationships were used with a modified version of the BJAN computer code to predict CIFV friction joint integrity for both Perryman III terrain test conditions for which DADS suspension data was available.

Single Connector Load Carrying Capability

A double lap shear specimen configuration was used to determine single connector load carrying capability. As seen in Figure 19, the thick S2 glass woven roving material was bolted between two 0.75" thick steel plates with a grade 9 bolt. This resulted in a 4" x 4" shear area. The diameter of the holes in the composite plate were oversized by 0.125" to allow for slippage between themselves and the metal plates. A bolt force sensor manufactured from a 0.225" thick x 1.105" outer diameter x 1.00" long steel cylinder was used to monitor axial bolt preload. Sensor instrumentation consisted of four BLH SR-4 type FAE-25-35 S13 E strain gages in a four arm Wheatstone bridge configuration. Prior calibration of these sensors was undertaken to insure both linearity and repeatability.

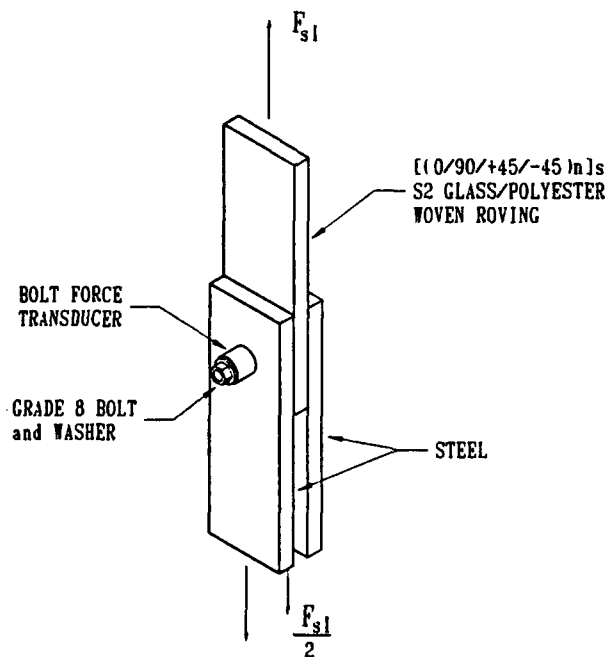


Figure 19 Single Connector Static Slip Test Specimen Configuration

The lap shear specimen was placed in an *Instron* mechanical testing machine and loaded in tension at a 0.02 inches/minute rate. A strip chart recording of load versus

crosshead displacement was recorded for various bolt preload values. As seen in Figure 20, typical strip chart readings appeared to show a peak slip load $F_{sl p}$ that initiated slip followed by a lower average slip load $F_{sl av}$ that maintained a sliding slip within the joint. Continual loading after this point was avoided since it resulted in a bolt bearing condition which increased joint tensile loads (F_b) and damaged the composite plate.

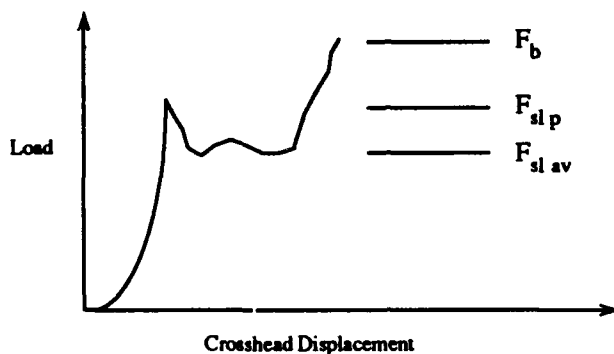


Figure 20 Typical Single Connector Static Slip Test Strip Chart Recording

Both peak and average slip loads were determined for increasing bolt preload values using two separate composite plate specimens. As shown by the least squares curve fit in Figure 21, a linear relationship existed between peak slip load and bolt preload. The linearization coefficient ($C = 0.270$) may be thought of as an effective friction joint coefficient of friction (μ_{eff}).

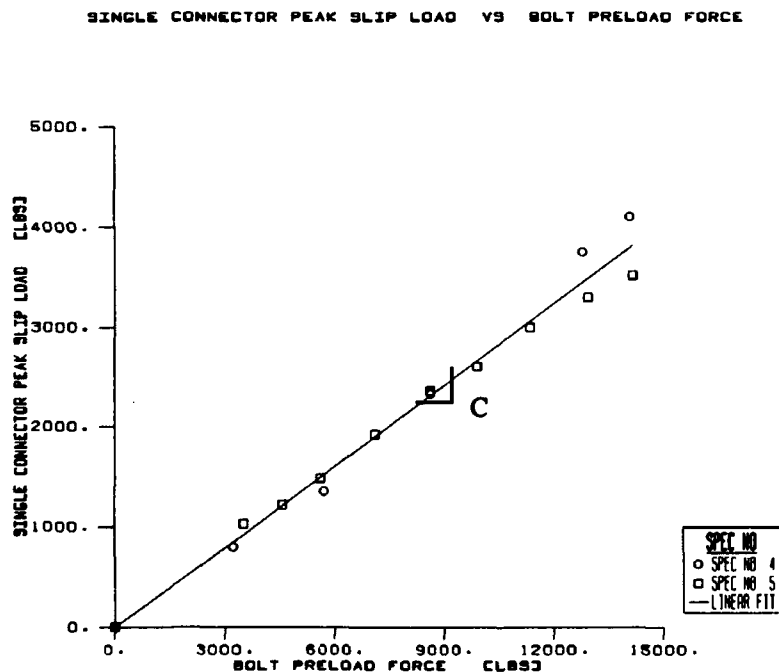


Figure 21 Single Connector Peak Slip Load Versus Bolt Preload Force

Variations in peak and average slip loads were found to be less than 3 % of peak slip loads. Repeatability of test results and effects of specimen loading rate were also investigated with multiple test runs of the 13,000 lb bolt preload case. A standard deviation of 3.68 % was observed in five separate test runs indicating extremely good repeatability. Variation of loading rates from 0.02-5.00 inches/minute yielded a peak load standard deviation of only 4.11 % thus indicating minimal loading rate effects.

Effects of Through Thickness Viscoelastic Material Relaxation

The effects of through thickness viscoelastic material relaxation on bolt preload was experimentally determined for the thick S2 glass/polyester woven roving material.¹¹ Both static and dynamic loading conditions were investigated with a single connector specimen configuration.

Static Loading Conditions

Static relaxation specimens, shown in Figure 22, were used along with bolt force sensors to monitor bolt preload relaxation at room temperature. The thick S2-glass/polyester woven roving material was sandwiched between 4" x 4" steel and aluminum plates and through bolted using a 0.625" diameter grade 9 bolt which was torqued to 158 ft-lbs. Standard size grade 9 washers were placed on either side of the bolt force sensor. Output voltage from the bolt force sensor Wheatstone bridge was recorded at 10 minute intervals by a *Megadac* data acquisition system for a 42-day test duration. A total of three static relaxation specimens were tested simultaneously. A power failure during the first 48 hours of testing required a repeat of this test. Two test specimens and a 21-day test duration was used for this second test.

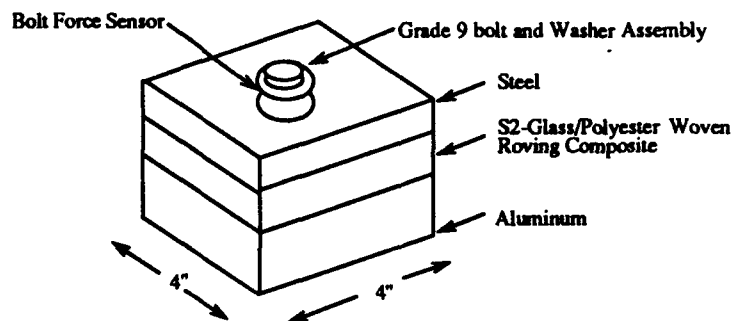


Figure 22 Static Bolt Force Preload Relaxation Specimen

Dynamic Surface Traction Fatigue Loading Conditions

A dynamic relaxation test specimen was used to determine the effects of roadwheel housing surface traction fatigue on through thickness viscoelastic relaxation of the hull

11. DOOLEY, R. and PASTERNAK, R. *Experimental Determination of Bolt Preload Decay in Single Connector Friction Joints Subjected to Static and Dynamic Loading Environments*. AMTL-TR, manuscript being prepared.

material.¹² As seen in Figure 23, four separate 4" X 4" S2 glass/polyester woven roving pads were sandwiched in-between an inner aluminum center plate and two outer metal plates. As with the double lap shear specimen, the diameter of the holes in the composite plate were oversized by 0.125" to allow for slippage between themselves and the metal plates. Grade 9 0.625" diameter bolts were used to through bolt each of the four connections. Bolt force sensors were sandwiched between standard sized grade 9 washers and used to monitor bolt preloads. The entire dynamic relaxation specimen was placed in a 60,000 lb *MTS* fatigue testing machine.

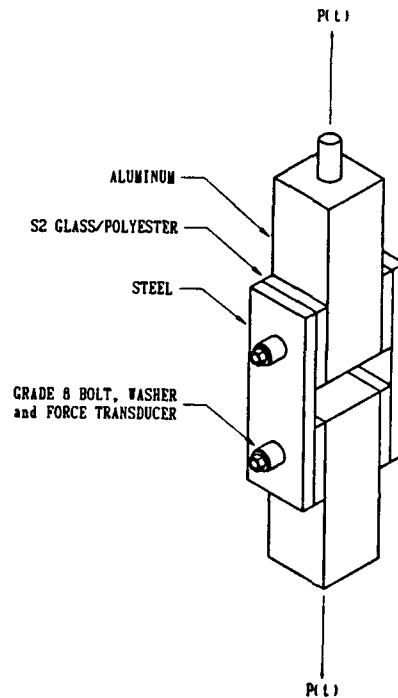


Figure 23 Dynamic Bolt Force Preload Relaxation Specimen

Fatigue loading of the dynamic relaxation test specimen was done to simulate the surface traction fatigue loading of the CIFV hull material by the roadwheel housing. Fatigue loading of the specimen and data acquisition of bolt force sensors were accomplished using the test configuration depicted in Figure 24. A wave generator was employed to activate the *MTS* testing machine. Output voltages from each of the four bolt force sensor Wheatstone bridges were amplified and routed into a *Megadac* data acquisitions system in addition to *MTS* load and stroke information. A second channel of the wave generator was used to trigger data acquisition at the positive peak of the fatigue load. Stroke displacement conditions were set in the *Megadac* data acquisition system in relation to the variation in composite and metal plate hole diameters to activate a test shutdown if significant preload relaxation and ensuing bolt bearing conditions prevailed.

12. ANASTASI, R.F., *On the Design of CIFV Friction Joint Dynamic Preload Relaxation Test Specimens*. AMTL-Technical Note, *manuscript being prepared*.

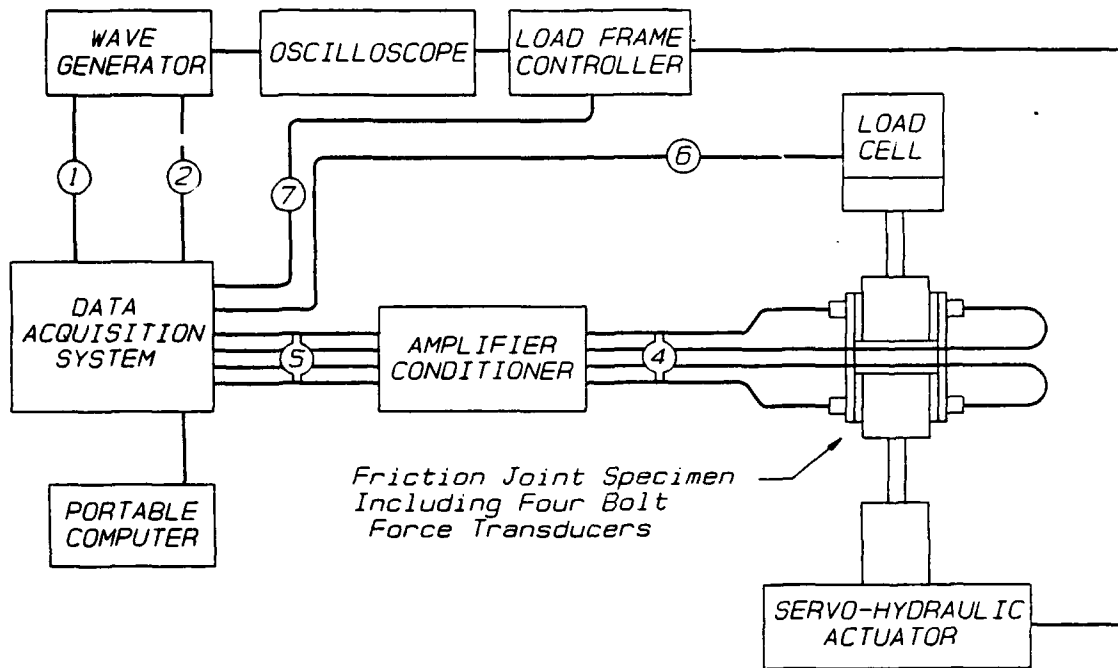


Figure 24 Dynamic Bolt Force Preload Relaxation Test Configuration

Two fatigue tests were conducted. As shown in Figure 25, each test used a separate mean (F_{mean}) and fatigue (F_{fatigue}) tensile load amplitude and frequency (f) which was indicative of the maximum resultant connector dynamic force characteristics obtained from the BJAN roadwheel housing simulations. The first test consisted of a 800 lb mean tensile load with a 200 lb fatigue load at 0.20 Hz. The second test consisted of a 1,350 lb mean tensile load with a 750 lb fatigue load at 1.0 Hz. Fresh composite specimens were used for each fatigue test.

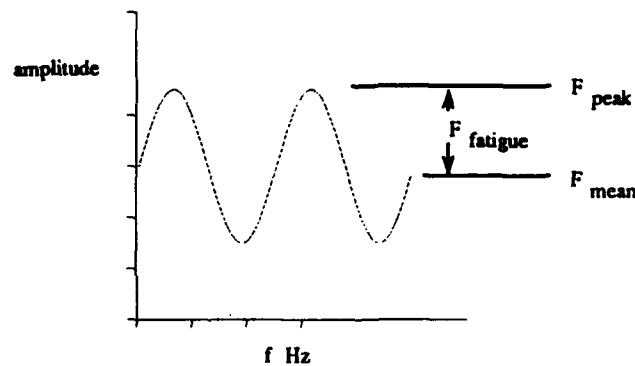


Figure 25 Dynamic Bolt Force Preload Relaxation Test Configuration

Experimental Results

Bolt preload relaxation results from the static tests may be seen in Figures 26 and 27. The 158 ft-lb torquing of the bolts produced initial bolt force readings ranging from 16,750 lbs-23,000 lbs. Results from test one, seen in Figure 26, indicate that minimal preload decay (500 lbs) occurred over the 45-1038 hour test time span. Results from test two, depicted in Figure 27, show that the signal from the second bolt force transducer appeared to be somewhat erratic while the third bolt force transducer failed within hours of test inception. The first bolt force transducer produced satisfactory results which showed an initial decay of about 500 lbs within the first 45 hour time period.

Bolt preload relaxation results for the dynamic test may be seen in Figures 28 and 29. Bolt force transducer repairs corrected all instrumentation problems encountered in the previous static relaxation tests. Results indicate that dynamic surface traction loading did not appear to significantly alter the through thickness viscoelastic material relaxation. As with the static test, average preload decay was limited to approximately 1,000 lbs.

Although minimal relaxation effects were observed for both the static and dynamic tests, it is not safe to conclude that a similar response will be observed in a fielded CIFV. Environmental factors such as temperature and long term exposure to moisture could affect these present conclusions. As mentioned in section 1.4, Slepetz *et al*⁴ showed that elevated temperatures produced significant bolt preload decay in high modulus graphite epoxy composites.

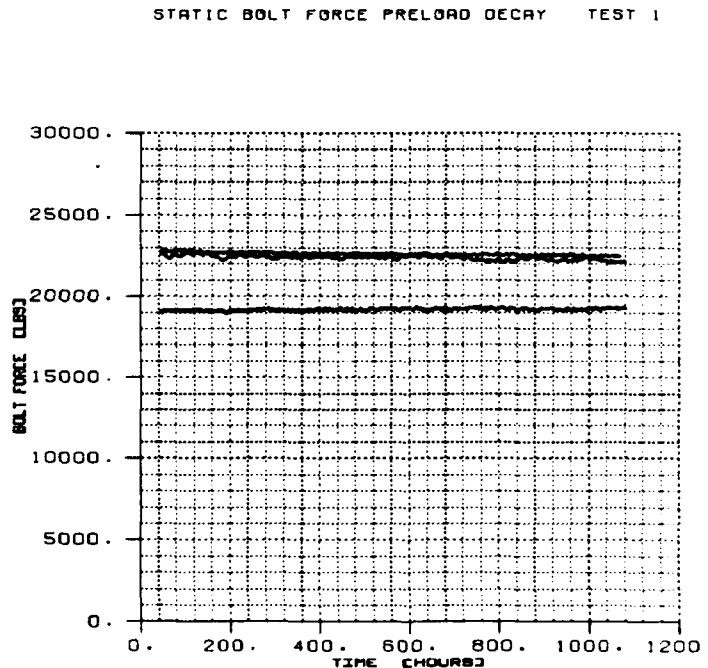


Figure 26 Static Loading Bolt Force Preload Decay (Test 1)

STATIC BOLT FORCE PRELOAD DECAY TEST 2

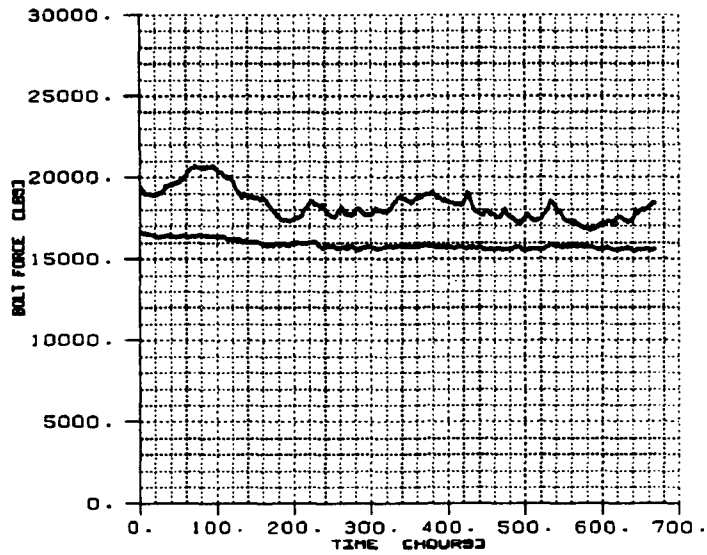


Figure 27 Static Loading Bolt Force Preload Decay (Test 2)

DYNAMIC SURFACE TRACTION FATIGUE BOLT FORCE PRELOAD DECAY
(1000 LB MEAN LOAD 200 LB FATIGUE LOAD 0.2 HZ FREQUENCY)

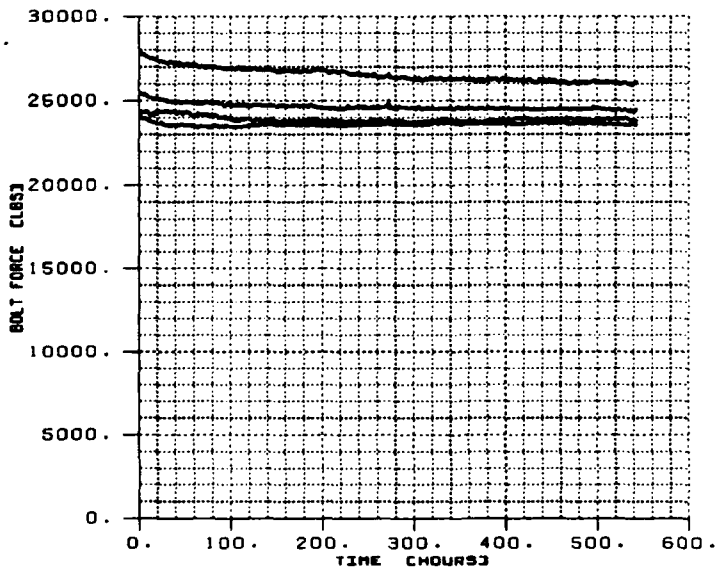


Figure 28 Dynamic Surface Traction Fatigue Bolt Force Preload Decay (Terrain 1)

DYNAMIC SURFACE TRACTION FATIGUE BOLT FORCE PRELOAD DECAY
 (2100 LB MEAN LOAD 750 LB FATIGUE LOAD 1 Hz FATIGUE LOAD)

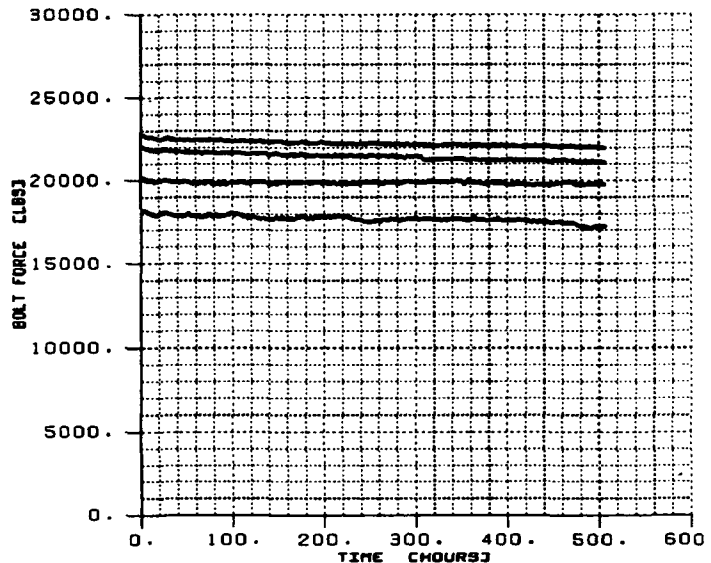


Figure 29 Dynamic Surface Traction Fatigue Bolt Force Preload Decay (Terrain 2)

PREDICTION OF CIFV FRICTION JOINT PERFORMANCE

CIFV friction joint performance was predicted as a function of roadarm displacement using a modified shear/moment analysis of the roadwheel housing joint which incorporated the single connector static slip test results. In addition to this, friction joint lifetimes for the Perryman III terrain condition were also predicted using this modified analysis and surface traction fatigue preload relaxation test results.

Friction Joint Mechanical Slip Analysis

Prediction of joint slippage was done by an incremental analysis for a given DADS force/moment load pair. Out-of-plane forces (F_x) and moments (M_y and M_z) affecting bolt preload were also included in the analysis thus forming a complete force/moment load set. During the analysis, a check for connector slip was made based on the single connector static slip test results. In addition to this, an option was included to relax bolt preloads according to the experimental results from the surface traction fatigue tests. A computer code entitled BJSAN (Bolted Joint Slip ANalysis) was written to perform this analysis. Modifications to the incremental BJSAN load stepping algorithm was implemented within this code to improve

solution accuracy and enhanced computational speed.

The in-plane shear/moment joint analysis of the roadwheel housing was employed on an incremental basis. As seen in Figure 30, each force/moment loading pair (F_y, F_z, M_x) was divided into a given number of increments (inc) to calculate an incremental force/moment pair ($\Delta F_y, \Delta F_z, \Delta M_x$). As in the first analysis, roadwheel arm incremental forces ($\Delta F_y, \Delta F_z$) were

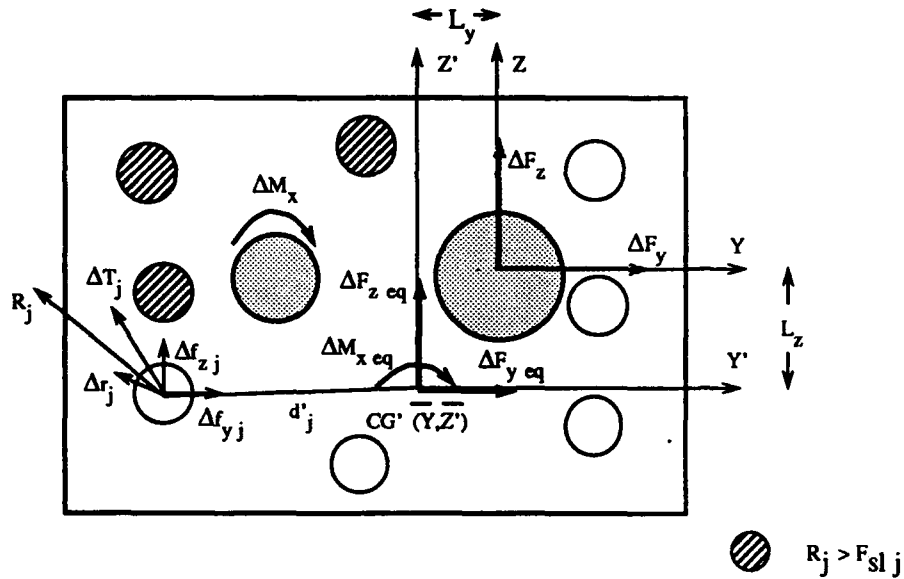


Figure 30 Shear/Moment Slip Analysis of Roadwheel Housing Joint

replaced by an incremental equivalent force ($\Delta F_{y \text{ eq}}, \Delta F_{z \text{ eq}}$) and incremental couple ($\Delta M_{x \text{ eq}}$) acting through the bolt pattern center of gravity (CG'). The total joint incremental moment (ΔM_x) was found by summing incremental roadwheel arm moment (ΔM_x) and incremental equivalent couple ($\Delta M_{x \text{ eq}}$) contributions. For a given incremental shear/moment loading, incremental resultant connector loads (Δr_j) were calculated by vectorially summing the incremental shear (Δf_j) and moment (Δt_j) reactive forces. These forces were calculated by assuming that incremental joint shear loading was equally distributed to each connector while incremental moment loading was distributed to each connector through forces (Δt_j) acting about the bolt pattern's center of gravity. Total connector resultant forces (R_j) were found by summing all incremental resultant connector loads (Δr_j).

These relationships may be stated simply as:

$$\Delta M_x = \frac{M_x}{inc} \quad (9) \quad \Delta F_y = \frac{F_y}{inc} \quad (10) \quad \Delta F_z = \frac{F_z}{inc} \quad (11)$$

$$\Delta M_{x \text{ eq}} = (\Delta F_y L_y + \Delta F_z L_z) \quad (12) \quad \Delta M_{x \text{ t}} = (\Delta M_x + \Delta M_{x \text{ eq}}) \quad (13)$$

$$\bar{Y}' = \frac{\sum_{j=1}^{n'} Y'_i A_i}{\sum_{j=1}^{n'} A_i} \quad (14)$$

$$\bar{Z}' = \frac{\sum_{j=1}^{n'} Z'_i A_i}{\sum_{j=1}^{n'} A_i} \quad (15)$$

where

ΔM_x = incremental roadwheel arm moment	$\Delta M_{x \text{ eq}}$ = incremental roadwheel arm equivalent moment
M_x = roadwheel arm moment	L_y, L_z = roadwheel arm joint CG distance
inc = total number of increments	$\Delta M_{x \text{ t}}$ = incremental total joint moments
ΔF_y = incremental roadwheel arm shear forces	(\bar{Y}', \bar{Z}') = joint CG' coordinates
ΔF_z = incremental roadwheel arm shear forces	(Y'_i, Z'_i) = connector coordinates
F_y = roadwheel arm shear forces	n' = total number of active connectors
F_z = roadwheel arm shear forces	

and:

$$\Delta f_{y j} = \frac{\Delta F_y}{n'} \quad (16)$$

$$\Delta f_{z j} = \frac{\Delta F_z}{n'} \quad (17)$$

$$\Delta t_j = \frac{\Delta M_{x \text{ t}} d'_j}{\sum_{j=1}^{n'} d_j'^2} \quad (18)$$

$$\vec{\Delta f}_j = \Delta f_{y j} \vec{i} + \Delta f_{z j} \vec{j} + \Delta t_j \vec{k} \quad (19)$$

$$\vec{R}_j = \sum_{i=1}^{inc} \vec{\Delta f}_j \quad (20)$$

where

$\Delta f_{y j}$ = incremental connector shear force	$\vec{\Delta f}_j$ = total incremental resultant connector load
$\Delta f_{z j}$ = incremental connector shear force	\vec{R}_j = total resultant connector load
Δt_j = incremental connector couple force	d'_j = perp. connector CG' distance

During each increment of a given force/moment loading pair, incremental resultant connector loads were checked for slip conditions by comparison to calculated static slip loads based on current bolt preloads and the effective coefficient of friction previously determined. In this comparison, bolt preloads were determined for the given time value of the terrain data base from the static or surface traction fatigue bolt preload relaxation test results. Bolt preloads (P_j) were adjusted to account for incremental out-of-plane forces (ΔF_x) and moments ($\Delta M_y, \Delta M_z$). Incremental out-of-plane forces were distributed equally among all

connectors (Δf_{xj}). Incremental out-of-plane moments were assumed to generate a rigid body translation of the roadwheel housing that produced incremental connector working loads (Δw_{yj} , Δw_{zj}). The distribution of these moments to the connectors forming the bolt working loads was found to be of the same form as the in-plane moments. It was assumed that out-of-plane forces and working loads affected connector slip loads as bolt preload did and that linear superposition could be applied to obtain total connector preloads. These relationships may be stated by.

$$\Delta F_x = \frac{F_x}{inc} \quad (21)$$

$$\Delta M_y = \frac{M_y}{inc} \quad (22)$$

$$\Delta M_z = \frac{M_z}{inc} \quad (23)$$

$$\Delta f_{xj} = - \frac{\Delta F_x}{n} \quad (24)$$

$$\Delta w_{yj} = - \frac{\Delta M_y z_j}{\sum_{j=1}^n z_j^2} \quad (25)$$

$$\Delta w_{zj} = \frac{\Delta M_z y_j}{\sum_{j=1}^n y_j^2} \quad (26)$$

$$\Delta p_j = \Delta f_{xj} + \Delta w_{yj} + \Delta w_{zj} \quad (27)$$

$$P_{tj} = P_r + \sum_{i=1}^{inc} \Delta p_j \quad (28)$$

where;

ΔF_x = incremental roadarm out-of-plane force
 ΔM_y = incremental roadarm out-of-plane moment
 ΔM_z = incremental roadarm out-of-plane moment
 Δf_{xj} = incremental out-of-plane connector force
 Δw_{yj} = incremental connector working loads
 Δw_{zj} = incremental connector working loads

z_j = perp. connector z CG' distance
 y_j = perp. connector y CG' distance
 Δp_j = total incremental connector preload adjustment due to out-of-plane loading
 P_{tj} = total connector preload
 P_r = relaxed connector preload

Connector slip loads (F_{slj}) were calculated from total connector preloads (P_{tj}) and the experimental single connector effective coefficient of friction (μ_{eff}). Connector slip conditions presented themselves when the total resultant connector load was equal to or greater than the connector slip load (F_{slj}). These relationships may be stated as;;

$$F_{slj} = \mu_{eff} P_{tj} \quad (29)$$

$$R_j \geq F_{slj} \text{ (slip)} \quad (30)$$

It was assumed that when connectors satisfied this slip condition, additional incremental connector in-plane shear and couple forces were distributed among the remaining number of "active" connectors (n') in the housing. Bolt pattern center of gravity (CG') location (X'Y') were also calculated from these remaining active connectors. Total friction joint slippage was assumed to occur when all housing connectors reached this experimental connector slip load.

Initial running of the BJSAN code on simplistic trial friction joint problems indicated that small increments were necessary to insure that total resultant connector loads closely approximated connector slip forces when slip conditions presented themselves. This resulted in excessive number of increments and relatively long computer times for terrain simulations. Modifications to the incremental analysis were done in order to reduce calculation time and improve solution accuracy. Reduced computation times were obtained by developing a load stepping algorithm that efficiently located force-moment load levels that induced connector slip. Solution accuracy was accomplished by introducing a slip load tolerancing parameter which enforced connector total resultant and connector slip force load equality within a user defined tolerance.

Connector participation in reacting joint force-moment loads was defined in terms of a slip load tolerancing parameter (T). As seen in Figure 31, connectors were removed from loading participation if their total resultant forces (R_j) were greater than or equal to their slip loads (F_{slj}). Connectors previously removed from loading participation were allowed to participate again if their total resultant forces were less than their slip loads. Both a high and low bounding of these actions were established by forming a high (UPTOL) and low (BOTOL) tolerance level with the slip load tolerancing parameter.

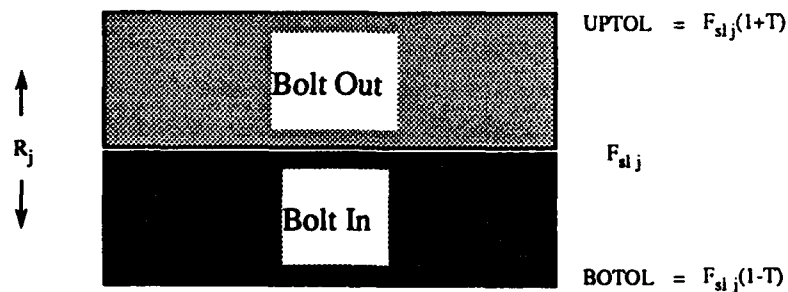


Figure 31 Connector Participation Relationships

Location of force-moment magnitudes that altered connector participation within each terrain time interval were found with the modified load stepping algorithm. In this algorithm, continual halving of an initial total force-moment loading of the joint was done until such time that connector participation updating occurred by the relations shown in Figure 31. This procedure was iteratively followed using residual force-moment loading of the joint for the

given terrain time value until such time that total force-moment loading had occurred or all connectors had slipped. A flow chart of the BJSAN code is shown below in Figure 32.

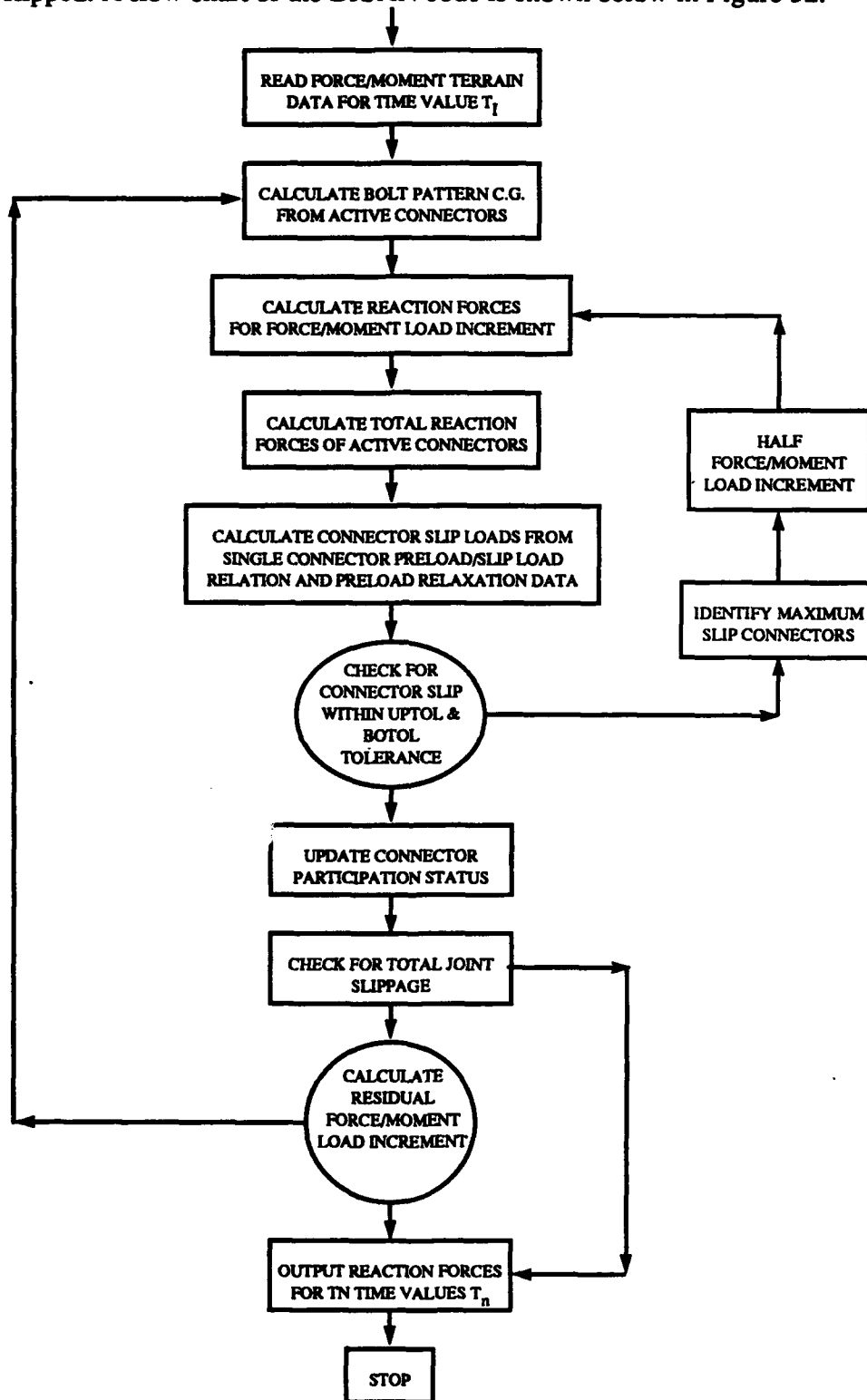


Figure 32 Computer Program BJSAN Flow Chart

Static Roadarm Displacement Results

Resultant connector loads as a function of roadwheel arm displacement are shown in Figure 33 for the original roadwheel housing design and Figure 34 for the modified design. In both instances, the additional out-of-plane moment (ΔM_y) altered the once linear relationship between resultant connector loads and roadwheel arm displacement. Slip loads for those connectors located above the bolt pattern CG increased over similar no slip results while decreases were observed for those connectors located below. These variations were more pronounced in the original roadwheel housing design than in the modified design. Maximum connector loads rose from the 5,757 lb no slip value to 9,395 lbs for the original design while an increase to 5,774 lbs from 5,204 lbs was found for the modified design. As indicated by a leveling in resultant connector loads, the modified roadwheel housing design had fewer connectors in the slip state (4) than the original design (7) at the largest roadarm displacement.

ORIGINAL ROADWHEEL HOUSING RESULTANT CONNECTOR LOADS VS ROADWHEEL ARM DISP
(0.270 FRICTION COEFFICIENT)

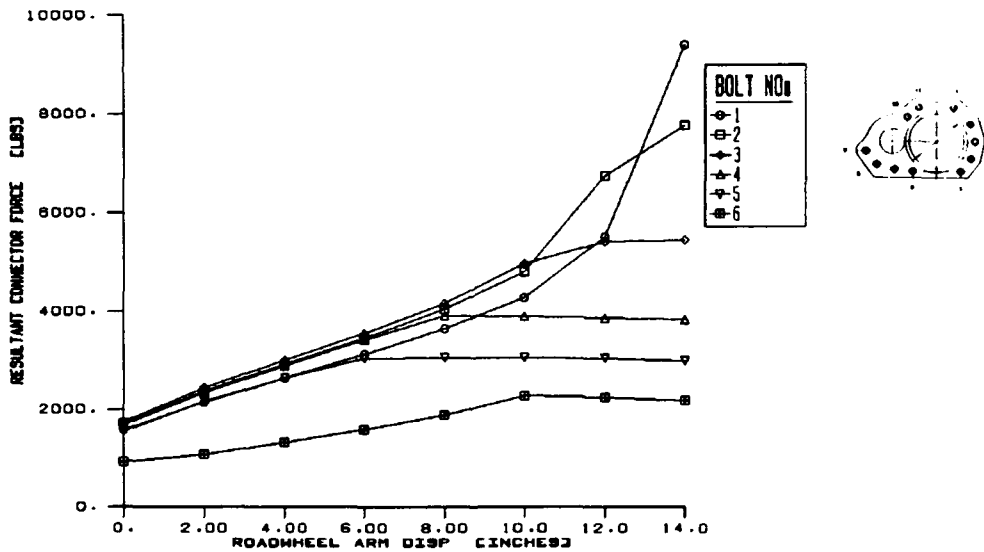


Figure 33a Original Roadwheel Housing Resultant Connector Loads as a Function of Roadwheel Arm Displacement ($\mu_{eff} = 0.270$)

ORIGINAL ROADWHEEL HOUSING RESULTANT CONNECTOR LOADS VS ROADWHEEL ARM DISP
(0.270 FRICTION COEFFICIENT)

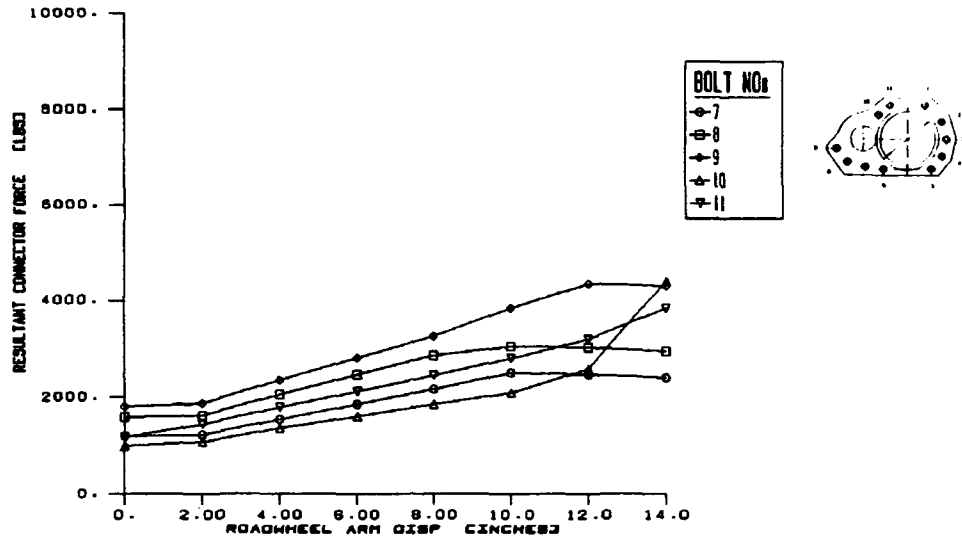


Figure 33b Original Roadwheel Housing Resultant Connector Loads as a Function of Roadwheel Arm Displacement ($\mu_{eff} = 0.270$)

MODIFIED ROADWHEEL HOUSING RESULTANT CONNECTOR LOADS VS ROADWHEEL ARM DISP
(0.270 FRICTION COEFFICIENT)

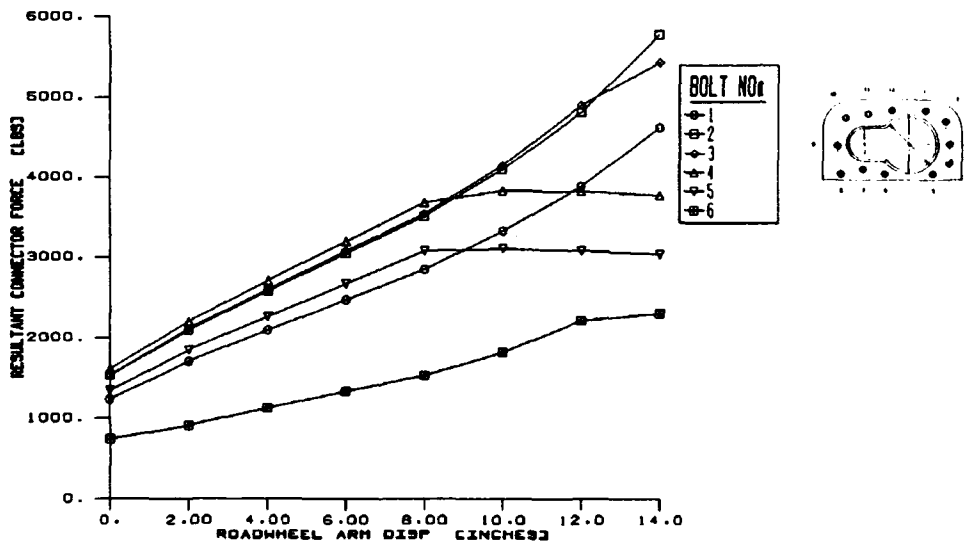


Figure 34a Modified Roadwheel Housing Resultant Connector Loads as a Function of Roadwheel Arm Displacement ($\mu_{eff} = 0.270$)

MODIFIED ROADWHEEL HOUSING RESULTANT CONNECTOR LOADS VS ROADWHEEL ARM DISPL
(0.270 FRICTION COEFFICIENT)

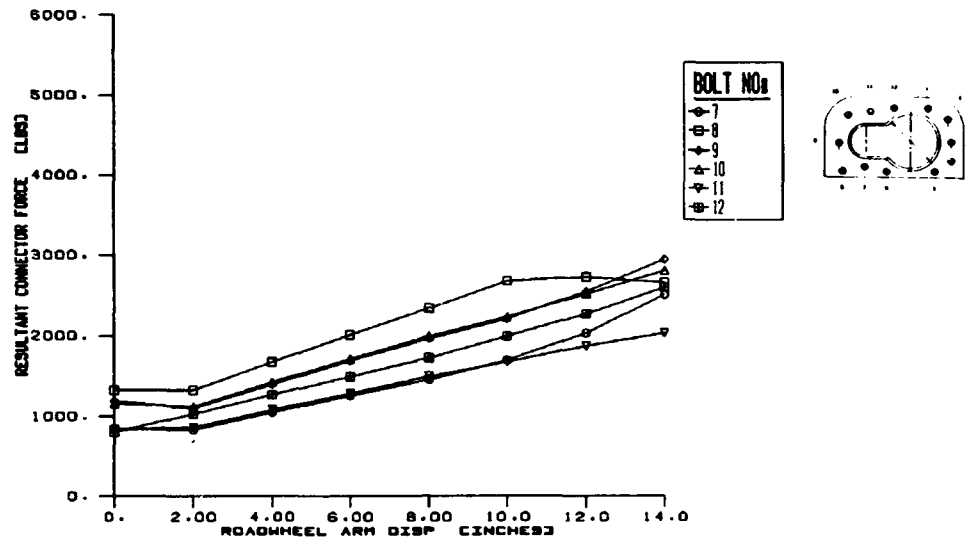


Figure 34b Modified Roadwheel Housing Resultant Connector Loads as a Function of Roadwheel Arm Displacement ($\mu_{eff} = 0.270$)

Dynamic Perryman III Terrain Results

Friction joint lifetimes for both Perryman III terrain conditions were predicted using the modified load stepping slip BJSAN analysis code. Total resultant connector loads were calculated for both roadwheel housing configurations using the experimentally determined single connector effective friction coefficient (μ_{eff}). In both of these calculations, bolt preloads were allowed to decay to 19,000 lbs from 20,000 lbs over a 500-hour time period in accordance to typical dynamic surface traction fatigue test results. In addition to this, a minimum value of connector bolt preload for incipient slip conditions was calculated using the BJSAN code for both the original and modified roadwheel housing designs.

Figures 35 and 36 illustrates results for both the original and modified roadwheel housing configurations under terrain test case 1 loading. Figures 37 and 38 illustrate similar results for terrain test case 2. Predictions indicated that each roadwheel housing design configuration did not slip when subjected to either terrain test conditions for the total 500-hour time period. Slip assumptions did however produce some variations in resultant connector loads for the Perryman III terrain 1 test condition for the original roadwheel housing design. The peak connector load for this housing design rose to 4,293 lbs from 3,936 lbs while slight increases or decreases were observed for other connectors through out the entire terrain 1 simulation. Peak modified housing resultant connector loads also increased using the slip assumptions for terrain 1. A 4,129 lb value was predicted in comparison to the 3,575 lb value found for the no slip conditions while, as with the original housing design, slight increases or decreases were observed for other connectors through out the entire

terrain 1 simulation. Resultant connector forces for both housing designs appeared to be unaffected for terrain 2 test conditions. This was anticipated since only the F_y out of plane force was included in the terrain 2 data base.

Minimum connector bolt preloads to sustain no slip conditions were lower for the less severe Perryman III terrain 1 test conditions. In either terrain test conditions, the modified roadwheel housing design required less bolt preload to sustain no slip conditions. Analysis results indicated that for terrain 1 test conditions 14,109 lbs of bolt preload was required for the original roadwheel housing design while 12,125 lbs was required for the modified design. Similarly, analysis results indicated that for terrain 2 test conditions 15,110 lbs of bolt preload was required for the original roadwheel housing design while 13,327 lbs was required for the modified design.

ORIGINAL ROADWHEEL HOUSING RESULTANT CONNECTOR FORCE/TIME HISTORIES
 (80,000 LB COMPOSITE SPV, PERRYMAN III, 4 MPH, 30 DEGREE TRAVERSING ANGLE)
 (0.270 FRICTION COEFFICIENT) (BOLT PRELOAD DECAY)

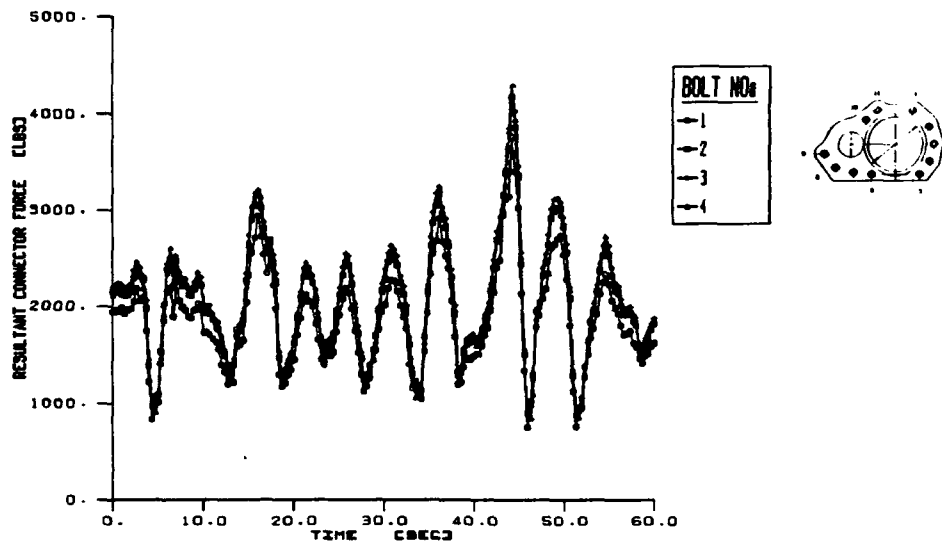


Figure 35a Original Roadwheel Housing Resultant Connector Force-Time Histories
 [terrain 1] [$\mu_{eff} = 0.270$] [19,000 lb bolt preload] [bolts 1-4]

ORIGINAL ROADWHEEL HOUSING RESULTANT CONNECTOR FORCE/TIME HISTORIES
 (80,000 LB COMPOSITE SFY, PERRYMAN III, 4 RPM, 30 DEGREE TRAVERSING ANGLE)
 (0.270 FRICTION COEFFICIENT) (BOLT PRELOAD DECAY)

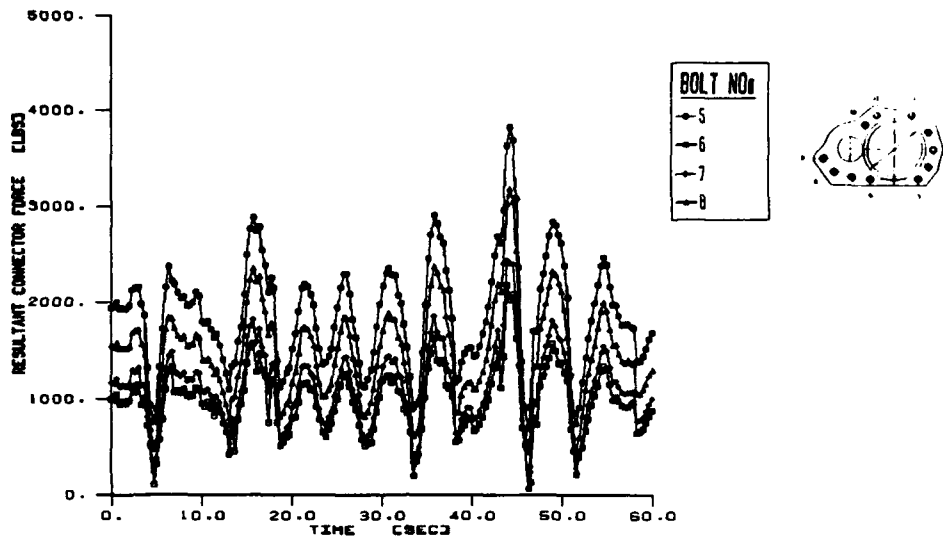


Figure 35b Original Roadwheel Housing Resultant Connector Force-Time Histories [terrain 1] [$\mu_{eff} = 0.270$] [19,000 lb bolt preload] [bolts 5-8]

ORIGINAL ROADWHEEL HOUSING RESULTANT CONNECTOR FORCE/TIME HISTORIES
 (80,000 LB COMPOSITE SFY, PERRYMAN III, 4 RPM, 30 DEGREE TRAVERSING ANGLE)
 (0.270 FRICTION COEFFICIENT) (BOLT PRELOAD DECAY)

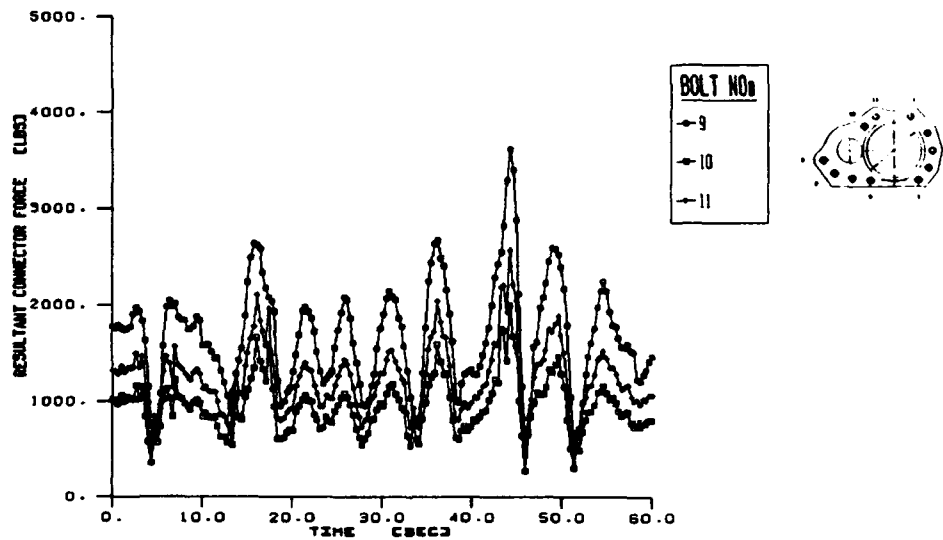


Figure 35c Original Roadwheel Housing Resultant Connector Force-Time Histories [terrain 1] [$\mu_{eff} = 0.270$] [19,000 lb bolt preload] [bolts 9-11]

MODIFIED ROADWHEEL HOUSING RESULTANT CONNECTOR FORCE/TIME HISTORIES
 (80,000 LB COMPOSITE OPV, PERRYMAN III, 4 MPH, 30 DEGREE TRAVERSING ANGLE)
 (0.270 FRICTION COEFFICIENT) (BOLT PRELOAD DECAY)

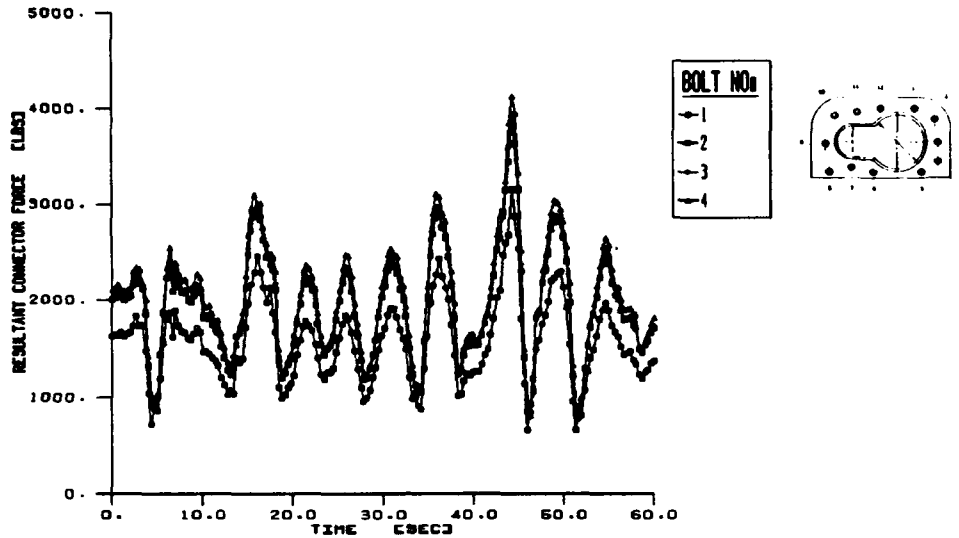


Figure 36a Modified Roadwheel Housing Resultant Connector Force-Time Histories
 [terrain 1] [$\mu_{eff} = 0.270$] [19,000 lb bolt preload] [bolts 1-4]

MODIFIED ROADWHEEL HOUSING RESULTANT CONNECTOR FORCE/TIME HISTORIES
 (80,000 LB COMPOSITE OPV, PERRYMAN III, 4 MPH, 30 DEGREE TRAVERSING ANGLE)
 (0.270 FRICTION COEFFICIENT) (BOLT PRELOAD DECAY)

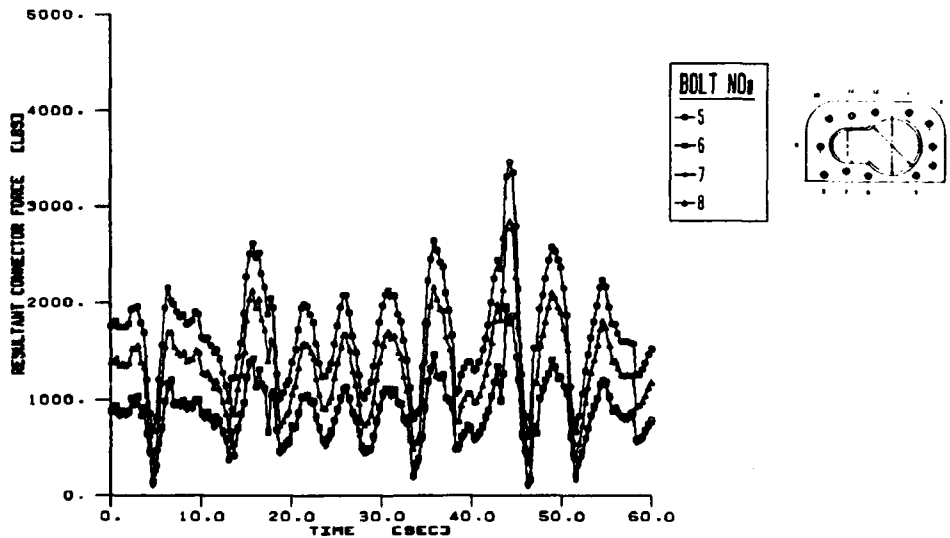


Figure 36b Modified Roadwheel Housing Resultant Connector Force-Time Histories
 [terrain 1] [$\mu_{eff} = 0.270$] [19,000 lb bolt preload] [bolts 5-8]

MODIFIED ROADWHEEL HOUSING RESULTANT CONNECTOR FORCE/TIME HISTORIES
 (80,000 LB COMPOSITE SPV, PERRYMAN III, 4 MPH, 30 DEGREE TRAVERSING ANGLE)
 (0.270 FRICTION COEFFICIENT) (BOLT PRELOAD DECAY)

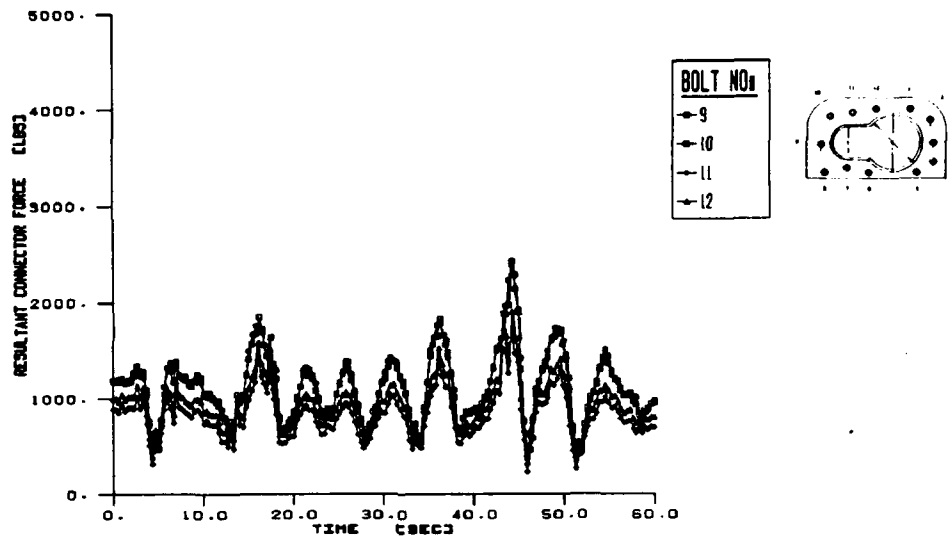


Figure 36c Modified Roadwheel Housing Resultant Connector Force-Time Histories
 [terrain 1] [$\mu_{eff} = 0.270$] [19,000 lb bolt preload] [bolts 9-12]

ORIGINAL ROADWHEEL HOUSING RESULTANT CONNECTOR FORCE/TIME HISTORIES
 (49,000 LB ALUMINUM SPV, PERRYMAN III, 20 MPH, 0 DEGREE TRAVERSING ANGLE)
 (0.270 FRICTION COEFFICIENT) (BOLT PRELOAD DECAY)

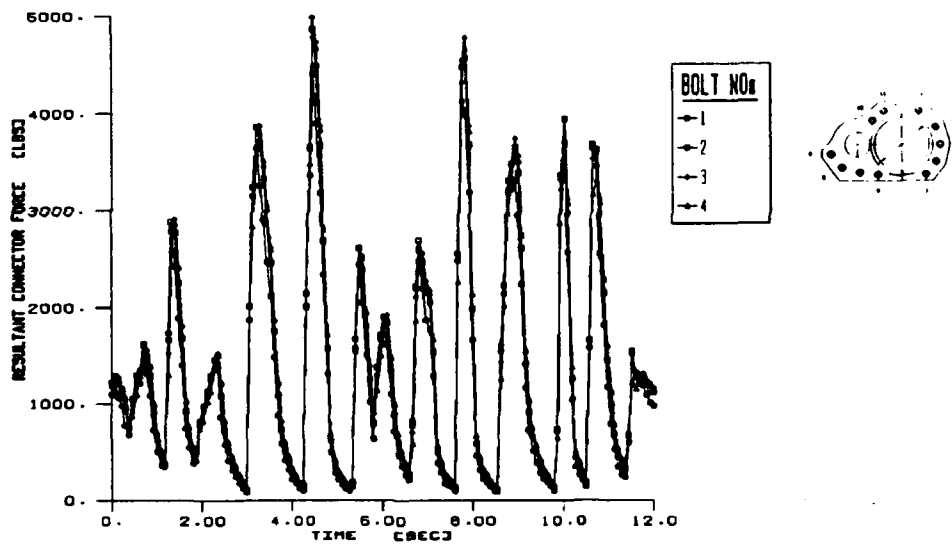


Figure 37a Original Roadwheel Housing Resultant Connector Force-Time Histories
 [terrain 2] [$\mu_{eff} = 0.270$] [19,000 lb bolt preload] [bolts 1-4]

ORIGINAL ROADWHEEL HOUSING RESULTANT CONNECTOR FORCE/TIME HISTORIES
 (48,000 LB ALUMINUM SPV, PERRYMAN III, 20 MPH, 0 DEGREE TRAVERSING ANGLE)
 (0.270 FRICTION COEFFICIENT) (BOLT PRELOAD DECAY)

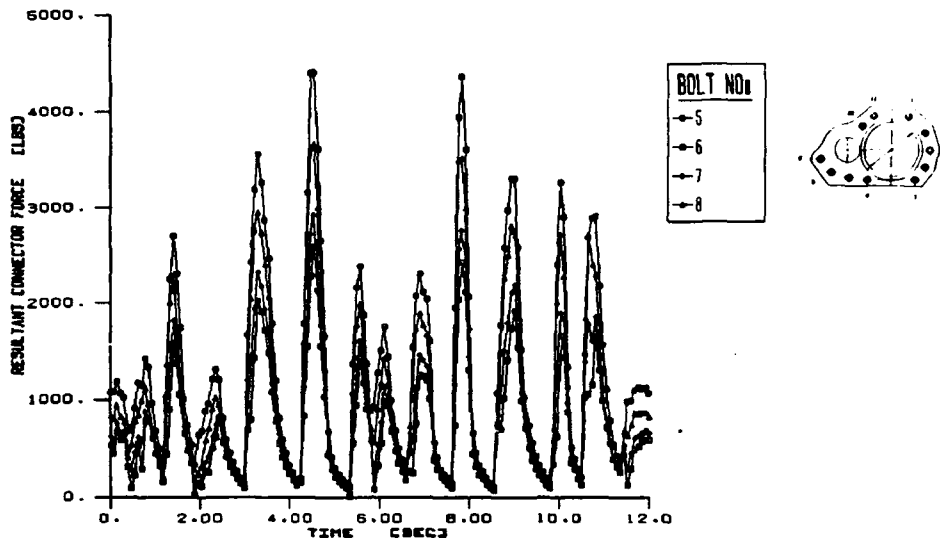


Figure 37b Original Roadwheel Housing Resultant Connector Force-Time Histories
 [terrain 2] [$\mu_{eff} = 0.270$] [19,000 lb bolt preload] [bolts 5-8]

ORIGINAL ROADWHEEL HOUSING RESULTANT CONNECTOR FORCE/TIME HISTORIES
 (48,000 LB ALUMINUM SPV, PERRYMAN III, 20 MPH, 0 DEGREE TRAVERSING ANGLE)
 (0.270 FRICTION COEFFICIENT) (BOLT PRELOAD DECAY)

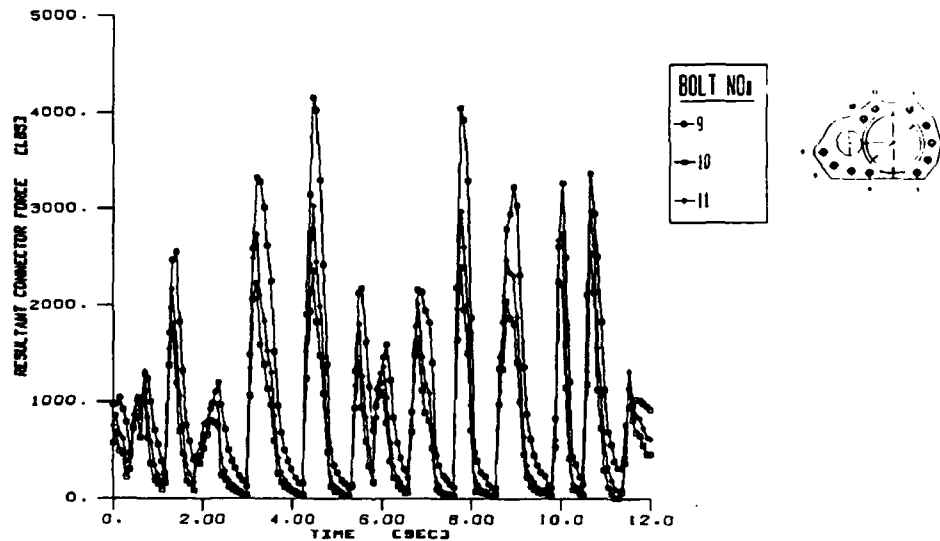


Figure 37c Original Roadwheel Housing Resultant Connector Force-Time Histories
 [terrain 2] [$\mu_{eff} = 0.270$] [19,000 lb bolt preload] [bolts 9-11]

MODIFIED ROADWHEEL HOUSING RESULTANT CONNECTOR FORCE/TIME HISTORIES
 (48,000 LB ALUMINUM SPV, PERRYMAN III, 20 MPH, 0 DEGREE TRAVERSING ANGLE)
 (0.270 FRICTION COEFFICIENT) (BOLT PRELOAD DECAY)

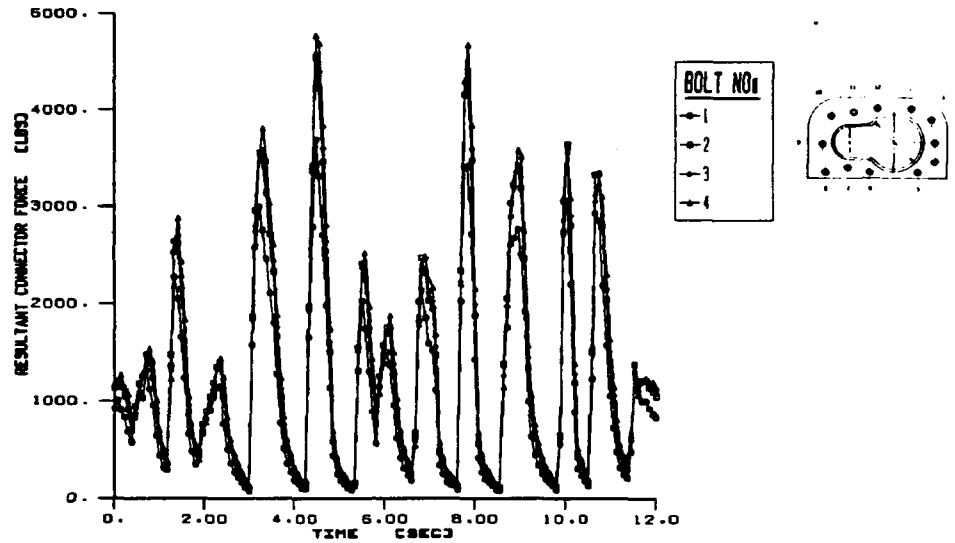


Figure 38a Modified Roadwheel Housing Resultant Connector Force-Time Histories
 [terrain 2] [$\mu_{eff} = 0.270$] [19,000 lb bolt preload] [bolts 1-4]

MODIFIED ROADWHEEL HOUSING RESULTANT CONNECTOR FORCE/TIME HISTORIES
 (48,000 LB ALUMINUM SPV, PERRYMAN III, 20 MPH, 0 DEGREE TRAVERSING ANGLE)
 (0.270 FRICTION COEFFICIENT) (BOLT PRELOAD DECAY)

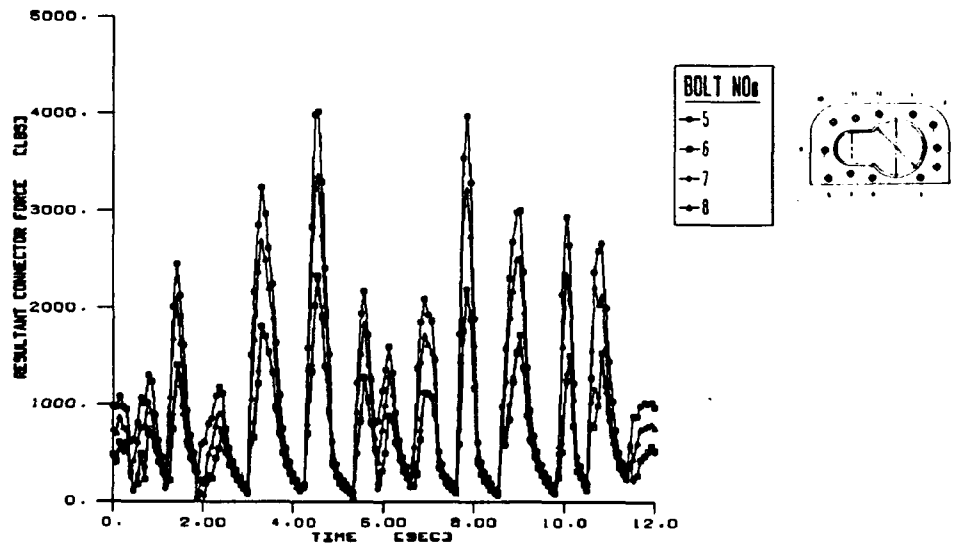


Figure 38b Modified Roadwheel Housing Resultant Connector Force-Time Histories
 [terrain 2] [$\mu_{eff} = 0.270$] [19,000 lb bolt preload] [bolts 5-8]

MODIFIED ROADWHEEL HOUSING RESULTANT CONNECTOR FORCE/TIME HISTORIES
 (48,000 LB ALUMINUM SPV. PERRIN 111, 20 MPH, 0 DEGREE TRAVERSING ANGLE)
 (0.270 FRICTION COEFFICIENT) (BOLT PRELOAD DECAY)

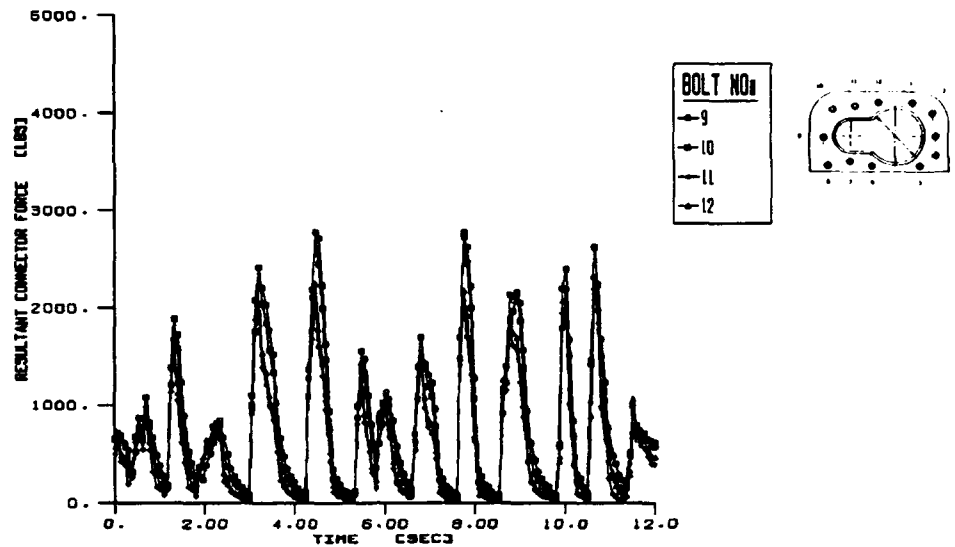


Figure 38c Modified Roadwheel Housing Resultant Connector Force-Time Histories
 [terrain 2] [$\mu_{eff} = 0.270$] [19,000 lb bolt preload] [bolts 9-12]

[0/90/+45/-45]_ns S2 WOVEN ROVING MECHANICAL PROPERTY CHARACTERIZATION

A mechanical property characterization of the CIFV hull material was conducted to establish a data base from which three dimensional orthotropic constitutive equation could be developed. These constitutive equations were employed in a three dimensional finite element model of a single connector arrangement. Tension, through thickness compression, interlaminar shear, and intralaminar shear tests were conducted.

Tension Testing

Tension tests were conducted on the S2 glass/polyester woven roving material to determine the in-plane modulus (E_1) and Poisson ratio (ν_{12}). Two tensile test specimens of approximately 0.625" x 1.00" x 24" dimensions were manufactured and instrumented with back-to-back BLH type FEA-13-125-WT-350 biaxial strain gages. Dual active arm Wheatstone bridges were used for signal conditioning. Two X-Y recorders were used to record load (L_{11}) versus longitudinal strain (ϵ_{11}) and transverse strain (ϵ_{22}) versus longitudinal strain (ϵ_{11}) respectively. Each specimen was cycled up to approximately 10,000 lbs a total of three times.

Table 2 details the tensile specimen crosssectional dimensions. Figures 39 and 40 illustrate the longitudinal stress-strain plots of both tensile test specimens. Figures 41 and 42 illustrate the transverse strain-longitudinal strain plots of both specimens.

Table 2 Tensile Test Specimen Dimensions

Specimen No	W (in)	t (in)
σ_{xx-1}	0.621	1.005
σ_{xx-2}	0.621	1.004

Compression Testing

Compression tests were conducted on the S2 glass/polyester woven roving material to determine the through thickness modulus (E_3) and Poisson ratio (ν_{31}). A 0.632" x 0.631" x 0.628" compression specimen was manufactured. Two of its' adjoining sides were instrumented with *BLH* type FEA-13-125-WT-350 biaxial strain gages. Dual active arm Wheatstone bridges were used for signal conditioning. Two X-Y recorders were used to record through thickness load (L_{33}) versus through thickness strain (ϵ_{33}) and transverse strain (ϵ_{22}) versus through thickness strain (ϵ_{33}). The compression specimen was cycled up to 2,000 lbs twice.

Figure 43 illustrates the through thickness load versus through thickness strain response of the specimen while Figure 44 illustrates transverse strain versus through thickness strain response of the specimen.

SIGMA XX VS EPSILON XX (SPEC SIGXX-1) (IN-PLANE TENSION)
 (E-Glass/Polyester woven roving material)

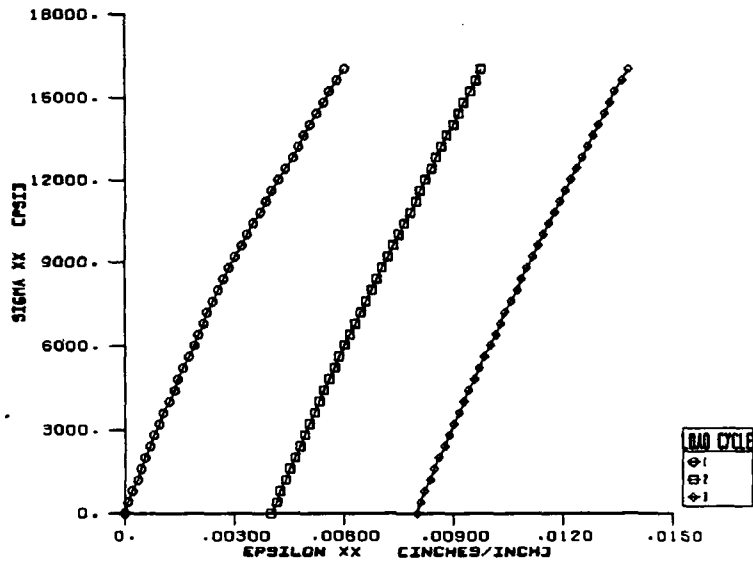


Figure 39 σ_{xx} vs ϵ_{xx} (specimen σ_{xx} -1)

SIGMA XX VS EPSILON XX (SPEC SIGXX-2) (IN-PLANE TENSION)
 (E-Glass/Polyester woven roving material)

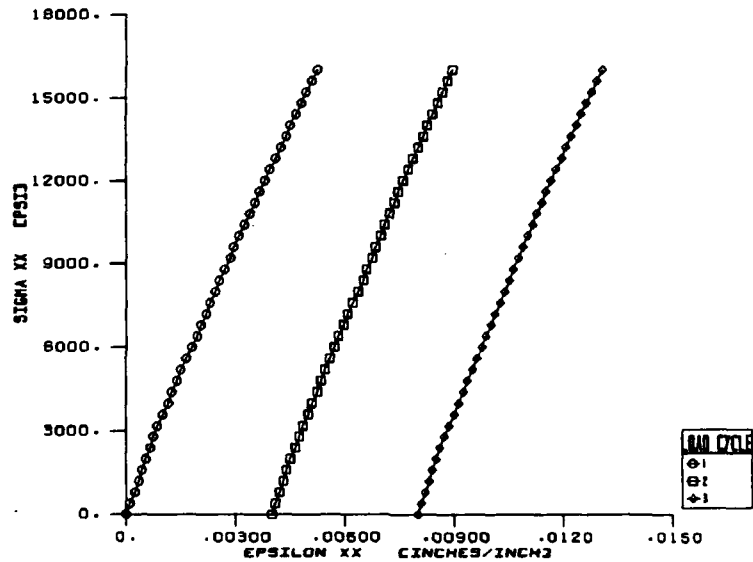


Figure 40 σ_{xx} vs ϵ_{xx} (specimen σ_{xx} -2)

EPSILON YY VS EPSILON XX (SPEC SIGXX-1) CIN-PLANE TENSION
 (E-G/POLYESTER WOVEN ROVING MATERIAL)

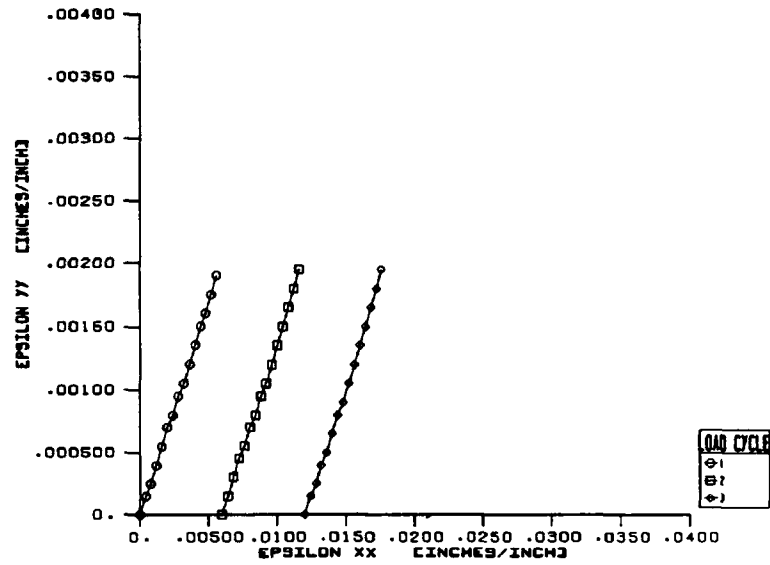


Figure 41 ϵ_{yy} vs ϵ_{xx} (specimen σ_{xx} -1)

EPSILON YY VS EPSILON XX (SPEC SIGXX-2) CIN-PLANE TENSION
 (E-G/POLYESTER WOVEN ROVING MATERIAL)

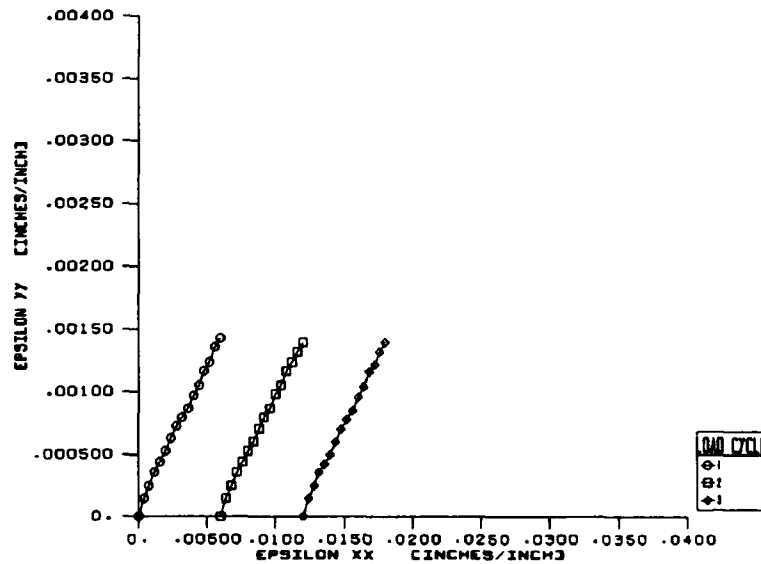


Figure 42 ϵ_{yy} vs ϵ_{xx} (specimen σ_{xx} -2)

SIGMA ZZ VS EPSILON ZZ (SPEC SIGZZ-1) (THROUGH THICKNESS COMPRESSION)
 (E2-CLASS/POLYESTER WOVEN ROVING MATERIAL)

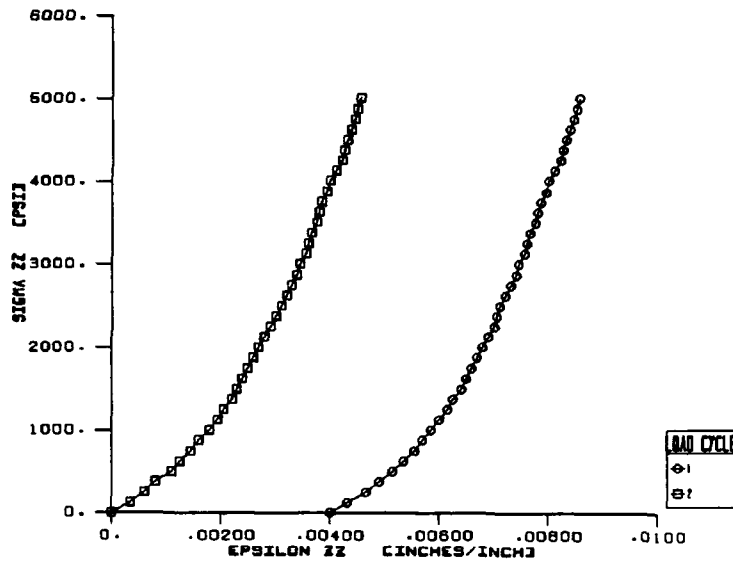


Figure 43 σ_{zz} vs ϵ_{zz} (specimen σ_{zz} -1)

EPSILON XX VS EPSILON ZZ (SPEC SIGZZ-1) (THROUGH THICKNESS COMPRESSION)
 (E2-CLASS/POLYESTER WOVEN ROVING MATERIAL)

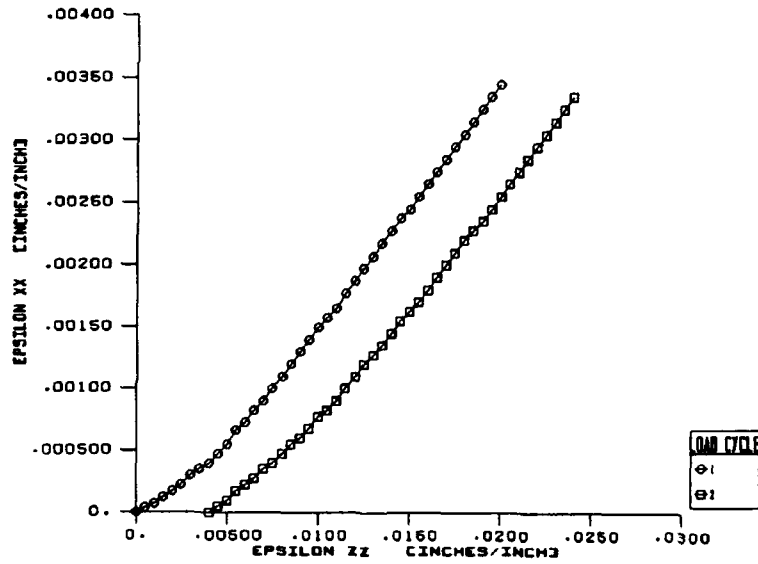


Figure 44 ϵ_{xx} vs ϵ_{zz} (specimen σ_{zz} -1)

Intra and Inter Laminar Shear Testing

Both intralaminar and interlaminar stress-strain response of the S2 glass/polyester woven roving material were experimentally determined by the asymmetric four point bend test (AFPB) developed by Slepetz *et al.*¹³ Similar to the more popular Iosipescu test method, the AFPB test uses two counteracting moments generated from force couples to produce a constant state of shear force through the middle section of the notched specimen. Figure 45 illustrates the ASFB test set-up.

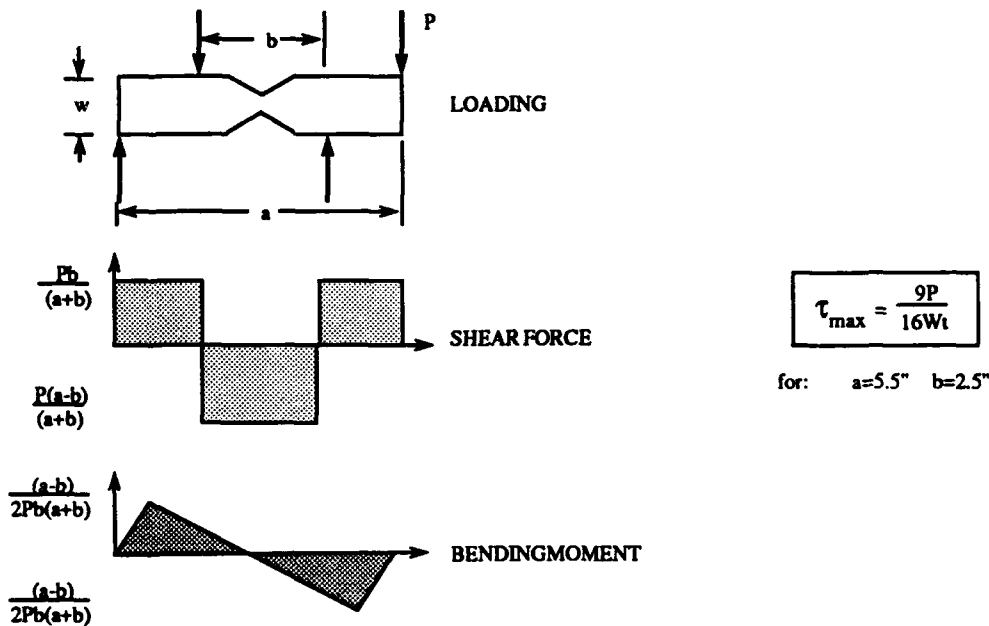


Figure 45 Load, Shear, and Bending Moment Relationships for AFPB Specimens

Interlaminar and intralaminar test specimens of 0.625" width and 6.0" length were manufactured from a 1" thick plate of the S2 glass/polyester woven roving material. A 120 degree notch angle was employed. Figure 46 illustrates the orientation of each specimen in relation to the plate's material properties axes while Table 3 details their shear section dimensional characteristics. Steel tabs were mounted on each specimen to provide a bearing surface to eliminate premature specimen failure caused by jig loading. *BLH* type FAED-12D-35-S13 shear gages were adhered on both sides of each specimen to avoid bending effects. A dual active arm Wheatstone bridge was used for signal conditioning.

- SLEPETZ, J.M., ZAGAESKI, T.F., and NOVELLO, R.F., *In-Plane Shear Test for Composite Materials*. Army Materials and Mechanics Research Center, AMMRC TR 78-30, July 1978.

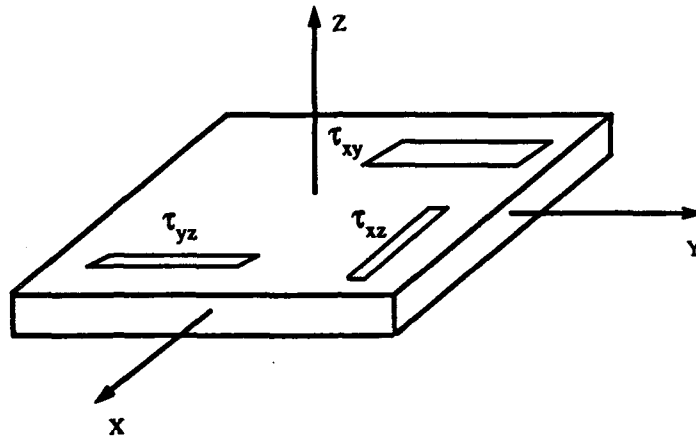


Figure 46 AFPB Specimen Material Axes Orientation

Tests were conducted at a rate of 0.02 inches/minute on a 20K *Instron* tension/compression testing machine. Table 3 lists specimen ultimate shear stress and shear strain values. Figures 47 through 49 illustrate all interlaminar and intralaminar test results.

Table 3 AFPB Specimen Dimensions and Test Results

Specimen No	W (in)	t (in)	τ_{max} (psi)	γ_{max} (μstrain)
τ_{xy} -1	0.614	0.630	19,285	9,200
τ_{yz} -1	0.546	0.100	11,264	11,930
τ_{yz} -2	0.552	0.100	10,417	9,940
τ_{xz} -1	0.594	0.097	9,910	14,150
τ_{xz} -2	0.589	0.104	9,060	9,500

TAU XY VS GAMMA XY
 (E2-CLASS/POLYESTER HOVEN ROVING)

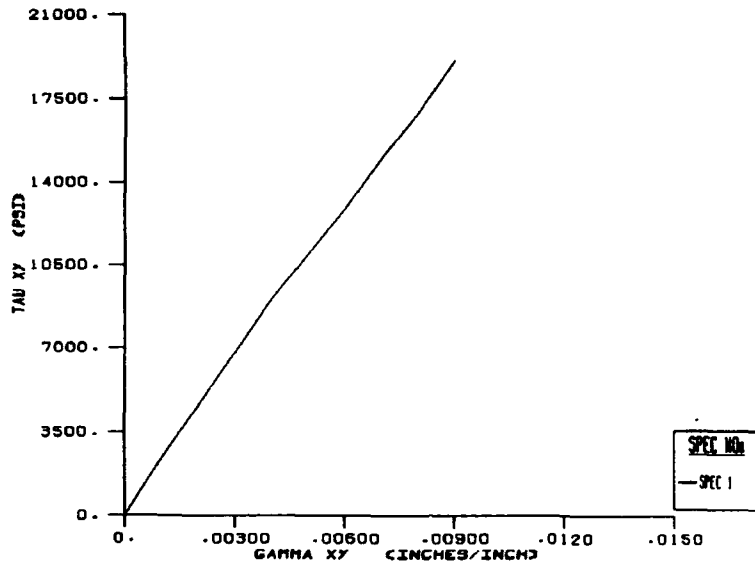


Figure 47 τ_{xy} vs γ_{xy}

TAU XZ VS GAMMA XZ
 (E2-CLASS/POLYESTER HOVEN ROVING)

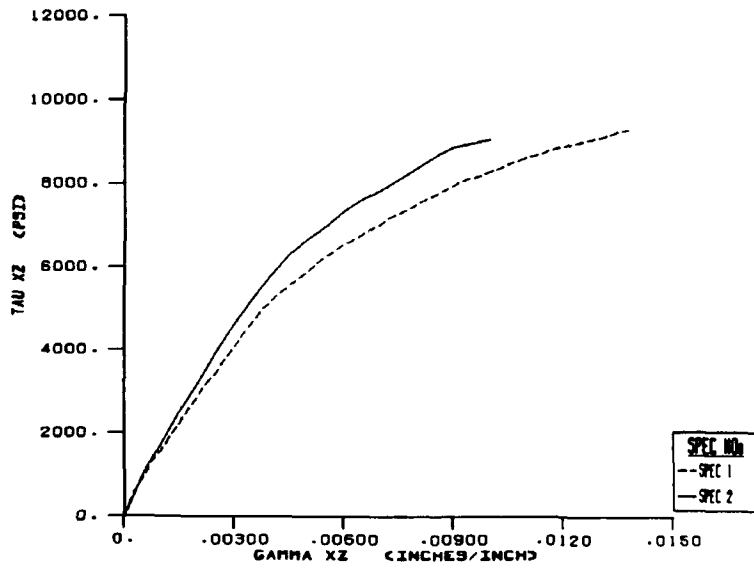


Figure 48 τ_{xz} vs γ_{xz}

TAU YZ VS GAMMA YZ
 (S2-GLASS/POLYESTER WOVEN ROVING)

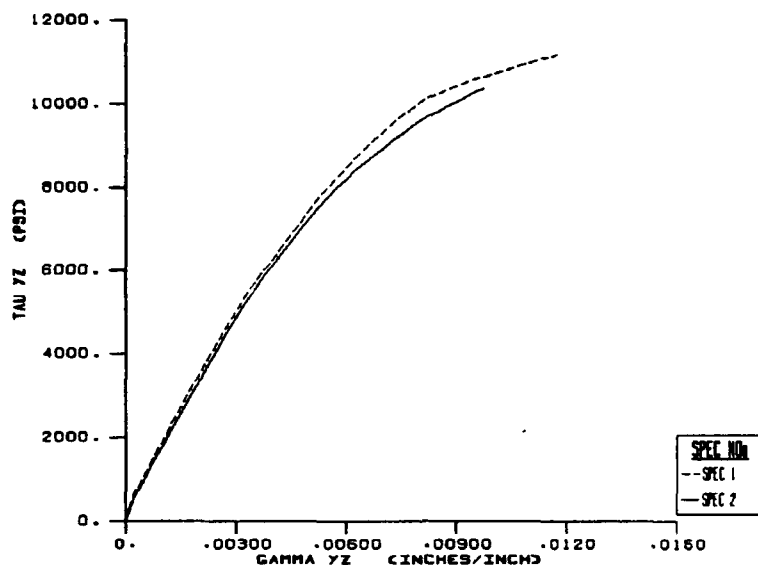


Figure 49 τ_{yz} vs γ_{yz}

BOLT BEARING STRESS STATE PREDICTIONS

Both bolt preload and combined bolt preload/bolt bearing stress state conditions were predicted with a 3D, nonlinear elastic, *Abaqus* finite element model of a typical single connector arrangement. Finite element constitutive equations were developed for the S2 woven roving material from mechanical properties obtained from tension, compression, intralaminar shear, and interlaminar shear tests. A nonlinear material subroutine was developed to effectively model interlaminar material behavior. Model stress states for an increasing series of axial bolt compressive preloads were obtained and superimposed with a uniform far field stress representation of peak bolt bearing loads obtained from BJan calculations using the maximum permissible roadarm vertical displacement.

Single Connector Three Dimensional Finite Element Model

A quarter symmetry model of a typical single connector of the roadwheel housing joint was constructed using the model generation features of *Patran*. Shown in Figure 50, the model consisted of the steel roadwheel housing plate, an S2 glass/polyester woven roving composite plate, and a steel bolt washer. Half symmetry was used in both the in-plane and through thickness directions to create a quarter symmetric model of minimum size.

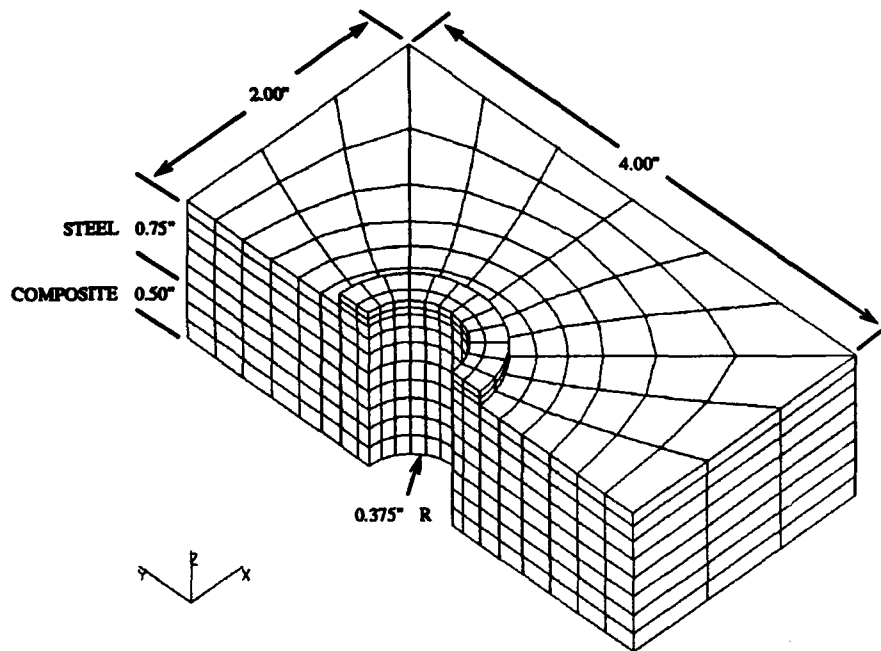


Figure 50 CIFV Friction Joint Finite Element Model

Three isoparametric element types were used from the Abaqus element library in the finite element representation of the model. Twenty noded quadratic displacement C3D20 solid continuum elements were used to model the steel and composite plates as well as the bolt washer. Eighteen noded INTER9 gap/interface friction elements were used to model contact between the common surfaces of the plates and washer. Two noded IRS13 contact elements were used to form a circular rigid surface which fit the model's bolt hole identically with zero clearance. Quadratic displacement C3D27 variable node solid continuum elements were used in those elements of the plates and washer that surrounded the rigid surface and sandwiched the gap/interface elements. The first ring of model elements were sized to the chamfered region underneath the bolt head to facilitate the application of axial compressive bolt preloads on the model. The model was bounded by symmetry conditions. All nodes on the Y-Z plane @ $X = 0$ were constrained from moving in the x direction while all nodes on the X-Y plane @ $Z = 0$ were constrained from moving in the z direction. Frictionless contact was assumed for all INTER9 elements. All rigid surface degrees of freedom were also constrained.

Conventional continuum element formulations and theories governed all continuum element behavior while Lagrangian multiplier theory was employed with all IRS13 and INTER9 elements to enforce contact between the plates, washer, and rigid surface.¹⁴ Contact was said to have occurred at a zero separation distance between respective nodes of each IRS13 and INTER9 element. Displacements of nodes in contact were limited to tangential directions.

14. HIBBIT, KARLSSON, and SORENSON, "ABAQUS Theory Manual", Version 7.1 Hibbit, Karlsson, and Sorenson Inc., Providence, R.I.

Constitutive Equation Development

Mechanical test results were evaluated to obtain mechanical property constants to form stress-strain constitutive equations for the S2 glass/polyester woven roving material. Average in-plane and out-of-plane tangent moduli (E_{xx} , E_{zz}) were determined from tension and compression test results respectively. Average in-plane and out-of-plane tangent Poisson ratios (ν_{xy} , ν_{zx}) were also obtained from these tests as well. An intralaminar shear modulus (G_{xy}) was obtained from the linear intralaminar AFPB test results. Numerical expressions were found for the nonlinear interlaminar shear moduli (G_{xz} , G_{yz}) by a least squares curve fitting of average interlaminar shear stress-strain AFPB test results. Remaining mechanical properties were found from the quasi-isotropic nature of the woven roving and the well known Poisson ratio reciprocity relationship which is expressed as;

$$\frac{\nu_{ij}}{E_i} = \frac{\nu_{ji}}{E_j} \quad (31)$$

Table 4 lists the interlaminar shear curve fit constants while Table 5 lists all mechanical property values obtained from the mechanical property tests and Equation 31.

Table 4 S2-Glass/polyester Woven Roving Shear Curve Fit Constants

	γ_{ij}	C_0	C_1	C_2
τ_{xz}	< 0.01	1.837xE6	1.379xE8	4.187xE9
τ_{xz}	> 0.01	5.405xE3	3.368xE5	
τ_{yz}	< 0.01	1.820xE6	7.037xE7	7.245xE8
τ_{yz}	> 0.01	7.904xE3	2.544xE5	

Table 5 S2-Glass/polyester Woven Roving Mechanical Properties

E_{xx} (psi)	E_{yy} (psi)	E_{zz} (psi)	G_{xy}	ν_{xy}	ν_{yx}	ν_{xz}	ν_{yz}	ν_{zx}	ν_{zy}
3.431xE6	3.431xE6	5.900xE5	2.098xE6	0.2812	0.2812	0.6688	0.6688	0.1150	0.1150

Three dimensional constitutive equations for the S2 glass/polyester woven roving material were calculated using the mechanical properties in Table 5 and the 3D orthotropic stress strain relations given from Reference 15 as;

15. JONES, R.M., Mechanics of Composite Materials, McGraw-Hill Book Company, New York, 1975.

$$\begin{pmatrix} \sigma_x \\ \sigma_y \\ \sigma_z \\ \tau_{xy} \\ \tau_{xz} \\ \tau_{yz} \end{pmatrix} = \begin{pmatrix} C_{11} & C_{12} & C_{13} & 0 & 0 & 0 \\ C_{12} & C_{22} & C_{23} & 0 & 0 & 0 \\ C_{13} & C_{23} & C_{33} & 0 & 0 & 0 \\ 0 & 0 & 0 & C_{44} & 0 & 0 \\ 0 & 0 & 0 & 0 & C_{55} & 0 \\ 0 & 0 & 0 & 0 & 0 & C_{66} \end{pmatrix} \begin{pmatrix} \epsilon_x \\ \epsilon_y \\ \epsilon_z \\ \gamma_{xy} \\ \gamma_{xz} \\ \gamma_{yz} \end{pmatrix}$$

where;

(32)

$$\begin{aligned} C_{11} &= \frac{[1 - (v_{23})(v_{32})]}{[(E_2)(E_3)(\Delta)]} & C_{12} &= \frac{[v_{21} + (v_{31})(v_{23})]}{[(E_2)(E_3)(\Delta)]} & C_{44} &= G_{xy} \\ C_{22} &= \frac{[1 - (v_{13})(v_{31})]}{[(E_1)(E_3)(\Delta)]} & C_{13} &= \frac{[v_{31} + (v_{21})(v_{32})]}{[(E_2)(E_3)(\Delta)]} & C_{55} &= G_{xz} \\ C_{33} &= \frac{[1 - (v_{12})(v_{21})]}{[(E_1)(E_2)(\Delta)]} & C_{23} &= \frac{[v_{32} + (v_{12})(v_{31})]}{[(E_1)(E_3)(\Delta)]} & C_{66} &= G_{yz} \end{aligned}$$

and;

$$\Delta = \frac{[1 - (v_{12})(v_{21}) - (v_{23})(v_{32}) - (v_{13})(v_{31}) - 2(v_{21})(v_{32})(v_{13})]}{[(E_1)(E_2)(E_3)]}$$

Table 6 lists the S2 glass/polyester woven roving constitutive equation constants resulting from the mechanical property values of Table 5 and applications of Equations 32.

Table 6 S2-Glass/polyester Woven Roving Constitutive Equation Constants

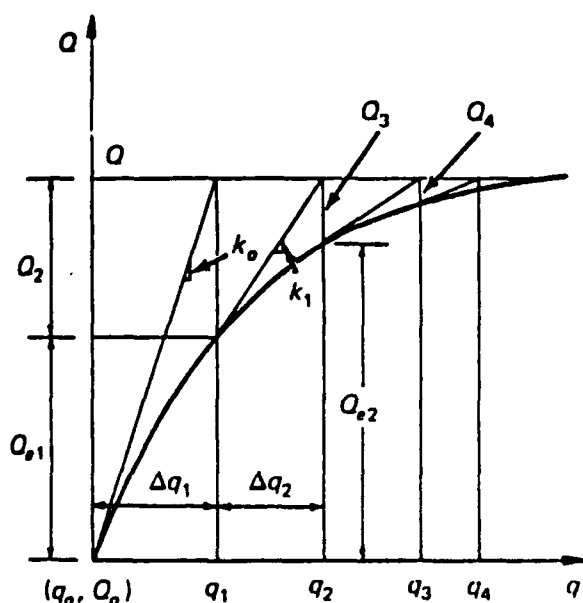
STACKINGSEQUENCE	C ₁₁ (psi)	C ₁₂ (psi)	C ₁₃ (psi)	C ₂₂ (psi)	C ₂₃ (psi)	C ₃₃ (psi)
[(0/90/45) _n]	4.3754xE6	1.6974xE6	6.9838xE5	4.3754xE6	6.9838xE5	7.5064xE5

Abaqus User Material Subroutine

The constitutive equations were implemented in the *Abaqus* finite element code through use of a user material subroutine (UMAT). The subroutine used a Newton-Raphson solution formulation to account for the nonlinear interlaminar shear behavior of the S2 glass/polyester woven roving material. Shown in Figure 51, the solution technique required the calculation of updated interlaminar stresses ($Q_{e,i-1}$) and interlaminar tangent moduli (k^i) from updated strains (q_i). These values were passed back to the finite element code where

equilibrium force residuals (Q_i) were calculated and applied to the system of equations in the next iteration. Iterations continued until the resulting equilibrium residuals fell below a specified tolerance ($Q_i < Q_{tol}$).

An *Abaqus* UMAT subroutine was written to 1) update current strains, 2) calculate updated stresses based on these updated strains, and 3) form the Jacobian of the present constitutive matrix. These three functions were performed using the constitutive equations and their constants.



$$\{Q_i\} = \{Q\} - \{Q_{e, i-1}\}$$

$$[k^{(i)}]\{\Delta q_i\} = \{Q_i\}$$

$$\{q_i\} = \{q_0\} + \sum_{j=1}^i \{\Delta q_j\}$$

$$[k^{(i)}] = [k_{i-1}]$$

Figure 51 Newton-Raphson Nonlinear Solution Technique

Finite Element Computations

Bolt preloads were applied to the single connector finite element model through four separate load steps in the *Abaqus* code. The steps applied a 20,000 lb axial compressive bolt preload in equal 5,000 lb increments. This force, whose value was based on the experimentally determined preloads, was applied through a stress boundary condition on the top face of the first ring of bolt washer elements. Each of the four bolt preload steps were subjected to a bolt bearing force of 5757 lbs resulting from maximum permissible roadwheel arm displacement. This was simulated by applying a 1440 psi and 960 psi far field uniform σ_y pressure distribution to opposite ends of the composite and steel plates respectively as shown in Figure 52. In keeping with the rigid pin assumption, the top surface of the washer was held in its deformed state while the far field pressure distributions were applied. All steps were divided into a maximum possible ten increments. Incrementation of each step was controlled by the automatic incrementation scheme of the *Abaqus* code.

Convergence of the analysis at each increment was controlled by dictating an acceptable solution tolerance level (P_{tol}) of the Lagrangian, virtual work based equilibrium

equations. Iteration of the Newton-Raphson nonlinear solution scheme was continued until minimum model maximum residual nodal forces ($MAX RES$) fell below the *Abaqus* suggested 0.1% value of model maximum nodal reaction forces ($R_{f \max}$).¹⁴ Each step's tolerance level, model maximum residual and reaction nodal forces, and resulting number of increments are shown in Table 7.

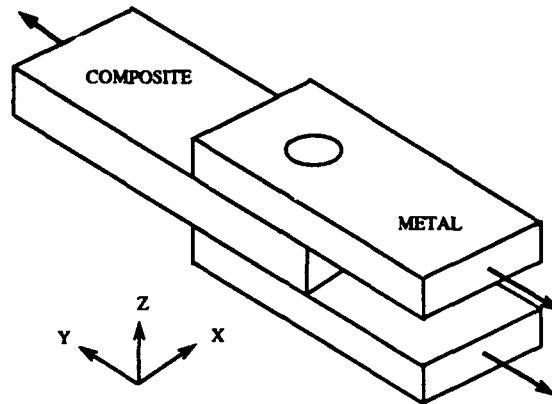


Figure 52 Single Connector Loading Scheme

Table 7 Friction joint FEA Convergence Criteria Results

LOAD (lbs)		STEP #	INC #	ITTER#	P_{TOL}	MAXRES	$R_{F \max}$	% $R_{F \max}$
PRELOAD	BEARING							
5,000	0	A1	1	8	0.01	4.06E-3	-6.04E+0	6.72E-2
10,000	0	B1	1	6	0.02	9.08E-3	-2.82E+1	3.21E-2
15,000	0	C1	1	6	0.03	8.84E-3	-4.26E+1	2.08E-2
20,000	0	D1	4	6	0.04	8.82E-3	-5.71E+1	1.54E-2
5,000	5,757	A2	4	6	0.01	1.03E-3	+4.58E+1	2.25E-3
10,000	5757	B2	4	6	0.02	1.11E-2	+5.94E+1	1.87E-2
15,000	5,757	C2	4	5	0.03	2.14E-2	+8.91E+1	2.40E-2
20,000	5,757	D2	4	5	0.04	1.08E-2	+1.19E+2	9.10E-2

14. HIBBIT, KARLSSON, and SORENSON, "ABAQUS Theory Manual", Version 7.1 Hibbit, Karlsson, and Sorenson Inc., Providence, R.I.

Finite Element Results

Results from the finite element computations may be seen in Figures 53-64. Uniform pressure loading of the first ring of washer elements in the through thickness direction produced contact between the majority of the washer elements and the steel plate. As seen in Figure 53a, a nearly symmetric compressive σ_{zz} pressure distribution developed within the steel plate from this simulated bolt preloading. The top two inner ring elements of the steel plate came in contact with the rigid surface. Radial stresses resulting from this contact appeared to be uniform around the bolt hole, but decayed rapidly with increasing depth. When normalized to axial bolt stress, they appeared independent of bolt preload as seen in Figure 54a.

Bolt preload also produced total contact between the steel and composite plates. A radially decaying symmetric σ_{zz} pressure distribution developed in the composite plate. As seen in Figures 59 and 60, higher bolt preloads increased the magnitude of this distribution. Maximum σ_{zz} pressure values rose from -899 psi to -3,441 psi as bolt preloads were increased from 5,000 lbs to 20,000 lbs. As with the steel plate, contact occurred between the composite plate and the rigid surface. However, only the top inner ring of nodes ($z=0.500$ ") contacted the rigid surface generating minimal radial stresses as seen in Figure 54b.

Application of the 5,757 lb bolt bearing load to each of the four preload stress states produced an asymmetry in the washer σ_{zz} pressure distribution. Poisson contraction of the non bearing portions of both the steel and composite plates combined with the rigid bolt assumptions (zero z displacement of preloaded washer top) reduced maximum washer σ_{zz} pressure to -17,900 psi and -15,650 psi from -22,400 psi over the steel and composite bearing sections respectively. The maximum magnitude and radially symmetric decay of the σ_{zz} pressure distribution in the steel plate was also altered by the bolt bearing load. As seen in Figure 53b, maximum steel plate σ_{zz} pressures fell from -29,150 psi to -20,150 psi at the washer interface above the composite plate bearing area. The decay of these stresses through the thickness of the steel plate was slower above the composite plate bearing area.

For the 5,000 lb bolt preload case, application of the bearing load increased the depth of contact between the steel plate and rigid surface to the next (sixth) nodal layer ($z=0.91665$ "). Steel plate radial stresses (normalized to pin bearing stresses) became highly dependent upon angular location. Increasing reductions of this normalized radial stress with depth were observed above the composite plate bearing area. As seen in Figure 55a, these reductions were large enough to create partial contact for both the fifth ($z=1.000$ ") and sixth ($z=0.91665$ ") nodal planes. This radial stress behavior varied significantly in peak magnitude and distribution from the often assumed $4/\pi (\cos \theta)$ function. Higher bolt preloads magnified these variations of normalized steel plate radial stress distribution while gradually eliminating the partial contact of the sixth nodal layer. Peak radial stresses were as high as thirteen times that of the $4/\pi (\cos \theta)$ function for the 20,000 lb bolt preload/bearing load case.

With the exception of the far field edges, the steel and composite plate remained in total contact for all but the 5,000 lb bolt preload/5757 bolt bearing load case. As seen in Figures 61 and 62, bolt bearing and net section Poisson contraction conditions disrupted the

symmetric radially decaying σ_{zz} pressure distribution in the composite plate. Bearing area "brooming" of the composite plate increased σ_{zz} pressures while net section Poisson contraction (from bolt hole in-plane σ_{yy} stress concentrations) reduced them. As would be anticipated, larger bearing area increases and net section decreases in σ_{zz} pressures were observed at lower bolt preloads. At the 5,000 lb bolt preload, bolt bearing conditions doubled bearing area maximum σ_{zz} pressure from -750 psi to 1,500 psi while zeroing maximum σ_{zz} pressures from -750 psi in the net section. At this bolt preload level, partial contact between the steel and composite plates was observed along the bolt hole boundary for the first two elements below the net section.

Application of the 5,757 lb bolt bearing load and resulting variations in the composite plate σ_{zz} pressure distribution slightly lowered the friction load carrying capabilities of the joint. As determined from the summation of composite plate bottom surface normal reaction forces, these reductions increased as bolt preload decreased. Table 8 summarizes these results.

Peak in-plane normal and shear composite plate stresses were observed in the 20,000 lb bolt preload/ 5757 lb bolt bearing load case. All peak stresses, as shown in Figure 64, were found on the top surface of the composite plate along the bolt hole boundary. The analysis predicted a maximum σ_{xx} stress values of -8,970 psi at approximately 45 degrees up from the net section. Maximum σ_{yy} stress values of -14,000 psi were predicted directly above the pin in the bearing area while a maximum τ_{xy} stress value of -8,100 psi was observed at approximately 18 degrees up from the net section. A maximum interlaminar τ_{xz} and τ_{yz} shear stress values of 1,540 psi and 1,670 psi was predicted in the bearing area. Most of these predicted maximum joint stresses were substantially lower than their ultimate stress counterparts obtained from the mechanical property tests. In direct comparison to these values ($\tau_{xy \text{ ult}} = 19,285$ psi, $\tau_{xz \text{ ult}} = 9,485$ psi, and $\tau_{yz \text{ ult}} = 10,840$ psi) respective joint design intralaminar and interlaminar factors of safety of 2.4, 6.1, and 6.5 presented themselves. However, maximum compressive bearing stresses (-14,000 psi) appear quite close to the in-plane compressive failure strength ($\sigma_{xx \text{ ult}} = \sigma_{yy \text{ ult}} = -16,000$ psi).¹⁶

Table 8 Effects of Bolt Preload on Ultimate Joint Friction Load

LOAD (LBS)		Σ RF	% Δ
PRELOAD	BEARING		
5000	0	5000.00	
10000	0	9999.30	
15000	0	15000.76	
20000	0	20001.19	
5000	5757	4281.59	14.30
10000	5757	9281.62	7.18
15000	5757	14279.62	4.80
20000	5757	19284.57	3.58

16. FAZILI, J, GOEKE, E., and NUNES, J., *Characterization of Thick Glass Reinforced Composites*. AMTL-TR, Watertown, MA, to be published

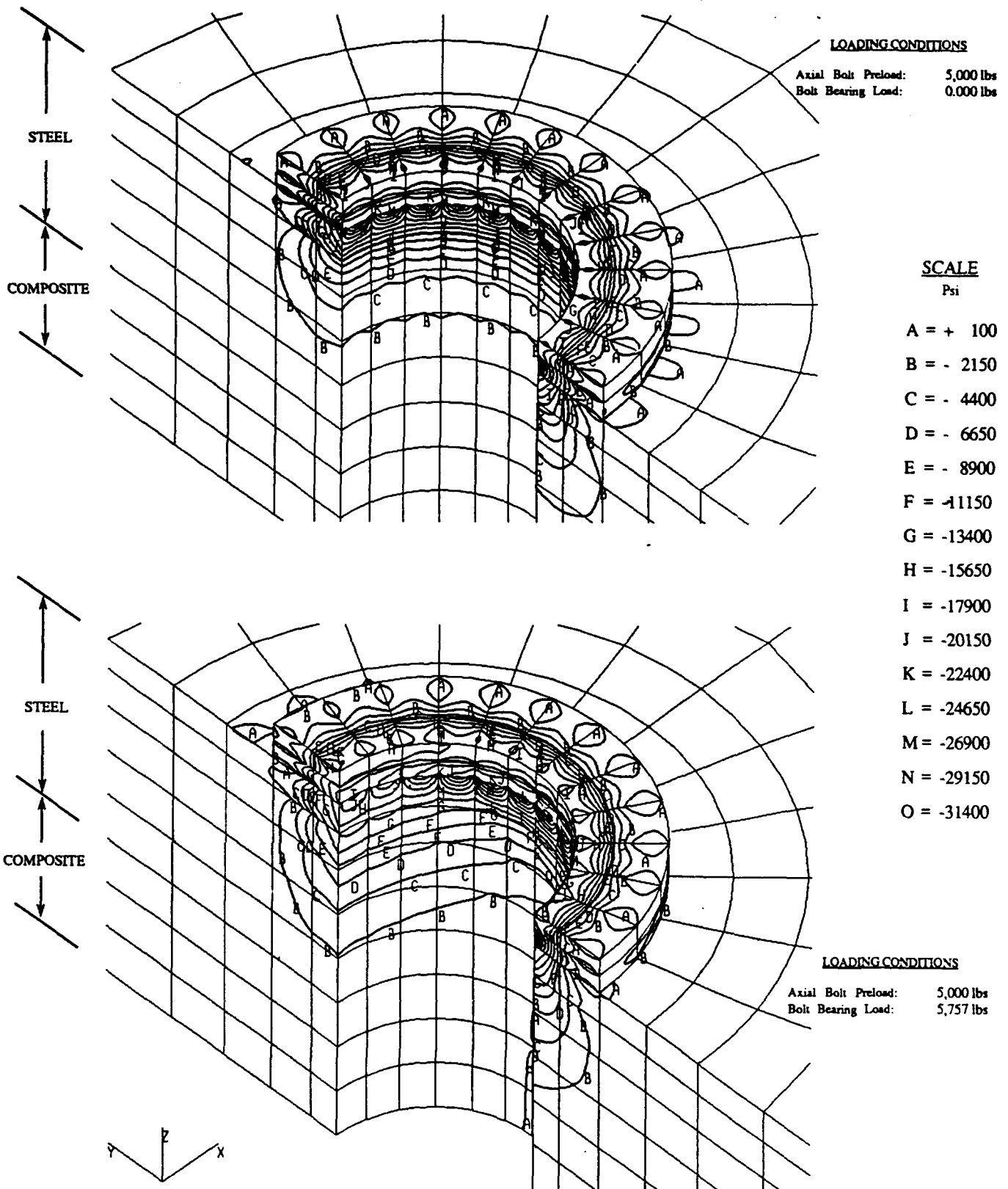
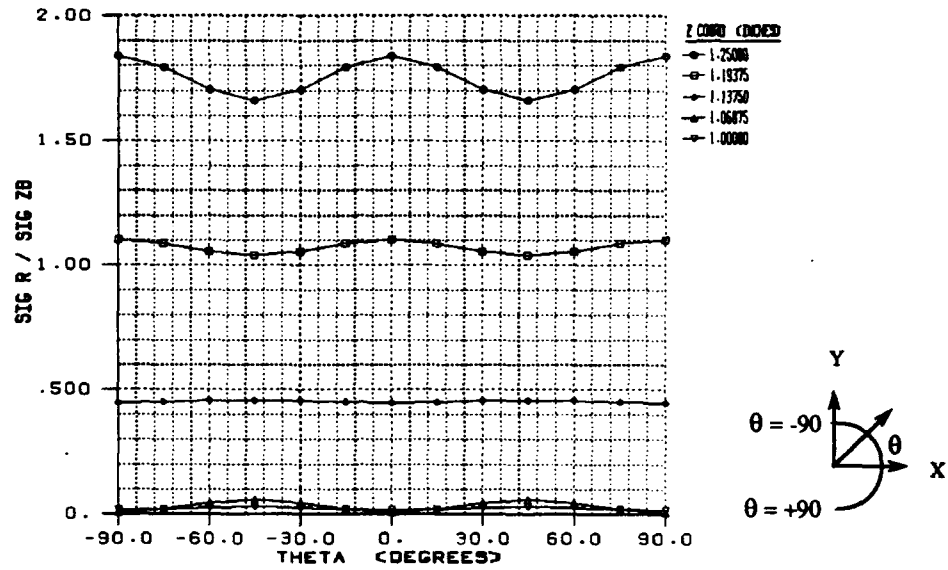


Figure 53 Complete Model σ_z Stress Distribution for Bolt Preload/Bearing Load Cases

NORMALIZED METAL PLATE RADIAL STRESS VS ANGULAR LOCATION
 (MODEL LOADING: BOLT PRELOAD)



NORMALIZED COMPOSITE PLATE RADIAL STRESS VS ANGULAR LOCATION
 (MODEL LOADING: BOLT PRELOAD)

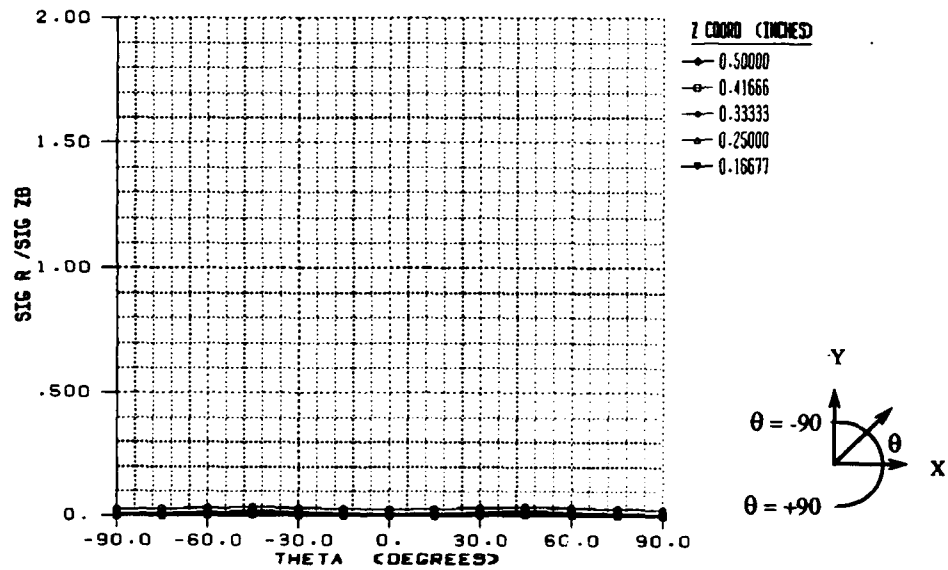
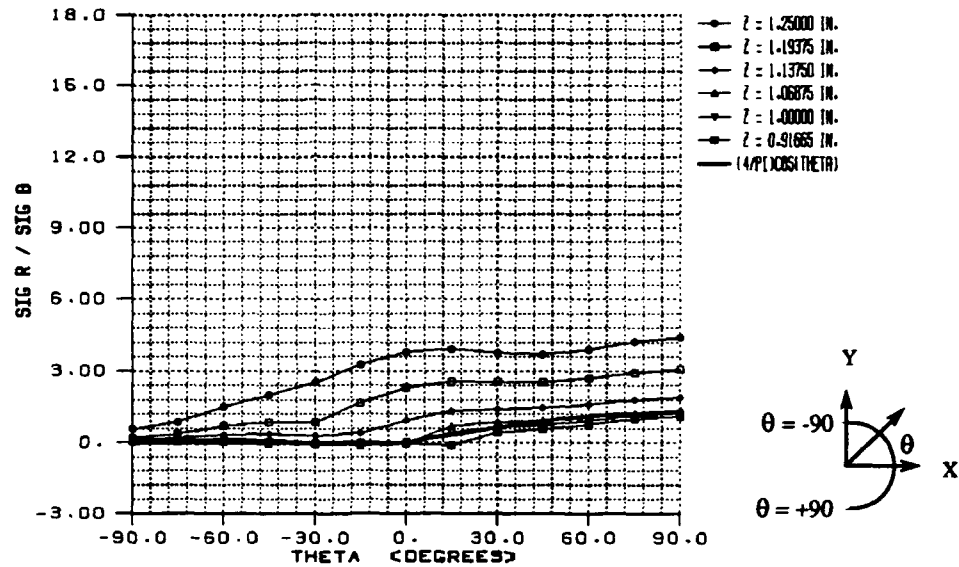


Figure 54 Normalized Metal and Composite Plate σ_r Stress vs. Angular Location
 (Bolt Preload Model Loading)

NORMALIZED METAL PLATE RADIAL STRESS VS ANGULAR LOCATION
 (MODEL LOADING: BOLT BEARING AND 5000 LB BOLT PRELOAD)



NORMALIZED METAL PLATE RADIAL STRESS VS ANGULAR LOCATION
 (MODEL LOADING: BOLT BEARING AND 10000 LB BOLT PRELOAD)

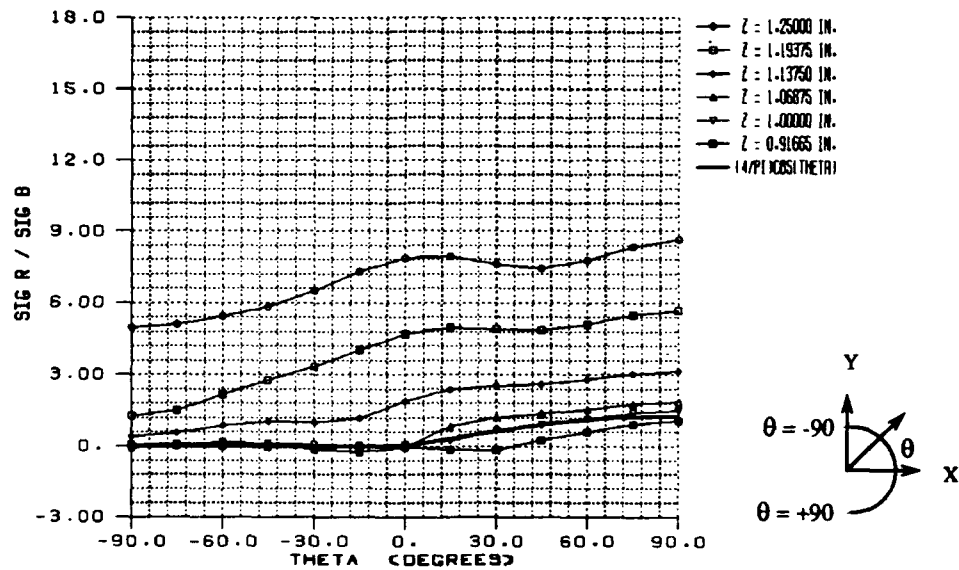
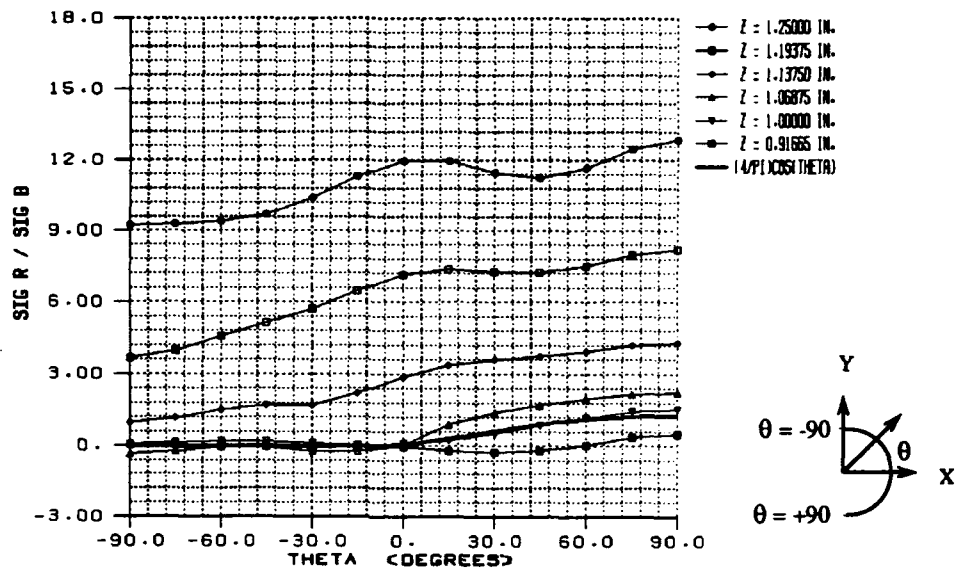


Figure 55 Normalized Metal Plate σ_r Stress vs. Angular Location
 (Bolt Preload and Bolt Bearing Model Loading)

NORMALIZED METAL PLATE RADIAL STRESS VS ANGULAR LOCATION
(MODEL LOADING: BOLT BEARING AND 15000 LB BOLT PRELOAD)



NORMALIZED METAL PLATE RADIAL STRESS VS ANGULAR LOCATION
(MODEL LOADING: BOLT BEARING AND 20000 LB BOLT PRELOAD)

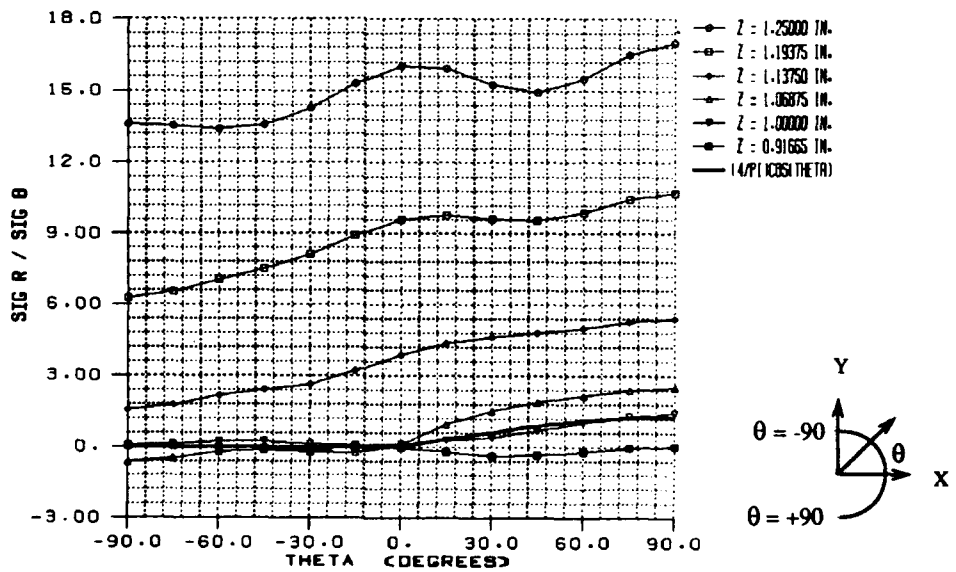
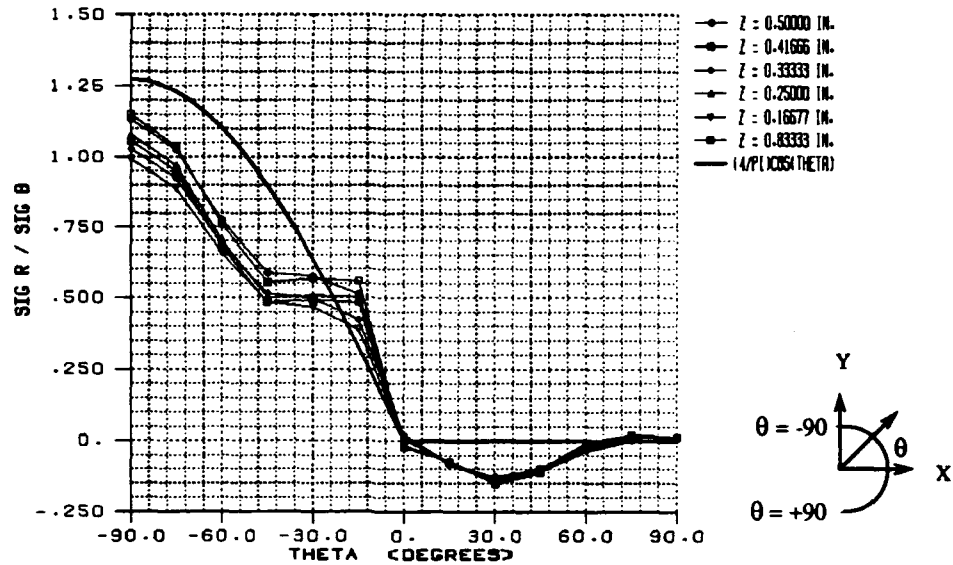


Figure 56 Normalized Metal Plate σ_r Stress vs. Angular Location
(Bolt Preload and Bolt Bearing Model Loading)

NORMALIZED COMPOSITE PLATE RADIAL STRESS VS ANGULAR LOCATION
 (MODEL LOADING: BOLT BEARING AND 5000 LB BOLT PRELOAD)



NORMALIZED COMPOSITE PLATE RADIAL STRESS VS ANGULAR LOCATION
 (MODEL LOADING: BOLT BEARING AND 10000 LB BOLT PRELOAD)

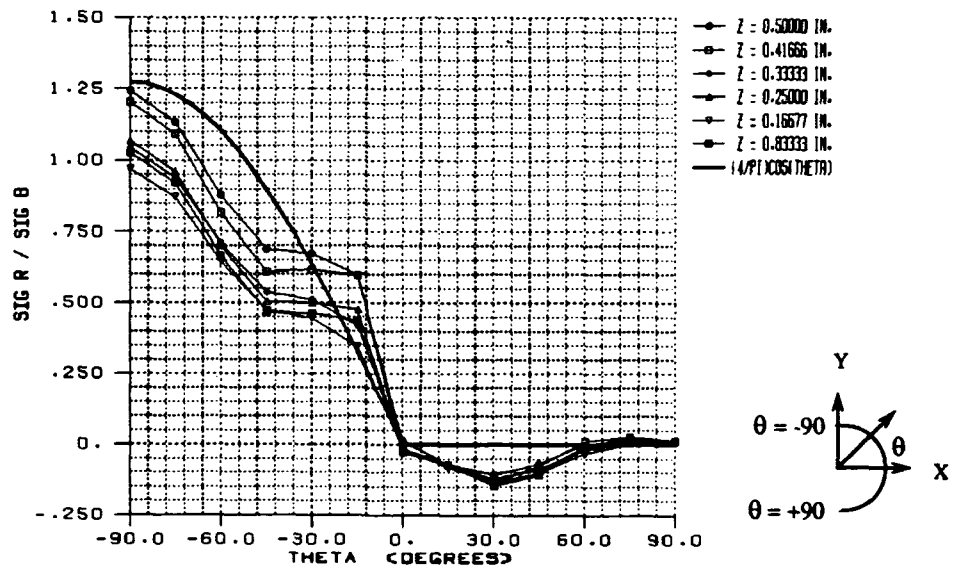
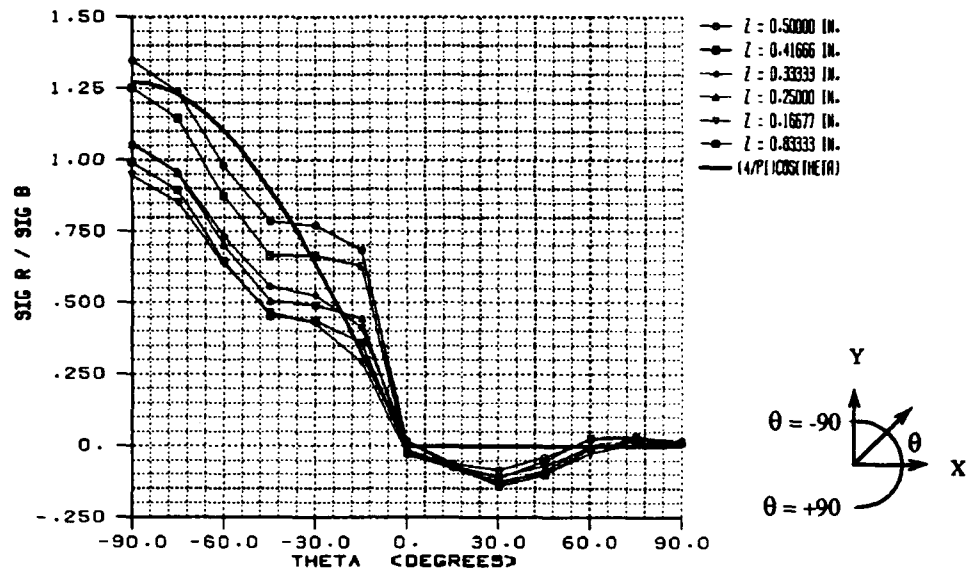


Figure 57 Normalized Composite Plate σ_r Stress vs. Angular Location
 (Bolt Preload and Bolt Bearing Model Loading)

NORMALIZED COMPOSITE PLATE RADIAL STRESS VS ANGULAR LOCATION
 (MODEL LOADING: BOLT BEARING AND 15000 LB BOLT PRELOAD)



NORMALIZED COMPOSITE PLATE RADIAL STRESS VS ANGULAR LOCATION
 (MODEL LOADING: BOLT BEARING AND 20000 LB BOLT PRELOAD)

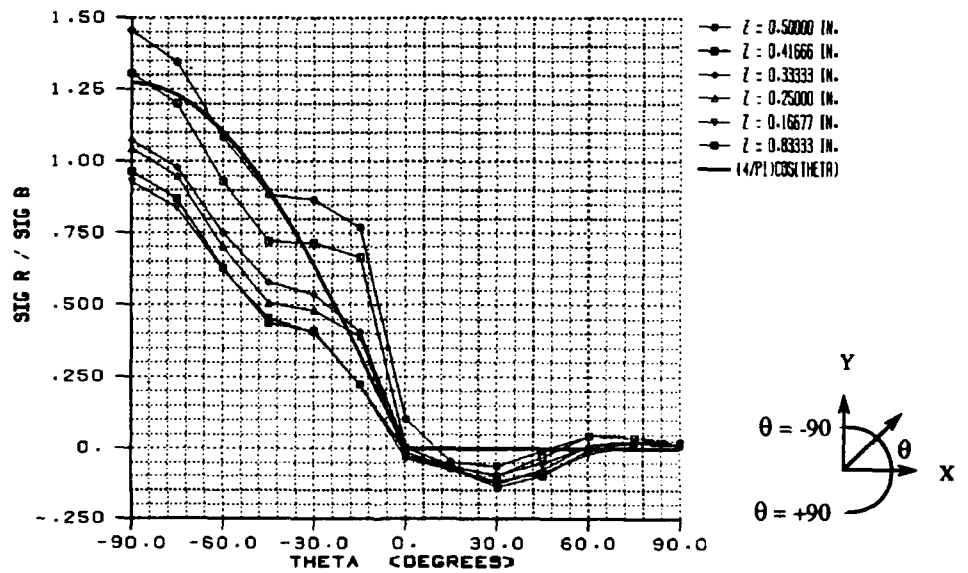
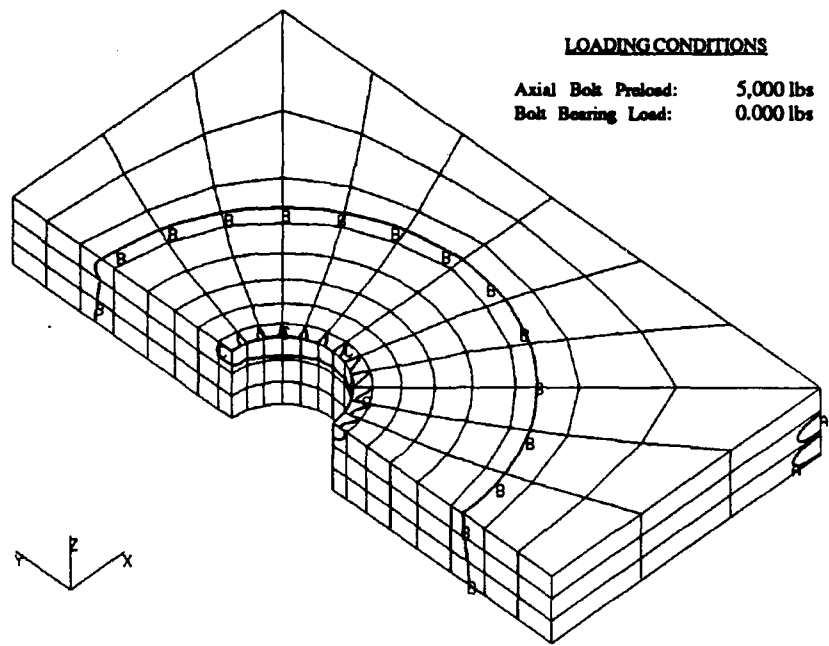


Figure 58 Normalized Composite Plate σ_r Stress vs. Angular Location
 (Bolt Preload and Bolt Bearing Model Loading)

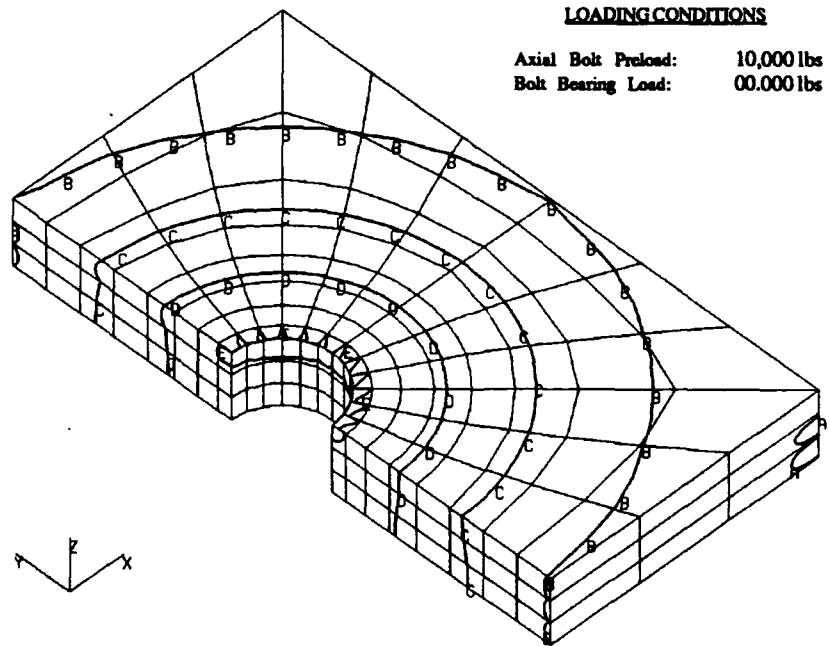


LOADING CONDITIONS

Axial Bolt Preload: 5,000 lbs
 Bolt Bearing Load: 0.000 lbs

SCALE
Psi

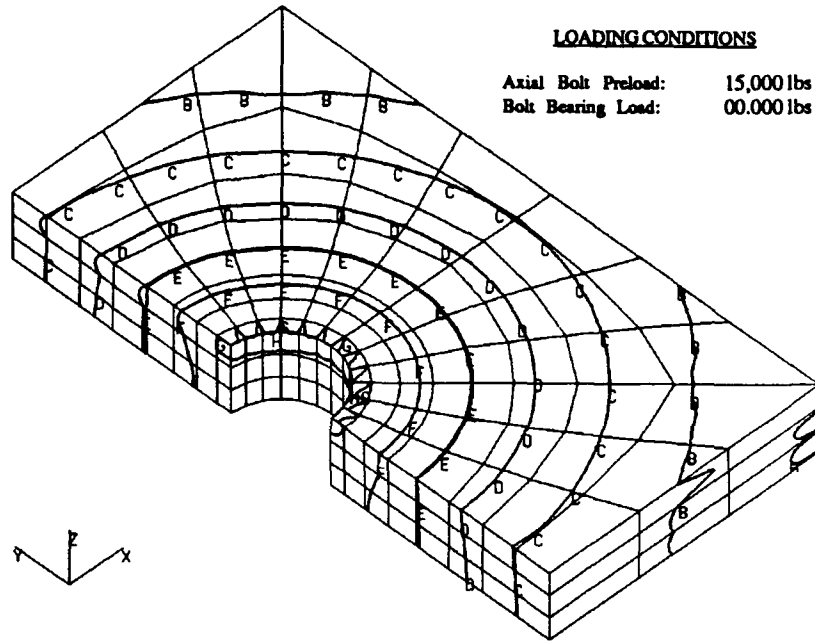
- A = - 0
- B = - 375
- C = - 750
- D = -1125
- E = -1500
- F = -1875
- G = -2250
- H = -2625
- I = -3000
- J = -3375
- K = -3750
- L = -4125
- M = -4500
- N = -4875
- O = -5250



LOADING CONDITIONS

Axial Bolt Preload: 10,000 lbs
 Bolt Bearing Load: 00.000 lbs

Figure 59 Composite Plate σ_z Stress Distribution for Bolt Preload Load Cases



SCALE
Psi

- A = - 0
- B = - 375
- C = - 750
- D = -1125
- E = -1500
- F = -1875
- G = -2250
- H = -2625
- I = -3000
- J = -3375
- K = -3750
- L = -4125
- M = -4500
- N = -4875
- O = -5250

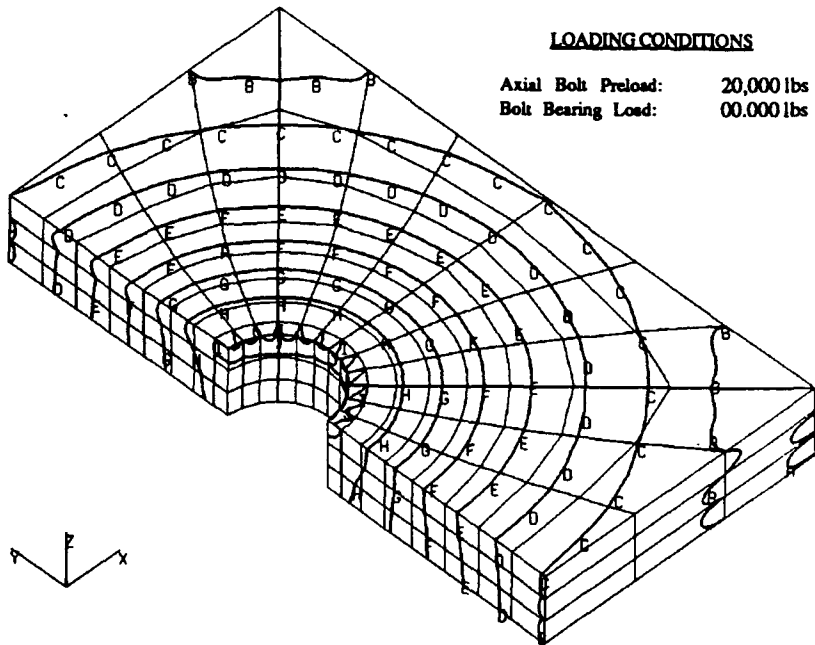
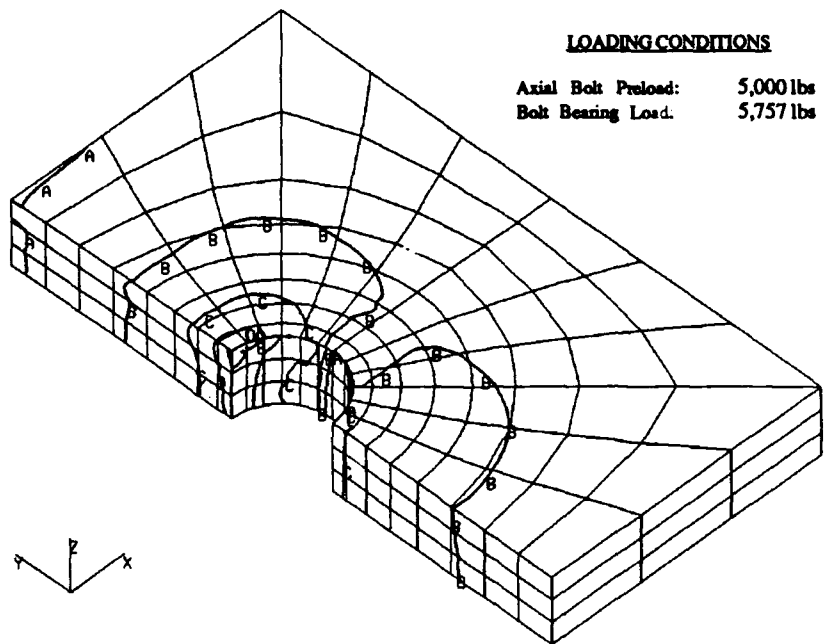


Figure 60 Composite Plate σ_z Stress Distribution for Bolt Preload Load Cases



SCALE
Psi

- A = - 0
- B = - 375
- C = - 750
- D = -1125
- E = -1500
- F = -1875
- G = -2250
- H = -2625
- I = -3000
- J = -3375
- K = -3750
- L = -4125
- M = -4500
- N = -4875
- O = -5250

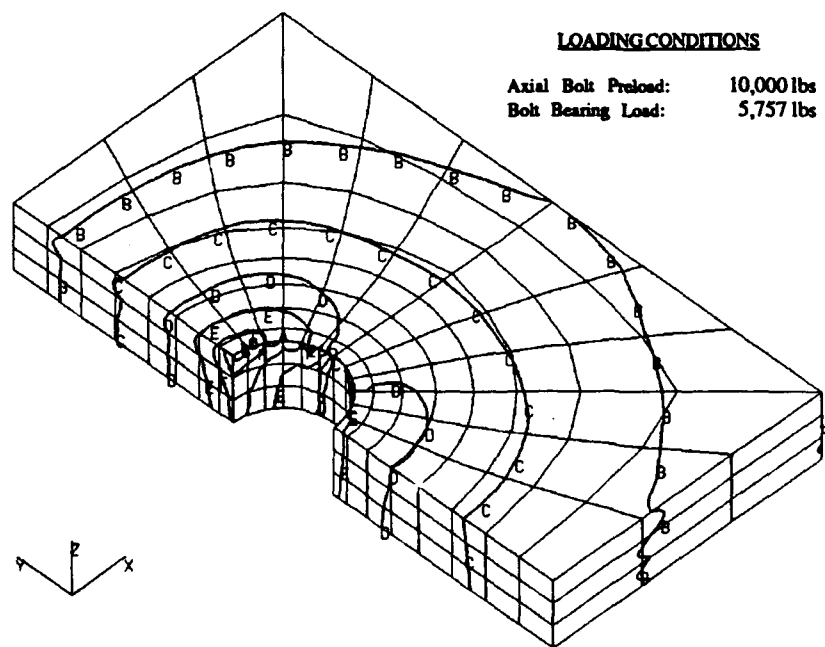
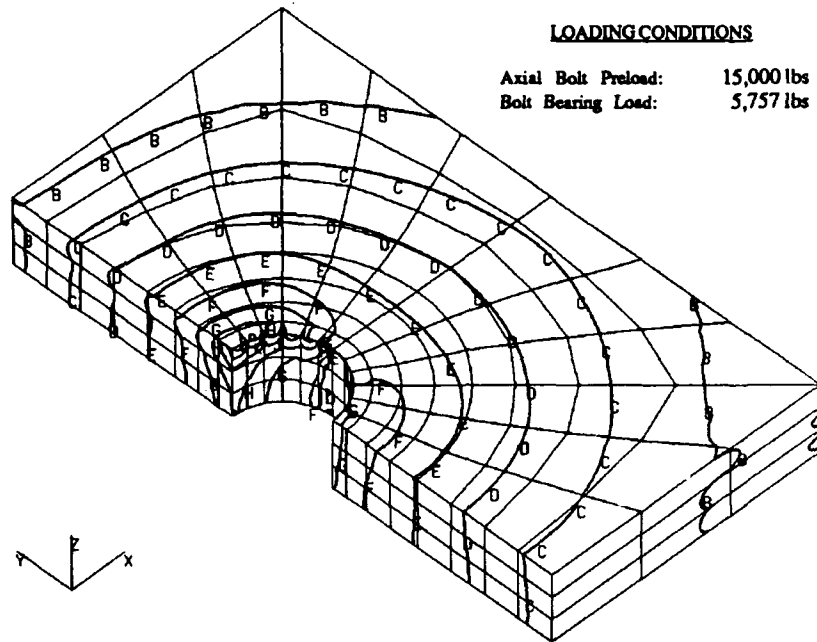


Figure 61 Composite Plate σ_z Stress Distribution for Combined Bolt Preload and Far Field Load Cases.



SCALE
Psi

- A = - 0
- B = - 375
- C = - 750
- D = -1125
- E = -1500
- F = -1875
- G = -2250
- H = -2625
- I = -3000
- J = -3375
- K = -3750
- L = -4125
- M = -4500
- N = -4875
- O = -5250

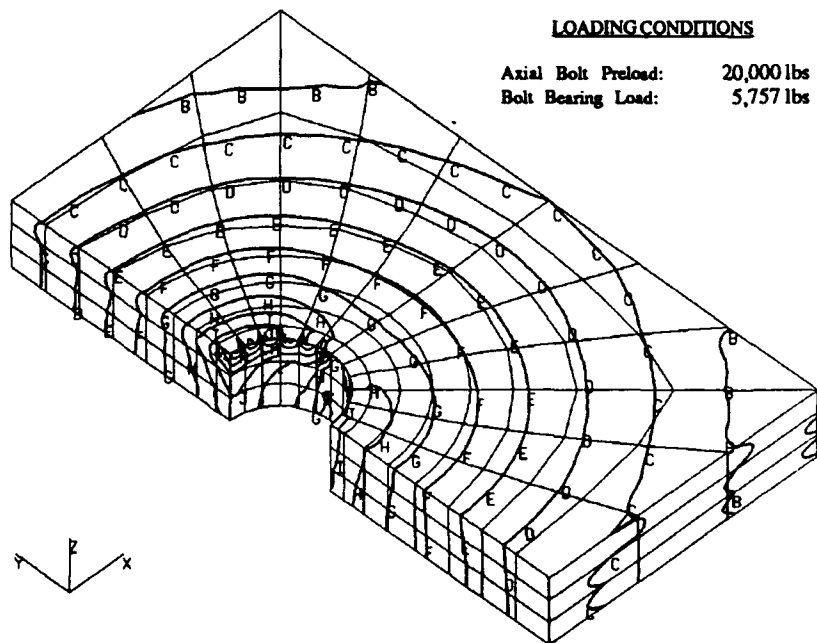
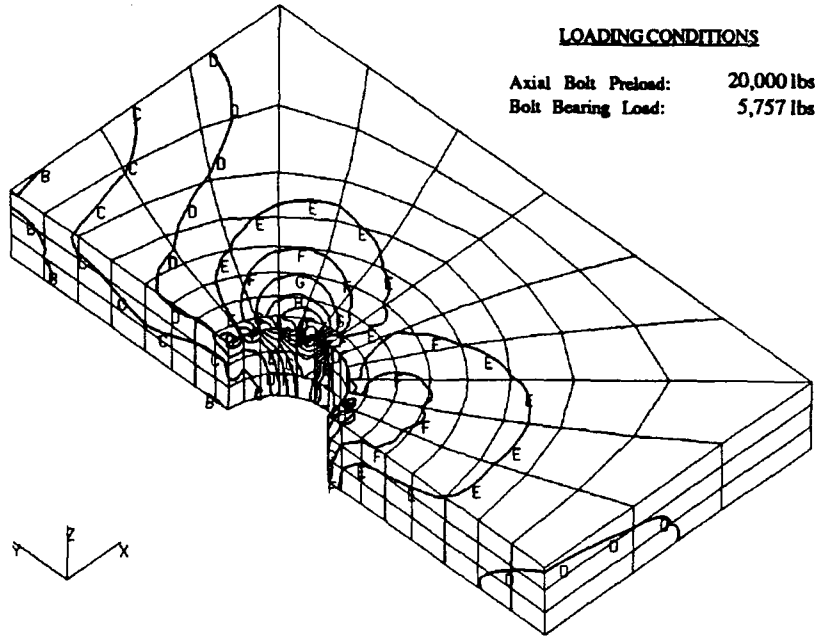


Figure 62 Composite Plate σ_z Stress Distribution for Combined Bolt Preload and Far Field Load Cases.

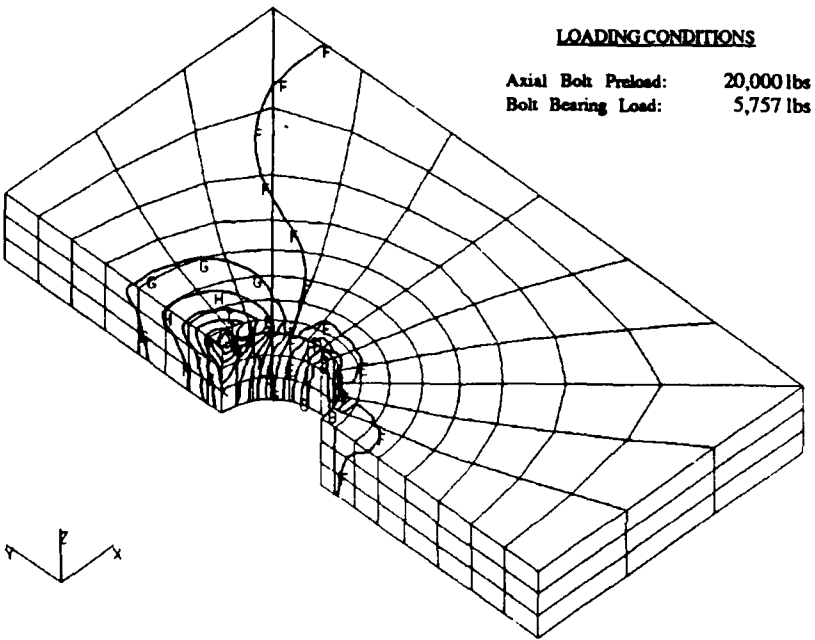


LOADING CONDITIONS

Axial Bolt Preload: 20,000 lbs
 Bolt Bearing Load: 5,757 lbs

SCALE
Psi

- A = +2900
- B = +2050
- C = +1200
- D = + 350
- E = - 500
- F = -1350
- G = -2200
- H = -3050
- I = -3900
- J = -4750
- K = -5600
- L = -6450
- M = -7300
- N = -8150
- O = -9000



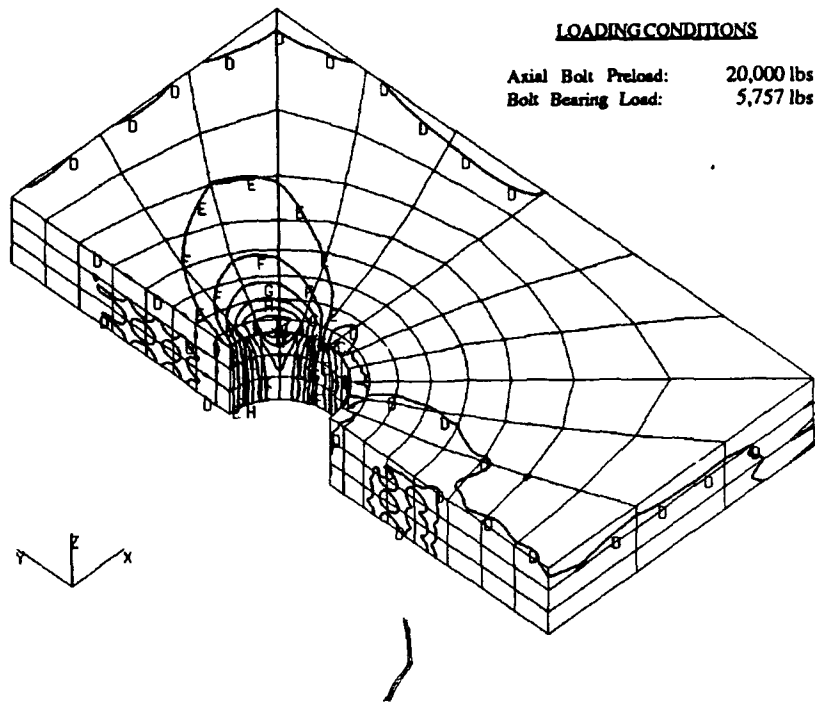
LOADING CONDITIONS

Axial Bolt Preload: 20,000 lbs
 Bolt Bearing Load: 5,757 lbs

SCALE
Psi

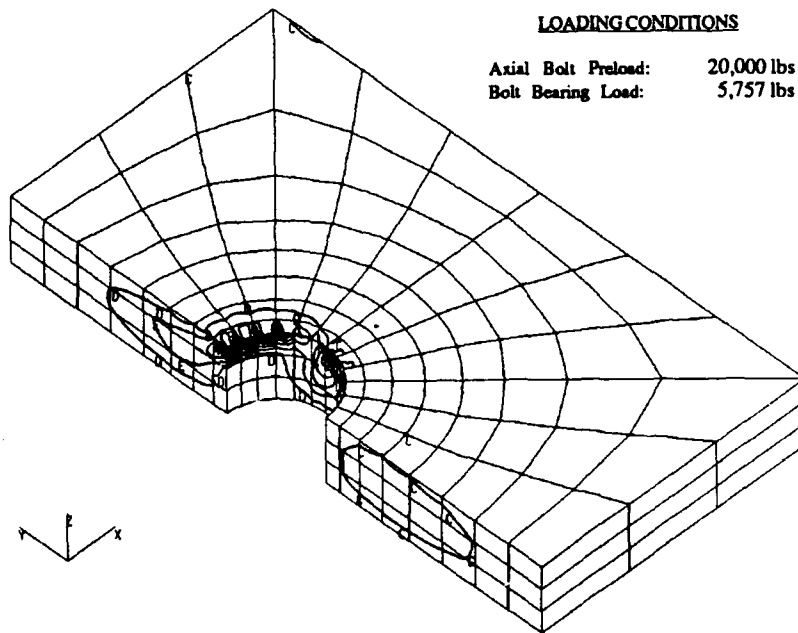
- A = + 8200
- B = + 6600
- C = + 5000
- D = + 3400
- E = + 1800
- F = + 200
- G = - 1400
- H = - 3000
- I = - 4600
- J = - 6200
- K = - 7800
- L = - 9400
- M = -11000
- N = -12600
- O = -14200

Figure 63 Composite Plate σ_{xx} and σ_{yy} Stress Distribution for Combined Bolt Preload and Far Field Load Cases.



SCALE
Psi

- A = +2250
- B = +1500
- C = + 750
- D = 0
- E = - 750
- F = -1500
- G = -2250
- H = -3000
- I = -3750
- J = -4500
- K = -5250
- L = -6000
- M = -6750
- N = -7500
- O = -8250



SCALE
Psi

- A = - 350
- B = - 200
- C = - 50
- D = + 100
- E = + 250
- F = + 400
- G = + 550
- H = + 700
- I = + 850
- J = +1000
- K = +1150
- L = +1300
- M = +1450
- N = +1600
- O = +1750

Figure 64 Composite Plate τ_{xy} and τ_{yz} Stress Distribution for Combined Bolt Preload and Far Field Load Case.

CONCLUSIONS

A shear/moment analysis program (BJAN) was developed and successfully used to determine the resultant connector loads of both the modified and original CIFV roadwheel housing joint designs as a function of static roadarm displacement and dynamic Perryman III DADS force/moment suspension data. Resultant connector forces were found to increase linearly with static roadwheel arm displacement for both roadwheel housing designs. A maximum connector force of 5,757 lbs was observed in the original housing design at a vertical roadarm distance of 14". Expansion of the bolt pattern in the modified housing design reduced this maximum static connector force by approximately 10%. Dynamic connector loads were larger for the more severe terrain 2 Perryman III test conditions. Terrain 2 simulation results indicate that a 4,576 lb maximum dynamic connector force presented itself in the original housing design. A 9% decrease in this force was observed in the modified housing design for these terrain conditions.

The effects of through thickness viscoelastic material relaxation on bolt preload was experimentally determined for the thick S2 glass/polyester woven roving material. Static relaxation tests indicated considerable variability in initial bolt preloads for the 158 ft-lbf pretorque while preload decay was limited to roughly only 5% of initial bolt preload over a 43 day test period. Effects of roadwheel housing surface traction fatigue loading on bolt preload decay were investigated in dynamic relaxation tests. Mean and fatigue load test conditions were obtained from a discrete fast Fourier transform of dynamic resultant connector loads which were determined for each Perryman III terrain situation. Both the high and low frequency dynamic tests did not show an appreciable effect on bolt preload decay.

Single connector slip tests were conducted to determine the relationship between bolt preload and joint slip load. Test results indicated that a linear relationship existed. The linearization coefficient (0.270) was used as an effective friction joint coefficient of friction in predicting multiple connector roadwheel housing slip.

A modified shear/moment slip analysis program (BJSAN) was developed to predict CIFV friction joint performance as a function of static roadarm displacement. The effective coefficient of friction determined in the single connector slip tests was employed to determine resultant connector loads and predict roadwheel housing slip. Results indicated that neither housing design slipped during the full range of roadarm vertical displacements. The additional out-of-plane moment significantly increased the load carrying capability of those connectors above the bolt pattern center of gravity while decreasing those below it. The modified roadwheel housing design had fewer connectors in slip (4) than the original design (7) at the largest roadarm displacement.

Bolt preload relaxation test results were used in conjunction with the modified shear moment slip analysis program BJSAN to predict friction joint lifetimes for both Perryman III terrain conditions. In these simulations, preloads were allowed to decay from 20,000 lbs to 19,000 lbs over a 500-hour time period. Results indicated that both roadwheel housing designs maintained their initial no slip status during this time frame under both terrain conditions. The BJSAN analysis code was then used to predict the minimum permissible value of bolt preload necessary to maintain slip conditions for each terrain. As anticipated, preloads were lower for the less severe Perryman III terrain 1 test condition. The modified

roadwheel housing design required approximately 12% less bolt preload than the original housing design to sustain no slip conditions for terrain 1. This value was found to rise to 14% for terrain 2. In either case, results indicated that substantial bolt preload loss would have to occur for slip conditions to prevail. It should be noted that conclusions regarding terrain 2 conditions are based on a partial set of force/moment DADS suspension data.

A mechanical property characterization of the quasi isotropic woven roving material was conducted to develop a material property data base for finite element analyses. Tension test results indicated near linear material response for in-plane mechanical properties. Asymmetric four point bend test results showed a linear intralaminar shear stress-strain response while interlaminar shear stress-strain response proved to be nonlinear. A nonlinear modulus was found from through thickness compression tests.

Both bolt preload and combined bolt preload/bolt bearing stress state conditions were predicted with a 3D, nonlinear elastic, *Abaqus* finite element model of a typical single connector arrangement. Finite element constitutive equations were developed for the S2 woven roving material from mechanical properties obtained from tension, compression, intralaminar shear, and interlaminar shear tests. A nonlinear material subroutine was developed to effectively model interlaminar material behavior. Model stress states for an increasing series of axial bolt compressive preloads were obtained and superimposed with a uniform far field stress representation of peak bolt bearing loads obtained from the maximum permissible roadarm vertical displacement.

Results from the finite element analysis predicted that bolt preloading produced a radially decaying σ_{zz} pressure distribution in the steel plate. Interface elements between the two plates transferred this pressure distribution to the composite plate. In direct contrast to the steel plate, there appeared to be minimal variation of this pressure distribution through the thickness of the composite plate. Maximum composite plate σ_{zz} pressure values rose from -899 psi to -3,441 psi as bolt preloads were increased from 5,000 lbs to 20,000 lbs. Application of the 5,757 lb bolt bearing load to each of the four preload stress states produced an asymmetry in the composite plate σ_{zz} pressure distribution. Bearing area "brooming" of the composite plate increased σ_{zz} pressures while net section Poisson contraction (from bolt hole in-plane σ_{yy} stress concentrations) reduced them. This asymmetry slightly lowered the friction load carrying capability of the single connector joint. A maximum reduction of 14% was observed for the 5,000 lb bolt preload case.

Peak in-plane normal and shear composite plate stresses were observed in the 20,000 lb bolt preload/ 5757 lb bolt bearing load case. Most maximum stress values appeared well below actual failure strengths of the quasi isotropic S2 glass/polyester woven roving material. However; maximum compressive bearing stresses (-14,000 psi) appear quite close to the in-plane compressive failure strength ($\sigma_{xx\text{ ult}} = \sigma_{yy\text{ ult}} = -16,000$ psi).

In closing, aside from these particular results, an advanced design rational has been developed for thick metallic/composite bolted friction joints. Hopefully the ideas of this new rational will be used in the future by other interested individuals to design reliable friction joints in thick composite structures.

RECOMMENDATIONS FOR FUTURE WORK

It is recommended that bolt preload relaxation tests be conducted at elevated temperatures and humidity to assess the effects of heat on the through thickness viscoelastic response of the [(0/90/+45/-45)_n], woven roving material. Future roadwheel housing terrain simulations, using the analysis codes described within this report, should include more severe CIFV test conditions. The *DADS* suspension modeling results for these simulations should contain a full set of roadarm force/moment data. The relationship between out-of-plane roadwheel housing moments and individual connector slip load should be firmly established. The effects of surface roughness on slip load should also be investigated. Rougher surfaces could lead to higher friction joint efficiencies. Effects of bolt elasticity on single connector finite element stress predictions should be investigated. Bolt bending, if sufficient, could significantly alter radial stress distributions. Ultimate strength properties of the woven roving material should be determined and appropriate failure theories should be applied to single connector finite element results. Ultimate bearing strength tests should also be conducted on single connector joints fabricated from the CIFV hull material.

ACKNOWLEDGMENTS

The authors would like to express their sincere thanks to Dr. Arthur Johnson, William Haskell, and Gordon Parsons of MTL as well as Eric Weerth, Paul Para and Dr. Baram Fatemi of FMC for their informative discussions regarding CIFV design and analysis. Special thanks to C.E. Freese of MTL for his many enlightening comments regarding FEA aspects as well as Bob Pasternak of MTL for his aid in the preload relaxation tests. The design of both static and dynamic preload relaxation test specimens by R. F. Anastasi of MTL was sincerely appreciated.

DISTRIBUTION LIST

No. of Copies	To
1	Office of the Under Secretary of Defense for Research and Engineering, The Pentagon, Washington, DC 20301
	Commander, U.S. Army Laboratory Command, 2800 Powder Mill Road, Adelphi, MD 20783-1145
1	ATTN: AMSLC-IM-TL
1	ATTN: AMSLC-CT
2	Commander, Defense Technical Information Center, Cameron Station, Building 5, 5010 Duke Street, Alexandria, VA 22304-6145
2	ATTN: DTIC-FDAC
1	MIAC/CINDAS, Purdue University, 2595 Yeager Road, West Lafayette, IN 47905
	Commander, Army Research Office, P.O. Box 12211, Research Triangle Park, NC 27709-2211
1	ATTN: Information Processing Office
	Commander, U.S. Army Materiel Command, 5001 Eisenhower Avenue, Alexandria, VA 22333
1	ATTN: AMCSCI
	Commander, U.S. Army Materiel Systems Analysis Activity, Aberdeen Proving Ground, MD 21005
1	ATTN: AMXSY-MP, H. Cohen
	Commander, U.S. Army Missile Command, Redstone Scientific Information Center, Redstone Arsenal, AL 35898-5241
1	ATTN: AMSMI-RD-CS-R/Doc
1	ATTN: AMSMI-RLM
1	Commander, U.S. Army Armament, Munitions and Chemical Command, Dover, NJ 07801
1	ATTN: Technical Library
	Commander, U.S. Army Natick Research, Development and Engineering Center, Natick, MA 01760-5010
1	ATTN: Technical Library
1	Commander, U.S. Army Satellite Communications Agency, Fort Monmouth, NJ 07703
1	ATTN: Technical Document Center
	Commander, U.S. Army Tank-Automotive Command, Warren, MI 48397-5000
1	ATTN: AMSTA-ZSK
1	ATTN: AMSTA-TSL, Technical Library
1	Commander, White Sands Missile Range, NM 88002
1	ATTN: STEWS-WS-VT
	President, Airborne, Electronics and Special Warfare Board, Fort Bragg, NC 28307
1	ATTN: Library
	Director, U.S. Army Ballistic Research Laboratory, Aberdeen Proving Ground, MD 21005
1	ATTN: SLCBR-TSB-S (STINFO)
	Commander, Dugway Proving Ground, Dugway, UT 84022
1	ATTN: Technical Library, Technical Information Division
	Commander, Harry Diamond Laboratories, 2800 Powder Mill Road, Adelphi, MD 20783
1	ATTN: Technical Information Office
	Director, Benet Weapons Laboratory, LCWSL, USA AMCCOM, Watervliet, NY 12189
1	ATTN: AMSMC-LCB-TL
1	ATTN: AMSMC-LCB-R
1	ATTN: AMSMC-LCB-RM
1	ATTN: AMSMC-LCB-RP
	Commander, U.S. Army Foreign Science and Technology Center, 220 7th Street, N.E., Charlottesville, VA 22901-5396
3	ATTN: AIFRTC, Applied Technologies Branch, Gerald Schlesinger
1	Plastics Technical Evaluation Center, (PLASTEC), ARDEC, Bldg. 355N, Picatinny Arsenal, NJ 07806-5000
	Commander, U.S. Army Aeromedical Research Unit, P.O. Box 577, Fort Rucker, AL 36360
1	ATTN: Technical Library

No. of Copies	To
1	Commander, U.S. Army Aviation Systems Command, Aviation Research and Technology Activity, Aviation Applied Technology Directorate, Fort Eustis, VA 23604-5577 ATTN: SAVDL-E-MOS
1	U.S. Army Aviation Training Library, Fort Rucker, AL 36360 ATTN: Building 5906-5907
1	Commander, U.S. Army Agency for Aviation Safety, Fort Rucker, AL 36362 ATTN: Technical Library
1	Commander, USACDC Air Defense Agency, Fort Bliss, TX 79916 ATTN: Technical Library
1	Clarke Engineer School Library, 3202 Nebraska Ave. North, Ft. Leonard Wood, MO 65473-5000
1	Commander, U.S. Army Engineer Waterways Experiment Station, P. O. Box 631, Vicksburg, MS 39180 ATTN: Research Center Library
1	Commandant, U.S. Army Quartermaster School, Fort Lee, VA 23801 ATTN: Quartermaster School Library
1	Naval Research Laboratory, Washington, DC 20375 ATTN: Code 5830
1	Dr. G. R. Yoder - Code 6384
1	Chief of Naval Research, Arlington, VA 22217 ATTN: Code 471
1	Edward J. Morrissey, WRDC/MLTE, Wright-Patterson Air Force, Base, OH 45433-6523
1	Commander, U.S. Air Force Wright Research & Development Center, Wright-Patterson Air Force Base, OH 45433-6523 ATTN: WRDC/MLLP, M. Forney, Jr.
1	WRDC/MLBC, Mr. Stanley Schulman
1	NASA - Marshall Space Flight Center, MSFC, AL 35812 ATTN: Mr. Paul Schuerer/EH01
1	U.S. Department of Commerce, National Institute of Standards and Technology, Gaithersburg, MD 20899 ATTN: Stephen M. Hsu, Chief, Ceramics Division, Institute for Materials Science and Engineering
1	Committee on Marine Structures, Marine Board, National Research Council, 2101 Constitution Ave., N.W., Washington, DC 20418
1	Librarian, Materials Sciences Corporation, 930 Harvest Drive, Suite 300, Blue Bell, PA 19422
1	The Charles Stark Draper Laboratory, 68 Albany Street, Cambridge, MA 02139
1	Wyman-Gordon Company, Worcester, MA 01601 ATTN: Technical Library
1	General Dynamics, Convair Aerospace Division, P.O. Box 748, Fort Worth, TX 76101 ATTN: Mfg. Engineering Technical Library
1	Department of the Army, Aerostructures Directorate, MS-266, U.S. Army Aviation R&T Activity - AVSCOM, Langley Research Center, Hampton, VA 23665-5225
1	NASA - Langley Research Center, Hampton, VA 23665-5225
1	U.S. Army Propulsion Directorate, NASA Lewis Research Center, 2100 Brookpark Road, Cleveland, OH 44135-3191
1	NASA - Lewis Research Center, 2100 Brookpark Road, Cleveland, OH 44135-3191
2	Director, U.S. Army Materials Technology Laboratory, Watertown, MA 02172-0001 ATTN: SLCMT-TML
4	Authors

U.S. Army Materials Technology Laboratory,
Watertown, Massachusetts 02172-0001
AN ASSESSMENT OF A FRICTION JOINT CONCEPT FOR THE
ROADWHEEL HOUSING ATTACHMENT OF THE COMPOSITE
INFANTRY FIGHTING VEHICLE -
Steven M. Serabian, Christopher Cavallaro,
Robert B. Dooley, and Kristen D. Weight

AD

UNCLASSIFIED
UNLIMITED DISTRIBUTION
Key Words

Composite materials
Bolted joints
Finite element analysis

Technical Report MTL TR 91-55, December 1991, 85 pp
illus-tables, D/A Project IL263102D081

Evaluation of a friction joint concept was undertaken to assess its viability as a critical joining technique for the Composite Infantry Fighting Vehicle. Through thickness viscoelastic relaxation effects of the thick [(0/90/45)_n] S2 glass/polyester woven roving C1FV hull material was experimentally investigated under dynamic surface traction fatigue and static loading conditions for a single connector configuration. Joint slip load as a function of bolt preload was also experimentally determined for this specimen configuration. Using this single connector information, a computer code was developed to predict friction joint lifetimes of multiple connector joints subjected to Perryman III terrain test conditions. Joint reaction forces and moments used in this code were obtained for the Composite Infantry Fighting Vehicle from DADS suspension modeling results. Bolt bearing stress state conditions resulting from friction joint slippage were predicted with a 3D nonlinear elastic finite element model. Finite element constitutive equations were developed for the S2 woven roving material from mechanical properties obtained from tension, compression, intralaminar, and interlaminar shear tests.

U.S. Army Materials Technology Laboratory,
Watertown, Massachusetts 02172-0001
AN ASSESSMENT OF A FRICTION JOINT CONCEPT FOR THE
ROADWHEEL HOUSING ATTACHMENT OF THE COMPOSITE
INFANTRY FIGHTING VEHICLE -
Steven M. Serabian, Christopher Cavallaro,
Robert B. Dooley, and Kristen D. Weight

AD

UNCLASSIFIED
UNLIMITED DISTRIBUTION
Key Words

Composite materials
Bolted joints
Finite element analysis

Technical Report MTL TR 91-55, December 1991, 85 pp
illus-tables, D/A Project IL263102D081

Evaluation of a friction joint concept was undertaken to assess its viability as a critical joining technique for the Composite Infantry Fighting Vehicle. Through thickness viscoelastic relaxation effects of the thick [(0/90/45)_n] S2 glass/polyester woven roving C1FV hull material was experimentally investigated under dynamic surface traction fatigue and static loading conditions for a single connector configuration. Joint slip load as a function of bolt preload was also experimentally determined for this specimen configuration. Using this single connector information, a computer code was developed to predict friction joint lifetimes of multiple connector joints subjected to Perryman III terrain test conditions. Joint reaction forces and moments used in this code were obtained for the Composite Infantry Fighting Vehicle from DADS suspension modeling results. Bolt bearing stress state conditions resulting from friction joint slippage were predicted with a 3D nonlinear elastic finite element model. Finite element constitutive equations were developed for the S2 woven roving material from mechanical properties obtained from tension, compression, intralaminar, and interlaminar shear tests.

U.S. Army Materials Technology Laboratory,
Watertown, Massachusetts 02172-0001
AN ASSESSMENT OF A FRICTION JOINT CONCEPT FOR THE
ROADWHEEL HOUSING ATTACHMENT OF THE COMPOSITE
INFANTRY FIGHTING VEHICLE -
Steven M. Serabian, Christopher Cavallaro,
Robert B. Dooley, and Kristen D. Weight

AD

UNCLASSIFIED
UNLIMITED DISTRIBUTION
Key Words

Composite materials
Bolted joints
Finite element analysis

Technical Report MTL TR 91-55, December 1991, 85 pp
illus-tables, D/A Project IL263102D081

Evaluation of a friction joint concept was undertaken to assess its viability as a critical joining technique for the Composite Infantry Fighting Vehicle. Through thickness viscoelastic relaxation effects of the thick [(0/90/45)_n] S2 glass/polyester woven roving C1FV hull material was experimentally investigated under dynamic surface traction fatigue and static loading conditions for a single connector configuration. Joint slip load as a function of bolt preload was also experimentally determined for this specimen configuration. Using this single connector information, a computer code was developed to predict friction joint lifetimes of multiple connector joints subjected to Perryman III terrain test conditions. Joint reaction forces and moments used in this code were obtained for the Composite Infantry Fighting Vehicle from DADS suspension modeling results. Bolt bearing stress state conditions resulting from friction joint slippage were predicted with a 3D nonlinear elastic finite element model. Finite element constitutive equations were developed for the S2 woven roving material from mechanical properties obtained from tension, compression, intralaminar, and interlaminar shear tests.

U.S. Army Materials Technology Laboratory,
Watertown, Massachusetts 02172-0001
AN ASSESSMENT OF A FRICTION JOINT CONCEPT FOR THE
ROADWHEEL HOUSING ATTACHMENT OF THE COMPOSITE
INFANTRY FIGHTING VEHICLE -
Steven M. Serabian, Christopher Cavallaro,
Robert B. Dooley, and Kristen D. Weight

AD

UNCLASSIFIED
UNLIMITED DISTRIBUTION
Key Words

Composite materials
Bolted joints
Finite element analysis

Technical Report MTL TR 91-55, December 1991, 85 pp
illus-tables, D/A Project IL263102D081

Evaluation of a friction joint concept was undertaken to assess its viability as a critical joining technique for the Composite Infantry Fighting Vehicle. Through thickness viscoelastic relaxation effects of the thick [(0/90/45)_n] S2 glass/polyester woven roving C1FV hull material was experimentally investigated under dynamic surface traction fatigue and static loading conditions for a single connector configuration. Joint slip load as a function of bolt preload was also experimentally determined for this specimen configuration. Using this single connector information, a computer code was developed to predict friction joint lifetimes of multiple connector joints subjected to Perryman III terrain test conditions. Joint reaction forces and moments used in this code were obtained for the Composite Infantry Fighting Vehicle from DADS suspension modeling results. Bolt bearing stress state conditions resulting from friction joint slippage were predicted with a 3D nonlinear elastic finite element model. Finite element constitutive equations were developed for the S2 woven roving material from mechanical properties obtained from tension, compression, intralaminar, and interlaminar shear tests.